

DISSERTATION

submitted to the

Combined Faculty of Natural Sciences
and Mathematics

of

Heidelberg University, Germany

for the degree of

Doctor of Natural Sciences

Put forward by

Jonas Karthein

born in Saarbrücken, Germany.

Oral examination: 13.05.2020

CERN-THESIS-2020-032
13/05/2020



Next-Generation Mass Spectrometry of Exotic Isotopes and Isomers

Referees:

Prof. Dr. Klaus Blaum

Priv.-Doz. Dr. Adriana Pálffy

Thesis content

1	Introduction	1
1.1	Nuclear Binding Energy Trends	3
1.2	Fundamental Physics Tests with Exotic Nuclei	5
1.2.1	Standard Model Tests	6
1.2.2	Neutrino-Mass Determination	8
2	Experimental Techniques	11
2.1	Radioactive Ion Beams at CERN/ISOLDE	11
2.2	MRTof-MS Basics	13
2.3	Penning Trap Basics	15
2.3.1	The ToF-ICR Technique	18
2.3.2	The PI-ICR Technique	19
2.4	The ISOLTRAP Experiment	23
2.4.1	Statistical and Systematic Uncertainties	24
3	Publications	27
3.1	Publication 1: Mirror Nuclei	29
3.2	Publication 2: Neutrino Mass	37
3.3	Publication 3: N-rich Cadmium	47
4	Discussion & Outlook	55
4.1	Mirror Nuclei	55
4.2	Neutrino Mass	58
4.3	N-rich Cadmium	59
5	Summary	63

List of Figures

<u>Figure 1.1:</u>	Nuclear chart with measured and extrapolated masses	2
<u>Figure 1.2:</u>	Nuclear observables deriving from a mass measurement	4
<u>Figure 1.3:</u>	Elementary particles of the Standard Model	6
<u>Figure 1.4:</u>	Schematic diagram of a β^+ -decay	7
<u>Figure 1.5:</u>	Complementary measurement principle of the ν_e mass	9
<u>Figure 2.1:</u>	Nuclear chart with isotope yield at ISOLDE	12
<u>Figure 2.2:</u>	Schematic diagram of an MRToF-MS	13
<u>Figure 2.3:</u>	Schematic overview of Penning traps	15
<u>Figure 2.4:</u>	Ion motion in a Penning trap	16
<u>Figure 2.5:</u>	Quantum-mechanical Penning trap eigen motions	17
<u>Figure 2.6:</u>	One/two-pulse ToF-ICR spectra	18
<u>Figure 2.7:</u>	Schematic diagram of the PI-ICR technique	20
<u>Figure 2.8:</u>	Mass-resolving power as function of the trapping time	22
<u>Figure 2.9:</u>	Schematic cross section of the ISOLTRAP experiment	23
<u>Figure 4.1:</u>	Temporal evolution of ν_c for $^{21}\text{Na}/^{21}\text{Ne}$ and $^{23}\text{Mg}/^{23}\text{Na}$	56
<u>Figure 4.2:</u>	$\Delta_{S_{1n}}(N=82)$ and $S_{1n}(N=82, 83)$ for $Z = \{40-68\}$	60

List of Abbreviations

CERN	European organization for nuclear research (<i>French: Conseil européen pour la recherche nucléaire</i>)
CKM	Cabibbo–Kobayashi–Maskawa quark-mixing matrix
CVC	Conserved vector current hypothesis
EC	Electron-capture decay
EMP	Electron multiplier particle detector
FAIR	Facility for antiproton and ion research (Darmstadt, Germany)
FRIB	Facility for rare isotope beams (East Lansing, USA)
GS	Ground state
IOI	Ion of interest
ISOLDE	CERN's isotope-separation on-line device
LS2	CERN's long shutdown 2 (2019-2020)
MCP	Micro-channel plate detector
MMC	Magnetic microcalorimetry
MRTof-MS	Multi-reflection time-of-flight mass spectrometer/separator
PDG	Particle data group
PI-ICR	Phase-imaging ion-cyclotron resonance technique
PSB	CERN's proton-synchrotron booster accelerator
PTMS	Penning trap mass spectrometry
QED	Quantum electrodynamic
RF	Radio-frequency field
RFQ	Radio-frequency quadrupole (Paul) trap
RIB	Radioactive ion beam facility
SM	Standard model of particle physics
ToF	Time of flight
ToF-ICR	Time-of-flight ion-cyclotron resonance technique
VS-IMSRG	Valence-space in-medium similarity renormalization group

Abstract

This cumulative dissertation comprises ISOLTRAP's transition from the well-established Penning-trap mass spectrometry (PTMS) technique, ToF-ICR, to the next-generation PTMS technique, called PI-ICR. **First**, the highest precision ever achieved at the ISOLTRAP experiment using ToF-ICR allowed for a reduction of the Q_{EC} -value uncertainty of the $^{21}\text{Na} \rightarrow ^{21}\text{Ne}$ and $^{23}\text{Mg} \rightarrow ^{23}\text{Na}$ electron-capture decays by a factor of five compared to their literature values. Within these findings, the most precise $\mathcal{F}t$ -values and, in the case of $^{21}\text{Na} \rightarrow ^{21}\text{Ne}$, a new V_{ud} -element value of the CKM quark-mixing matrix were derived and found to agree with the standard model of particle physics. **Second**, ISOLTRAP's first publication using PI-ICR demonstrated a supreme relative mass precision of $\delta m/m = 1.4 \times 10^{-9}$ in only 4 hours experiment time. The result reduced the uncertainty on the Q_{EC} -value of the $^{131}\text{Cs} \rightarrow ^{131}\text{Xe}$ decay by a factor of 25 and consequently precluded the decay as a possible candidate for a direct neutrino-mass determination. **Third**, ultra-high mass resolving powers exceeding 10^6 using PI-ICR allowed for the first spatial resolution of isomeric states in neutron-rich cadmium isotopes. Thus, this publication presented the first experimental data describing the $N=82$ neutron-shell closure below the proton-magic $Z=50$ while implying a drastic weakening of the $N=82$ shell. Furthermore, these measurements allowed for sophisticated comparison with state-of-the-art nuclear-theoretical models.

Kurzfassung

Diese kumulative Dissertation beschreibt ISOLTRAP's Übergang von der Standardmethode in Penningfallen-Massenspektrometrie (PFMS) ToF-ICR zur PFMS der nächsten Generation mittels PI-ICR. **Erstens** erlaubte die höchste je an ISOLTRAP erreichte Präzision mittels ToF-ICR eine Reduzierung der Q_{EC} -Wert-Unsicherheit der $^{21}\text{Na} \rightarrow ^{21}\text{Ne}$ und $^{23}\text{Mg} \rightarrow ^{23}\text{Na}$ Elektroneneinfangszfälle um einen Faktor fünf im Vergleich zu ihren Literaturwerten. Mit diesen Werten konnten höchst präzise $\mathcal{F}t$ -Werte und, im Falle von $^{21}\text{Na} \rightarrow ^{21}\text{Ne}$, ein neues V_{ud} -Matrixelement der CKM-Quarkmischungsmatrix bestimmt werden, welche mit der Vorhersage im Rahmen des Standardmodells übereinstimmen. **Zweitens** demonstrierte ISOLTRAP's erste Publikation mit PI-ICR höchste relative Massenpräzision von 1.4×10^{-9} in lediglich vier Stunden Messzeit. Das Ergebnis reduzierte die Q_{EC} -Wert-Unsicherheit des $^{131}\text{Cs} \rightarrow ^{131}\text{Xe}$ Zerfalls um einen Faktor 25 und schließt ihn als möglichen Kandidaten für eine direkte Neutrinomassenbestimmung aus. **Drittens** erlaubte eine ultrahohe Massenauflösung oberhalb 10^6 mittels PI-ICR die erste örtliche Auflösung metastabiler Zustände in neutronenreichen Cadmiumisotopen. Daraus resultierend präsentierte diese Veröffentlichung die ersten experimentellen Daten, welche den $N=82$ Neutronenabschluss unterhalb der magischen Protonenschale bei $Z=50$ beschreibt und eine drastische Schwächung der $N=82$ Schale impliziert. Zudem erlaubten diese Messungen Vergleiche der modernsten Kerntheoretischen Modelle.

1 Introduction

Einstein's famous $E = m \cdot c^2$ formula [Eins05] describes the fundamental link between energy, E , and mass, m , via the constant c , the speed of light. Hence, the mass of an atom summarizes all underlying energies, interactions, structure effects, and constituents in one quantity, unique to every particle like a fingerprint to a human. Studying the mass with the highest precision, therefore, allows for the revelation of all properties in a single measurement.

As such, scientists are trying to increase their mass measurement sensitivity since the inception of mass spectrometry in 1913 by the works of Thomson and Aston [Thom13]. For a recent review, see [Blau13]. During the time, relative mass precisions of $\delta m/m \sim 10^{-3}$ - 10^{-5} were enough to discover the concept of isotopes, which are particles of the same element (same proton number Z) but different mass number $A = Z + N$ (i.e., different neutron number N) [Asto19]. Besides, the concept of the nuclear and electronic binding energies, E_B and E_e , were discovered via the mass defect $\delta_x = (E_B + E_e) / c^2$ [Asto27], the amount of which a particle is lighter than the sum of its constituents:

$$M_{\text{atom}}(N, Z) = N \cdot m_n + Z \cdot m_p + Z \cdot m_e - (E_B(N, Z) + E_e(N, Z)) / c^2. \quad (1.1)$$

Technical developments [Münz13] of mass spectrometers have allowed for an increased relative mass precision of $\delta m/m \sim 10^{-6}$ - 10^{-8} ever since and led to breakthroughs in the model-independent understanding of nuclear structure. Detailed studies of nuclear binding energies reveal, among other things, enhanced nuclear binding (see black bars in Fig. 1.1 and Ch. 1.1 or [Caki13]) and help in the understanding of elemental creation in the universe for heavy elements in processes like the rapid neutron-capture (r) process (see red squares in Fig. 1.1 and [Clar13, Scha13]). Even better relative mass precisions of $\delta m/m \leq 10^{-9}$ of stable and exotic isotopes allow for tests of fundamental theories like quantum-electrodynamics (QED) [Köhl16], the Standard Model in mirror nuclei (see [Eron13, Kart19a] or Ch. 3.1) or electron-capture decay with the context of neutrino physics (see [Elis13b, Kart19b] or Ch. 3.2).

The challenging factor at radioactive ion beam (RIB) facilities (see Ch. 2) lies in the artificial creation of isotopes that do not exist on Earth (so-called exotic isotopes). Hence high-precision mass spectrometers of exotic isotopes require the

highest sensitivity and resolving power to access new areas of the nuclear chart and thus new physics, as displayed in Fig. 1.1 for ISOLTRAP since 2017.

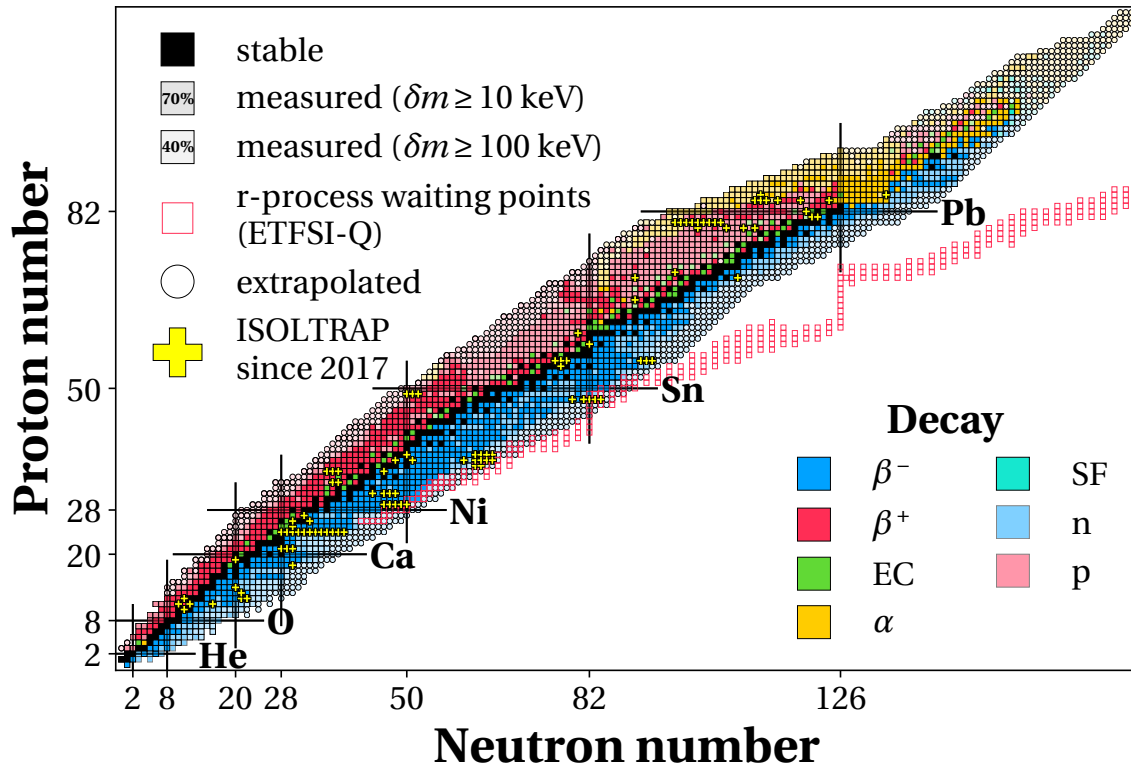


Figure 1.1: Nuclear chart showing stable isotopes (black squares), measured isotopes with their dominant decay mode in color (filled squares; ~2500) and extrapolated isotopes with their dominant decay mode in color (filled circles; ~1000). Isotopes measured or published by ISOLTRAP since 2017 are highlighted with yellow plus markers ranging from $A = 21$ up to $A = 219$. The waiting points of the r-process are displayed with red, empty squares [Graw07]. Additionally, mass uncertainties above 10 keV are indicated with a 30% transparency filter on the color and mass uncertainties above 100 keV with a 60% transparency filter on the color. Closed-neutron/proton shells are indicated with a black bar. The data was taken from the 2016 atomic-mass evaluation [Audi17, Wang17]. The figure was created using a Python script, which was programmed within the scope of this thesis. It was published on Github under the MIT license [Kart19f].

This thesis represents the transition to the next-generation mass spectrometry technique for the ISOLTRAP setup. With the so-called phase-imaging ion-cyclotron-resonance technique (see Ch. 2.3.2 and [Elis13a]), new or insufficiently known (see Fig. 1.1) areas of the nuclear chart can be accessed by overcoming the downsides of other state-of-the-art techniques (see Ch. 2.3.1), allowing for further advances in nuclear and astrophysics. The following introduces essential concepts and observables deriving from nuclear mass measurements.

1.1 Nuclear Binding Energy Trends

The power of a convoluted quantity as the mass, summarizing all underlying effects, comes with the task for the scientist to reveal as much information from just one quantity. Several derivative techniques (so-called mass filters) were found to be useful in unveiling substructure effects.

The general nuclear binding energy trend does not provide any distinct information about nuclear structure (see [Fig. 1.2](#)). However, the concave curve trend with a maximum at ^{62}Ni explains why fusion processes in stars stop around nickel and iron. Since adding further nucleons would consume energy rather than release, fusion is only energetically favorable until those isotopes. The one-neutron separation energy S_{1n} ,

$$S_{1n}(Z, N) = E_B(Z, N - 1) - E_B(Z, N), \quad (1.2)$$

which calculates from the difference in the binding energy of two neighboring isotopes, reveals more information. The quantity represents the amount by which the last neutron is bound. [Figure 1.2](#) depicts its general trend for all ~2500 experimentally known masses listed in the 2016 atomic mass evaluation [[Wang17](#)] with an inset for $Z = 50$ at $N \sim 82$. Besides the general downward trend with Z , two exciting effects expose:

1. A *small* (~3 MeV) staggering effect in energy between every even and odd isotope. This effect is caused by two-neutron pairing and is often compared to the electron-pairing seen in superconductors [[Coop56](#)].
2. A *significant* (>5 MeV) drop in energy at neutron numbers 2, 8, 20, 28, 50, 82, 126. These are typically referred to as *magic numbers* and correspond to configurations of enhanced stability. In the corresponding proton picture, the same stable configurations exist. In analogy to the electron shell model in an atom, a nuclear shell model was very successful in describing the nucleus [[Maye48](#)].

The S_{1n} provides essential information for models of the r-process, which is the process responsible for the creation of more than 50% of the elements heavier than nickel and iron. More specifically, enhanced neutron binding described in points 1 and 2 explains the so-called "waiting points" (see [Fig. 1.1](#)), where the rapid neutron capture stops and heavier elements form. Recent ISOLTRAP publications provide detailed additional information on this topic [[Atan15](#), [Wolf13a](#)].

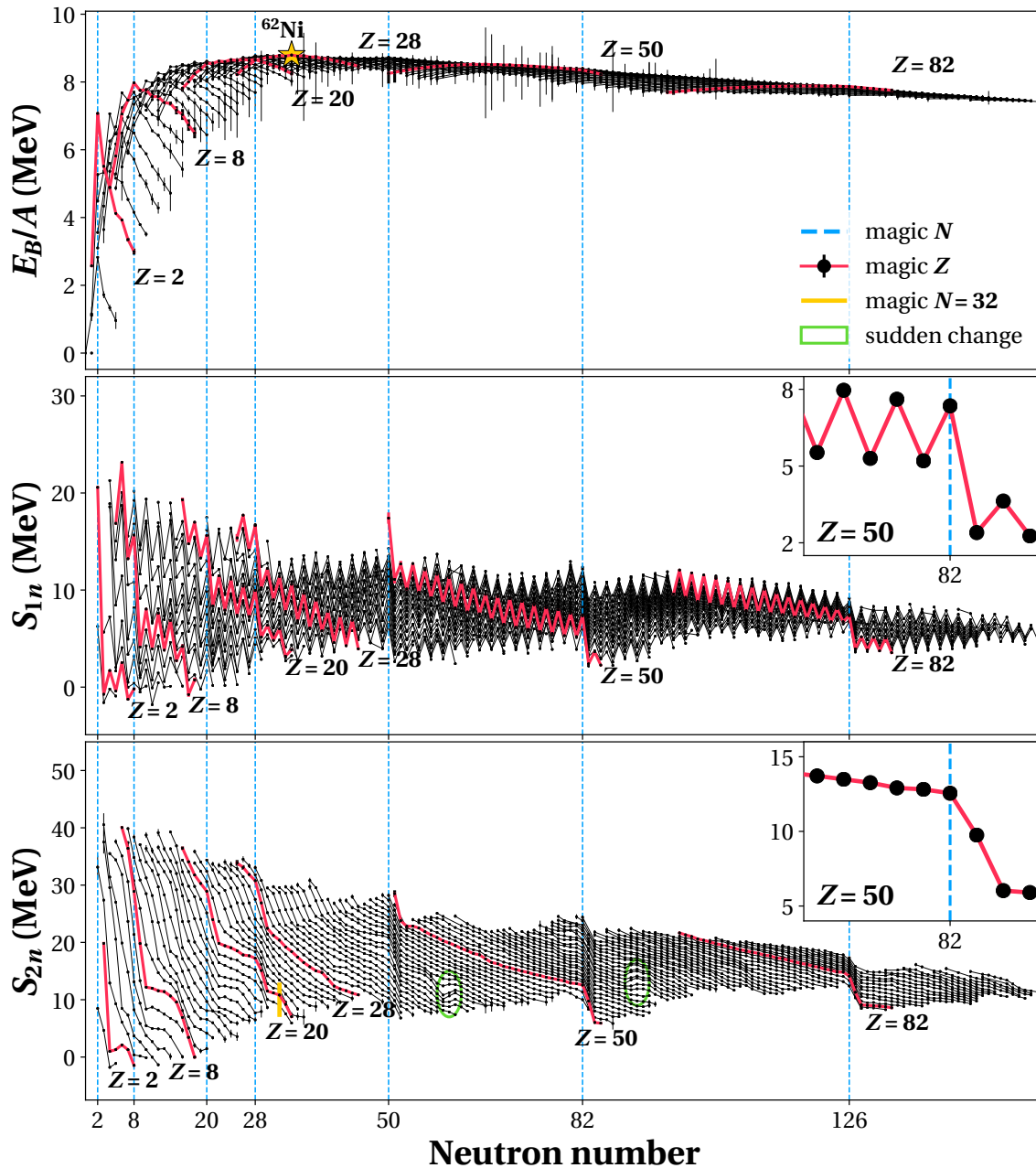


Figure 1.2: Nuclear observables deriving from mass measurements for isotopes with $1 \leq Z \leq 100$. Isotopes with closed proton shells $Z = \{2, 8, 20, 28, 50, 82\}$ are indicated with a solid red line and those with closed neutron shells $N = \{2, 8, 20, 28, 50, 82\}$ are indicated with a dashed blue line. *Top:* Nuclear binding energies per nucleon E_B/A for experimental data. The highest $E_B/A = 8.794553(7)$ MeV [Audi17] for ^{62}Ni is marked with a yellow star. *Middle:* One-neutron separation energies S_{1n} for experimental data. The inset shows S_{1n} for $Z = 50$ around $N = 82$. *Bottom:* Two-neutron separation energies S_{2n} for experimental data. Areas with sudden shape transitions are circled in green, and the $N = 32$ shell closure is highlighted in yellow [Wien13]. The inset shows S_{2n} for $Z = 50$ around $N = 82$. The data were taken from the 2016 atomic-mass evaluation [Audi17, Wang17]. The figure was created using a Python script, which was programmed within the scope of this thesis. It was published on Github under the MIT license [Kart19f].

Two-neutron separation energy S_{2n} ,

$$S_{2n}(Z, N) = E_B(Z, N - 2) - E_B(Z, N), \quad (1.3)$$

enhances the effect described in point 2 of the list, as mentioned earlier, by suppressing the staggering effect in energy. Besides the general downward trend in Z (see Fig. 1.2), the sharp drops in energy at magic N emphasize the strong binding and, consequently, the closed-shell character.

Even though treated as such for decades, these closed-shell nuclei do not seem to be universal. Recent measurements at, among others, ISOLTRAP show the appearance of new closed-shell configurations far away from stability. Measurements of neutron-rich $^{53,54}\text{Ca}$ at ISOLTRAP were of particular interest since they unambiguously confirmed the existence of the $N = 32$ shell closure (see Fig. 1.1) [Wien13]. Additionally, some existing magic-number configurations seem to undergo a substantial weakening in binding energy far away from stability, as discussed in Ch. 3.3 and Ch. 4. Furthermore, the S_{2n} overview uncovers areas of sudden change in energy (see Fig. 1.2) caused by nuclear phenomena such as nuclear deformation (i.e., the deviation from a spherical form; e.g., see [Naim10]), or nuclear halos (i.e., nuclei with a core and one to four decoupled and loosely bound nucleons; e.g., see [Riis13]).

In order to resolve the effects described in this section, typical relative mass precisions of $\delta m/m \sim 10^{-6}$ - 10^{-9} are required. Besides the technical limitations of the mass spectrometry apparatuses themselves, challenges are found in the artificial production of exotic isotopes far away from stability at high yield and low contamination (see Ch. 2).

1.2 Fundamental Physics Tests with Exotic Nuclei

With recent advances in mass spectrometry techniques, the achieved relative mass precisions of $\delta m/m \sim 10^{-9}$ and lower allow for additional fundamental physics tests using exotic nuclei. These measurements are complementary to high-precision experiments with stable nuclides [Rain04, Stur14, Köhl16], anti-matter [Smor19] or precision experiments performed in the field of high-energy particle physics [Erle19] which allow for a test of special relativity (essentially $E = m \cdot c^2$), quantum electrodynamics or the standard model of particle physics.

1.2.1 Standard Model Tests

The standard model (SM) of particle physics [Bamb15] is a quantum field theory which describes three of the four known fundamental forces in nature (electromagnetic, weak and strong – not yet gravitational) based on all known elementary particles. These include particles which form matter (so-called fermions with half-integer spin) and are categorized into quarks and leptons. These also include force carriers (so-called bosons with integer spin), which are categorized into gauge (vector) and scalar bosons. Figure 1.3 summarizes the elementary particles of the SM. The theory has been extremely successful in predicting experimental quantities even at high precisions (e.g., in predictions for the electron magnetic moment [Hann06]).

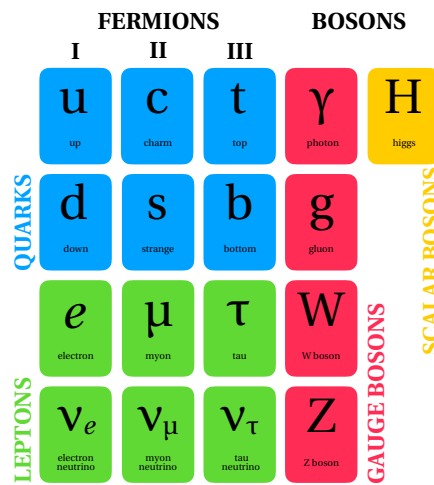


Figure 1.3: Elementary particles of the Standard Model made up from fermions (matter) and bosons (radiation).

The success of the SM triggered experimental programs in various physics fields in order to test the predictions or, in case of divergence, find physics beyond the SM. One approach appears to be the high-precision study of the β^+ -decay. This decay is one type of nuclear decay in which an *up* (u) quark bound inside a nucleon decays into a *down* (d) quark under the emission of a W^+ -boson. Consequently, the neutron and proton number changes by ± 1 . Figure 1.4 shows the Feynman diagram for a β^+ -decay. The interacting quarks are highlighted in red. It also shows the experimental observables, namely the half-life of the particle before the decay (so-called parent), the branching ratio BR of the decay into an observed particle after the decay (so-called daughter), and the Q -value of the decay. This quantity is essentially the energy difference of the parent and daughter atom, which directly results from a mass measurement:

$$Q = \left(M_{\text{parent}}(N, Z) - M_{\text{daughter}}(N + 1, Z - 1) \right) \cdot c^2. \quad (1.4)$$

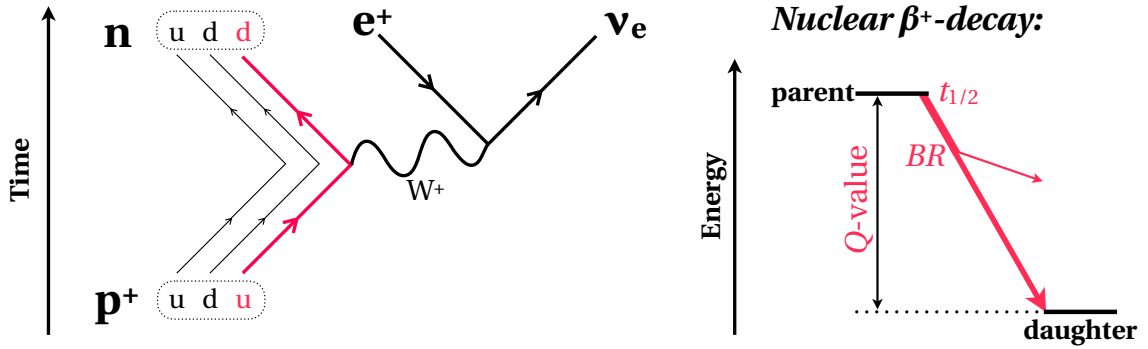


Figure 1.4: Schematic of a β^+ -decay. *Left:* Feynman diagram of a β^+ -decay with the participating up/down quarks highlighted in red. *Right:* Nuclear observables in a β^+ -decay marked in red. For details, see the text.

The W^+ -boson carries the released energy, which then decays into a positron e^+ and an electron neutrino ν_e . Measuring the observable quantities in the β^+ -decays of so-called mirror nuclei ($N_{\text{parent}} = Z_{\text{daughter}}$, $Z_{\text{parent}} = N_{\text{daughter}}$; i.e., very similar configurations of parent and daughter nucleus) very precisely allows for one of the best tests of the Conserved Vector Current (CVC) hypothesis, and the most precise determination of the V_{ud} -element of the Cabibbo–Kobayashi–Maskawa (CKM) quark-mixing matrix. Both values are calculated based on the $\mathcal{F}t$ -value,

$$\mathcal{F}t = f_V t \cdot (1 + \delta'_R) \cdot (1 + \delta_{\text{NS}}^V - \delta_C^V) = \frac{K}{V_{ud}^2 G_F^2 C_V^2 (1 + \Delta_R^V)}, \quad (1.5)$$

which corrects the vector parts of the statistical rate function f_V (derived from a mass measurement: $f_V \propto Q^5$) and the partial half-lives t (derived from half-life and branching-ratio measurements) by the isospin-symmetry-breaking correction, δ'_R , and nucleus dependent radiative corrections, δ_{NS}^V and δ_C^V [Seve08]. The $\mathcal{F}t$ -value can also be calculated from $K/(\hbar c)^6 = 2\pi^3 \ln 2 (m_e c^2)^{-5} = 8120.276(5) \times 10^{-10} \text{ GeV}^4 \cdot \text{s}$, the fundamental weak interaction coupling constant $G_F/(\hbar c)^3 = 1.16639(1) \times 10^5 \text{ GeV}^2$, the CVC constant $C_V = 1$ (assuming that the CVC hypothesis is correct; see [Hard15]), and the transition-independent correction $\Delta_R^V = 0.02361(38)$ [Seve08].

The CKM quark-mixing matrix is a unitary 3×3 matrix which contains information about the strength of the flavor-changing weak interaction. It is defined as [Koba73, PDG18]:

$$\text{CKM} = \begin{pmatrix} V_{ud} & V_{us} & V_{ub} \\ V_{cd} & V_{cs} & V_{cb} \\ V_{td} & V_{ts} & V_{tb} \end{pmatrix} = \begin{pmatrix} 0.97446(10) & 0.22452(44) & 0.00365(12) \\ 0.22438(44) & 0.97359(11) & 0.04214(76) \\ 0.00896(24) & 0.04133(24) & 0.999105(32) \end{pmatrix} \quad (1.6)$$

with the elements V_{ij} of an initial flavor i and a final flavor j . The indices correspond to flavors *up* (u), *down* (d), *top* (t), *bottom* (b), *charm* (c), and *strange* (s).

The measured matrix-element values are taken from the latest 2019 particle data group (PDG) evaluation update. The unitarity is fulfilled if the square sum of the row or column elements is equal to one. Using independently measured element values, one obtains [PDG18]:

$$\begin{aligned}
 \text{1st row:} & \quad |V_{ud}|^2 + |V_{us}|^2 + |V_{ub}|^2 = 0.9994(5) \\
 \text{2nd row:} & \quad |V_{cd}|^2 + |V_{cs}|^2 + |V_{cb}|^2 = 1.043(34) \\
 \text{1st column:} & \quad |V_{ud}|^2 + |V_{cd}|^2 + |V_{td}|^2 = 0.9967(18).
 \end{aligned} \tag{1.7}$$

The first row, which is dominated by the V_{ud} -element is the most precisely determined combination so far. Its determination derives from the study of super-allowed Fermi-type $0^+ \rightarrow 0^+$ mirror-nuclei transitions [Hard15].

This dissertation addresses transitions of mixed Fermi and Gamow-Teller type between mirror nuclei [Seve08]. These decays depend both on the vector and axial-vector part of the weak interaction. The formula (1.5) hence contains an additional correction term $(1 + \rho^2 f_V/f_A)$, where ρ is the Fermi and Gamow-Teller mixing ratio (determined in β - ν -asymmetry-coefficient measurements [Waut09]), and f_V/f_A is the ratio of the vector to axial-vector statistical rate functions, which is also calculated based on the Q -value. More information can be found in [Haye19].

1.2.2 Neutrino-Mass Determination

Neutrinos are the most abundant and lightest elementary particles. Even though the Standard Model assumes the neutrinos to be massless, there is profound experimental evidence based on neutrino oscillation [Bile87] for a non-zero neutrino mass and neutrino-flavor mixing. One approach for an experimental, model-independent determination of the neutrino mass lies in studying electron-capture (EC) decays.

EC decays are very similar to β^+ -decays (see Fig. 1.4) with the difference that the lepton number is conserved by absorbing an incoming, intra-atomic electron of the parent nucleus instead of expelling a positron. The captured electron is typically occupying the K, L, or M electronic shells due to their large wave-function-overlap with the nucleus. The particle, thus, ends up in an excited electronic state, which then decays via the emission of Auger electrons [Auge75] or Coster-Kronig photons (typically X-rays) [Cost35]. These secondary particles (i.e., electrons or photons) can be detected by calorimetric measurements [Gast17]. In summary, the ground-state parent nucleus decays in a two-step process to the ground-state daughter nucleus first by the emission of a neutrino and then by the emission of electrons or photons in a secondary atomic de-excitation:



One possibility to derive the neutrino mass from such a decay requires the comparison of two measurements. First, the total released energy in the EC decay is determined via the ground-to-ground-state Q -value ($\stackrel{\text{def}}{=} Q_{\text{EC}}$ -value; see Eq. (1.4)) using Penning-trap mass spectrometry (PTMS, [Fig. 1.5 left](#)). Second, the total released energy in the secondary atomic de-excitation is measured using low temperature metallic magnetic calorimeters (MMC, simulated in [Fig. 1.5 right](#)). If the neutrino is massless as predicted in the SM, the atomic de-excitation spectrum for many decays (simulated for 10^{14} events in [Fig. 1.5 right](#)) will span from 0 keV (at maximum kinetic energy of the neutrino $E_{\text{kin}}(\nu_e) = E_{\text{max}} = Q_{\text{EC}}$) up to $E_{\text{max}} = Q_{\text{EC}}$ (at zero kinetic energy of the neutrino $E_{\text{kin}}(\nu_e) = 0$). However, if the neutrino mass is non-zero, the atomic de-excitation spectrum for many decays will end at a value smaller than the Q_{EC} -value. The neutrino mass can then directly be determined from the difference between the measurements, as shown in the inset in [Fig. 1.5](#) simulated for three different proposed neutrino masses. More information on this specific experiment can be found in Ref. [[Elis15](#), [Gast17](#)]. The PTMS eventually requires a relative mass precision on the order of $\delta m/m \sim 10^{-12}$ to resolve a neutrino mass of 1 eV or lower.

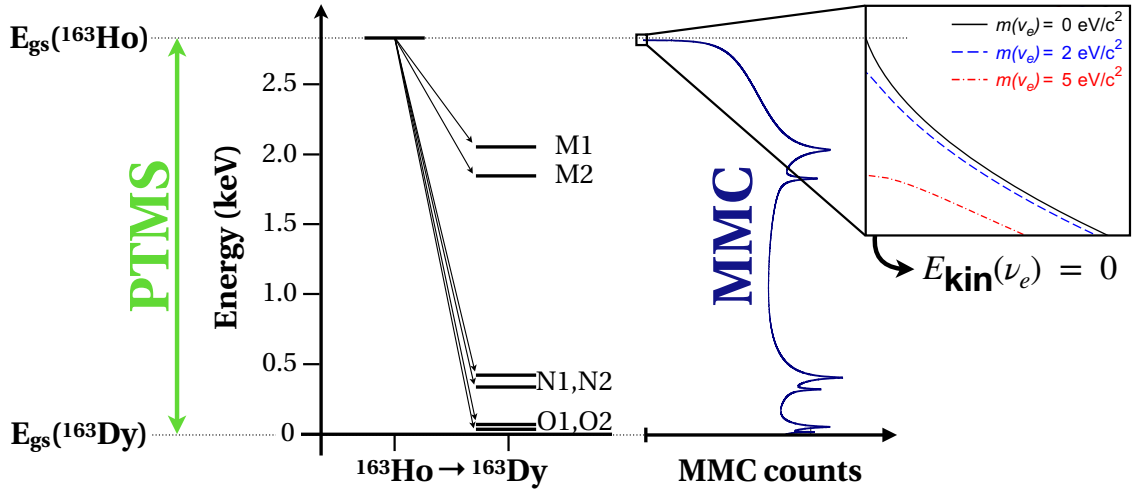


Figure 1.5: Complementary measurement principle of the ν_e mass via the EC in ${}^{163}\text{Ho}$. *Left:* The ground-state masses measured with PTMS. *Middle:* Decay branches of the ${}^{163}\text{Ho}$ EC-decay into atomic excited states in ${}^{163}\text{Dy}^*$. *Right:* Simulated atomic de-excitation spectrum of ${}^{163}\text{Dy}^*$ measured with MMC (rotated by 90°) [[Gast17](#)].

Important note: these measurements require detailed information about ground-state masses and electron-level schemes in order to find possible EC pairs with the lowest Q_{EC} -values prior to the actual experiment (see [Ch. 3.2](#)).

2 Experimental Techniques

Since the discovery of the atomic nucleus by E. Rutherford in 1909, nuclear physics has remained one of the most challenging fields in physics. The nuclear many-body problem with up to hundreds of interacting particles can neither be described by analytical solutions of the Schrödinger equation as seen in few-body systems nor by macroscopic approximations of systems with particles close to $N_A \sim 10^{23}$. Radioactive ion beam (RIB) facilities have been essential for breakthroughs in the understanding of elementary particles, nuclear structure, and elemental creation in the universe. RIBs artificially produce so-called "exotic" isotopes that do not exist on Earth for experiments of fundamental and applied nuclear research. This thesis lays focus on one of the most fundamental nuclear properties, namely the mass (= energy) of the aforementioned exotic isotopes.

2.1 Radioactive Ion Beams at CERN/ISOLDE

The isotope-separation on-line device (ISOLDE) facility is a RIB facility located at the European organization for nuclear research, CERN, in Geneva, Switzerland. Since its founding in 1967, and with a significant upgrade in accelerator energy in 1992 and a post-accelerator in 2015, it has been one of the pioneering facilities for the production of radioactive beams of more than 70 different chemical elements. Applications range among nuclear and atomic physics, solid-state physics, materials science, and life sciences. Besides, it also allows for high-precision experiments looking for physics beyond the Standard Model, which are complementary to high-energy experiments at CERN [Cath17, Borg18].

Integrated into CERN's accelerator complex, a 1.4 GeV proton beam from CERN's proton-synchrotron booster (PSB) accelerator is used to induce fission, spallation and fragmentation processes in a thick target (typical thickness tens of g/cm^2 [Köst01]). The target material is chosen depending on the desired isotopes to be measured and typically consists of uranium or silicon carbide. It is heated to $\sim 2 \times 10^3$ K to release the desired atoms via thermal diffusion and effusion into an ionization chamber. Besides surface and plasma ionization, resonant-laser ionization [Fedo17] of a growing number of chemical elements can also be applied. This technique has the advantage of being element selective already in the ionization process. The resulting ions (typically singly charged) are then accelerated to

30-50 keV and magnetically separated by their mass-to-charge ratio in order to obtain the mass number of interest. The typical mass resolving power of the magnetic separators at ISOLDE is on the order of 10^2 - 10^3 [Cath17], enough to separate isotopes of different mass numbers $A = (N + Z)$. The mass-separated beam is then sent to the subsequent experimental setups with the option of a post-acceleration step of tens of MeV/ u .

Figure 2.1 shows a nuclear chart with the available isotope yields at ISOLDE in color per μC of proton beam on target. Even though most isotopes lighter than the target material are created *inside* the thick target, it is not necessarily possible to extract them *out of* the target. Target and ion-source research and development is, therefore, an integral part of any RIB facility. Further information about the radiochemistry processes in different ISOLDE targets can be found in [Köst01].

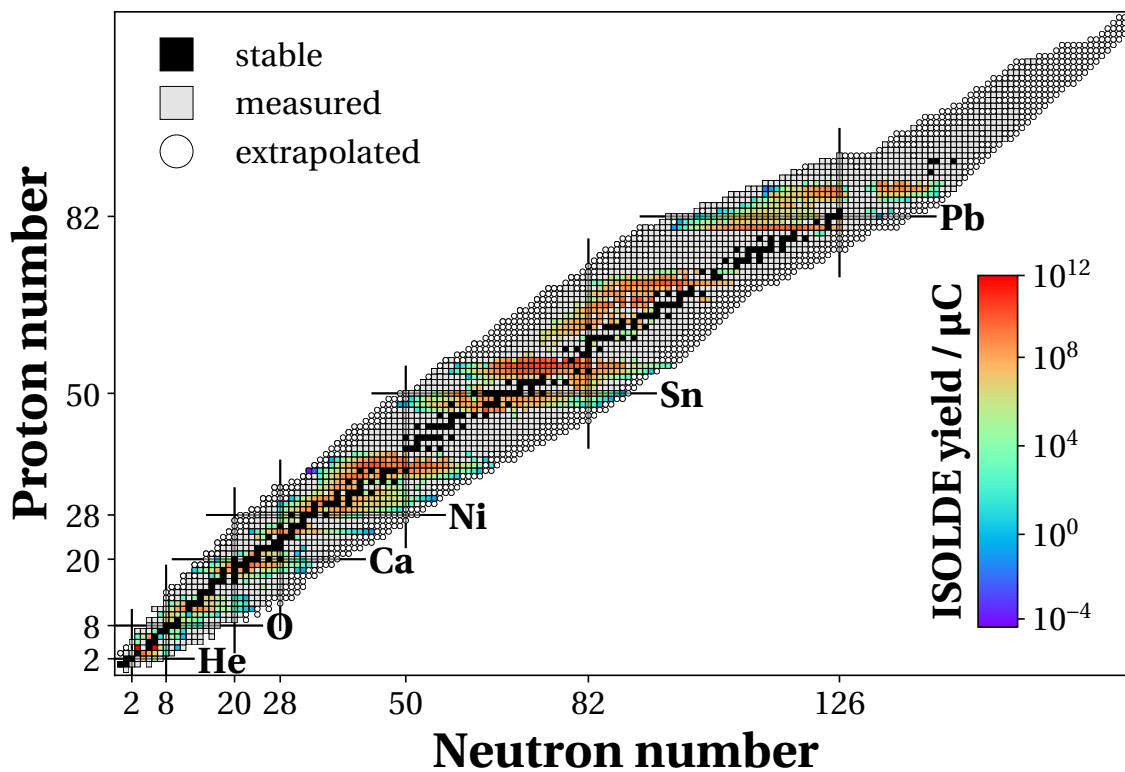


Figure 2.1: Nuclear chart showing isotopes with their detected yield in color per μC of proton beam on target at the CERN/ISOLDE facility in comparison with experimental and theoretically known isotopes. The data were taken from the 2016 atomic mass evaluation [Audi17, Wang17] and the ISOLDE target group [Ball19]. The figure was created using a Python script, which was programmed within the scope of this thesis. It was published on Github under the MIT license [Kart19f].

2.2 MRToF-MS Basics

The RIB facility ISOLDE produces a large variety of stable and radioactive species. Even though this allows the production of very exotic isotopes, their abundance (especially compared to stable or long-lived isobars which cannot be filtered out by conventional magnetic mass separators) and half-lives steeply decrease with distance to the stable elements (see Fig. 2.1). The main challenge for subsequent experiments is the time-efficient purification of the mass-selected beam of isobaric species, so-called "(isobaric) contaminants".

In recent years multi-reflection time-of-flight (MRToF) mass separators/spectrometers (MS) have become very popular at RIBs thanks to their success demonstrated at the ISOLTRAP experiment [Wien13, Welk17, Moug18]. Their comparably high speed in reaching high resolving powers ($m/\Delta m \cong 2.5 \times 10^5$ in tens of ms trapping time [Wien19]) and their capability of dealing with high contamination rates $R_{\text{cont}} > 10^5$ [Wolf13b] (so-called "high dynamic range") make them the perfect tool for mass separation and spectrometry of very short-lived species, which are not accessible by Penning traps ($10 \text{ ms} < t_{1/2} < 60 \text{ ms}$) [Wolf13b].

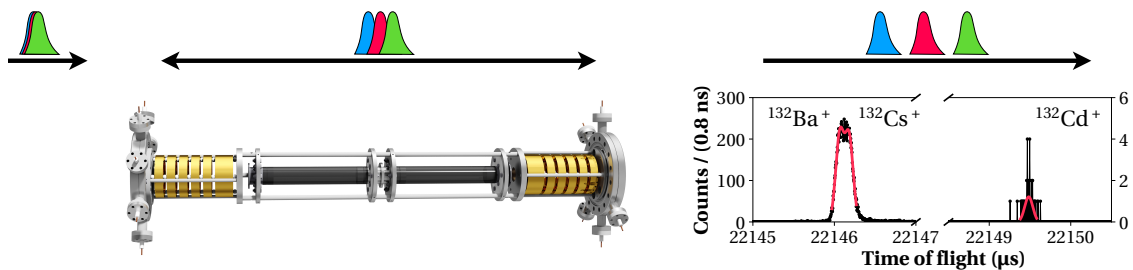


Figure 2.2: *Left:* Schematic diagram of the ISOLTRAP MRToF mass spectrometer/separator. Beam composed of different species with well-defined energy enters the device at the left and is trapped for a certain number of revolutions N_{rev} (typically $N_{\text{rev}} = 1 \times 10^3$ at ISOLTRAP). There, ions undergo a time-of-flight separation, and their time of flight can be measured. *Right:* Time-of-flight spectrum of $^{132}\text{Cd}^+$ with a mass resolving power of $m/\Delta m \sim 1 \times 10^5$.

Such an MRToF device consists of two electrostatic mirrors between which trapped ions are reflected back and forth (see Fig. 2.2). The ion's time of flight t ,

$$t = \alpha \sqrt{\frac{m}{q}} + \beta, \quad (2.1)$$

is directly proportional to its mass-to-charge ratio m/q and two device-specific calibration parameters α and β . These parameters can be determined by measur-

ing the time of flight $t_{1,2}$ of two well-known species. The mass of the ion of interest (IOI) m_{IOI} then results in

$$m_{\text{IOI}} = \left(C_{\text{ToF}} \times (\sqrt{m_1} - \sqrt{m_2}) + 0.5 \times (\sqrt{m_1} + \sqrt{m_2}) \right)^2, \quad (2.2)$$

with $C_{\text{ToF}} = (2t_{\text{IOI}} - t_1 - t_2)/[2(t_1 - t_2)]$, the masses of the reference ions $m_{1,2}$, and the ion of interest's time of flight t_{IOI} .

In the device's separation mode, the ion of interest is extracted after the time-of-flight separation by a fast-switching cavity [Wien17]. Figure 2.2 shows a typical example of $A = 132$. Even after "mass separation" using the ISOLDE mass separator, stable/long-lived (and therefore typically very abundant) $^{132}\text{Ba}^+ / ^{132}\text{Cs}^+$ cations still dominate the beam composition. However, after ~ 22 ms trapping time in ISOLTRAP's MRTof-MS, the much less abundant ion of interest, $^{132}\text{Cd}^+$, was successfully separated and measured.

The MRTof apparatus was used for all publications (see Ch. 3) in this dissertation as a mass separator or as a mass spectrometer. Additional information and recent developments of ISOLTRAP's MRTof can be found in Refs. [Wolf12, Wolf13b, Wien19]. These publications provide detailed information about ISOLTRAP's ion capture and time focusing techniques using a pulsed drift tube. Moreover, active and passive voltage stabilization of the mirror electrodes allow for mass resolving powers $m/\Delta m$ exceeding 2.5×10^5 in tens of ms trapping time and on a scale of hours of continuous data taking.

Within the scope of this thesis, a Python-based analysis software was written. It allows a full data analysis starting with the reconstruction of the raw, unbinned time-of-flight data taken by an electron multiplier particle detector. In addition to a regular spectral time-of-flight (ToF) analysis with unbinned, maximum likelihood estimation, and diverse cut parameters, the code includes a more advanced automated statistical ToF-drift detection tool based on rolling averages. Finally, a mass value is inferred from the fitted peaks by utilizing the atomic mass evaluation (AME16) database [Wang17]. The code was published on Github under the MIT license [Kart19e] and was used so far for the analysis of the $^{99-101}\text{In}$ masses [Moug20], in parallel with an analysis code using the ROOT analysis framework.

2.3 Penning Trap Basics

Besides MRTofF-MS, there are to-date two mass spectrometry devices for radioactive isotopes:

1. Storage rings using Schottky or isochronous mass spectrometry [Zhan16]. The first technique allows for mass determination with typical uncertainties of tens of keV but only for isotopes with half-lives down to several seconds. The latter technique provides access to isotopes with very low half-lives (microseconds), but only with accuracies of hundreds of keV, which is often insufficient for nuclear structure or Standard Model tests [Fran08].
2. Penning traps: first introduced at the ISOLTRAP setup in the 1980s have become the device of choice because they overcome both problems mentioned above: they provide typical uncertainties even down to the sub-keV regime for isotopes with half-lives of tens of milliseconds [Blau06].

A Penning trap is a device used to confine a charged particle in a defined volume. The radial confinement is achieved using a several Tesla linear magnetic field of strength $\vec{B} = B_0 \cdot \vec{z}$. A quadrupolar electrostatic field of strength \vec{E} provides the axial confinement. The electric field decomposes into axial and polar, dynamically independent components,

$$\vec{E}_z = -\frac{V_0}{d^2} \cdot \vec{z} \quad \text{and} \quad \vec{E}_\rho = \frac{V_0}{2d^2} \cdot \vec{\rho}, \quad (2.3)$$

using the characteristic length (see Fig. 2.3) in a Penning trap $d = (z_0^2/2 + \rho_0^2/4)$ and the applied electrode voltage V_0 . In the case of ISOLTRAP's hyperbolic precision Penning trap, $z_0 = 11.18$ mm and $\rho_0 = 13.0$ mm [Mukh08].

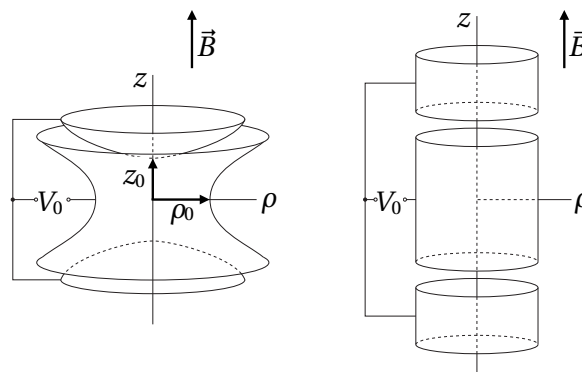


Figure 2.3: Schematic overview of a hyperbolic (left) and a linear Penning trap (right). Figure by Prof. K. Blaum.

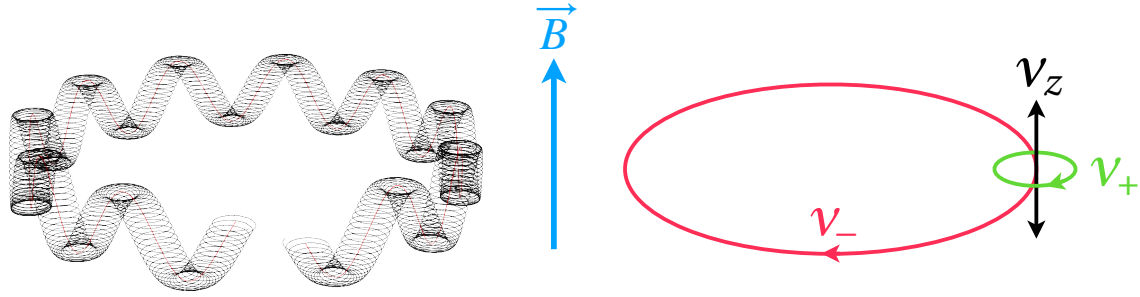


Figure 2.4: Ion motion in a Penning trap. *Left:* Schematic diagram of the superposition of the three eigenmotions of a trapped ion in a Penning trap. *Right:* Individual eigenmotions consisting of two radial motions, ν_- (red) and ν_+ (green), and one axial motion ν_z (black) along the magnetic field \vec{B} (blue).

Solving the equations of motion in space-coordinates,

$$m\ddot{z} = q\vec{E}_z \quad \text{and} \quad m\ddot{\vec{\rho}} = q\left(\vec{E}_\rho + \dot{\vec{\rho}} \times \vec{B}\right), \quad (2.4)$$

results in the ion motion in a Penning trap, which is shown in [Fig. 2.4](#). The motion is a superposition of three eigenmotions, one axial motion at ν_z and two radial motions, the reduced cyclotron motion at ν_+ and the magnetron motion at ν_- :

$$\nu_z = \sqrt{\frac{4\pi^2 qV_0}{m d^2}} \quad \text{and} \quad \nu_\pm = \frac{\nu_c}{2} \pm \sqrt{\frac{\nu_c}{4} - \frac{\nu_z}{2}}. \quad (2.5)$$

The last equation is the key to why Penning traps are so well suited for mass spectrometry. The cyclotron frequency ν_c of a singly charged cation,

$$\nu_c = \frac{q}{2\pi \cdot m} B = \nu_+ + \nu_-, \quad (2.6)$$

is directly proportional to the ion's charge-over-mass ratio q/m , which is equal to the sum of the two radial eigenfrequencies. The final atomic mass M_i is then determined by alternating measurements of the ion of interest (IOI) and a well-known reference ion (ref) in order to cancel the contribution of the magnetic field in Eq. (2.6) while using the cyclotron-frequency ratio $r_{\text{ref},\text{IOI}} = \frac{\nu_{c,\text{ref}}}{\nu_{c,\text{IOI}}}$ and the electron mass m_e [[Stur14](#)]:

$$M_{\text{IOI}} = r_{\text{ref},\text{IOI}} \cdot (M_{\text{ref}} - m_e) + m_e. \quad (2.7)$$

Individual, harmonic oscillators constitute an alternative picture on the three eigenmotions (see [Fig. 2.5](#)). This quantum-mechanical picture simplifies the understanding of the motion and its manipulation via external radio-frequency (RF) fields in a Penning trap. The negative energy contribution of ν_- results from the

electrostatic potential shape with a maximum in the center of the radial plane (see Eq. (2.3)). As shown in Fig. 2.5, the resonant excitation at their eigenfrequency allows for varying the amplitude quanta of each eigenmotion similar to a quantum harmonic oscillator (typically referred to as "dipolar excitation"). In analogy to Rabi oscillations, one can even couple two eigenmotions with the difference of two eigenfrequencies in order to shift energy between the modes (typically referred to as "quadrupolar excitation"). These two concepts are crucial for preparing trapped ions in a specific energy state to repeat a measurement always in the same fashion in order to increase statistics. Detailed quantum-mechanical calculations and descriptions of the ion dynamics in a Penning trap can be found in [Kret99].

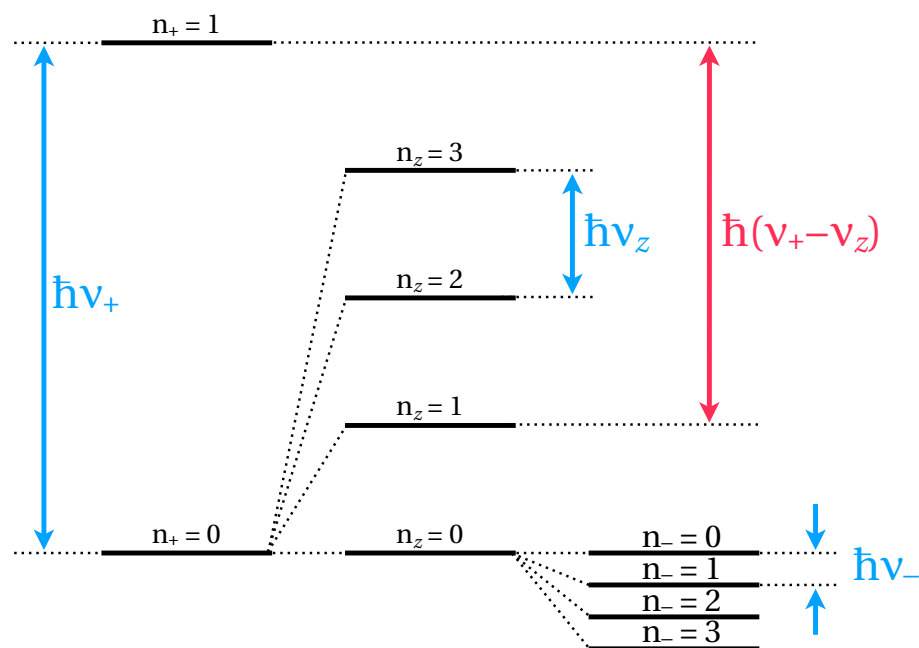


Figure 2.5: Quantum-mechanical energy-level scheme for the Penning-trap eigenmotions. Amplitude quanta of each eigenmotion can be increased or decreased by interaction with RF-fields at resonance frequency (blue). In analogy to Rabi oscillations, two eigenmotions can even be coupled with the difference of two eigenfrequencies (red).

2.3.1 The ToF-ICR Technique

The by far superior mass spectroscopy tool for radioactive ions to-date is the Penning trap. Since its first application in the 1980s at ISOLTRAP, the so-called time-of-flight ion-cyclotron-resonance technique [Gräf80] has become the mass spectroscopy technique of choice at RIB facilities worldwide due to its speed ($60 \text{ ms} \lesssim T_{\text{RF}} \ll 1 \text{ s}$), simplicity and one-ion sensitivity at room temperature allowing for high relative mass precisions $\delta m/m \sim 1 \times 10^{-9}$ and lower [Kart19a].

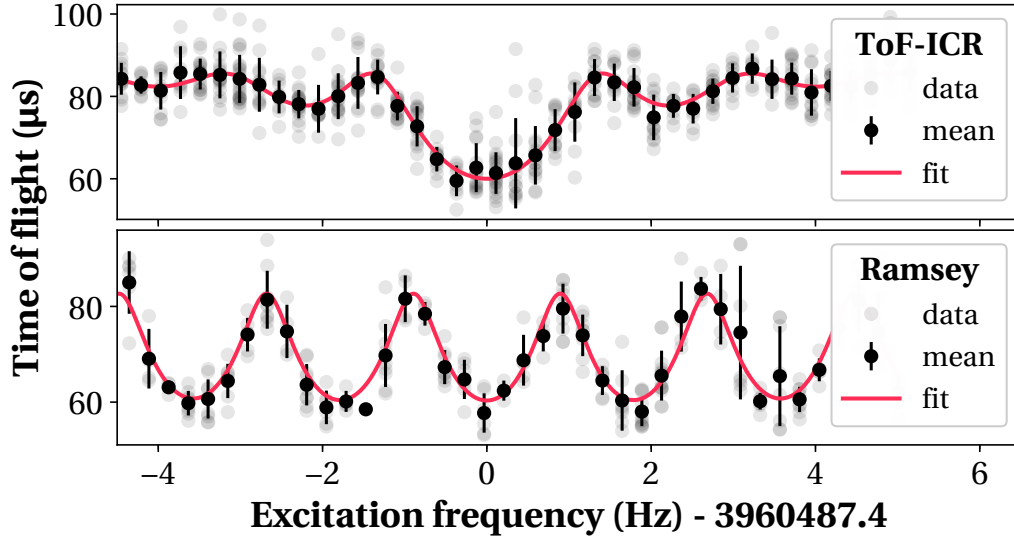


Figure 2.6: ToF-ICR spectra using a one-pulse (*top*) and two-pulse Ramsey-type (*bottom*) excitation scheme. Spectra shown for $^{23}\text{Mg}^+$ with a total measurement time of $T_{\text{RF}} = 600 \text{ ms}$.

In this technique, a quadrupolar excitation frequency around the true ν_c is scanned, coupling the two radial motions. The excited ions are then ejected from the Penning trap onto a micro-channel plate (MCP) detector while preserving their eigenmotions and the time of flight from the trap to the detector is measured destructively. Since the ions propagate through a strong magnetic field gradient (see Fig. 2.7), their magnetic moment μ ,

$$\mu = \frac{E_r}{B} \propto \frac{\nu_+^2 \rho_+^2 - \nu_-^2 \rho_-^2}{B} \quad (2.8)$$

with radial energy, E_r , and amplitudes of the radial motions, ρ_i , couples to the field and converts the radial motion into an additional transverse motion via an accelerating force $\vec{F}_\mu = -\mu(\nabla \vec{B})$. In other words, the ions are accelerated depending on the magnitude of their radial motion. Ions excited at the resonance frequency contain the largest radial energy and therefore arrive earlier at the detector than those out of resonance. Since the quadrupolar excitation frequency coupling the two radial motions in a Penning trap is exactly the cyclotron

frequency $\nu_c = \nu_+ + \nu_-$, the minimum in the ToF-ICR spectrum (as shown in [Fig. 2.6](#)) corresponds to the cyclotron frequency ν_c which is directly proportional to the ion's mass m in the formula (2.6) for ν_c . The side lobes result from the Fourier-transformed square-excitation pulse in the time domain [[Boll90](#)].

ToF-ICR was evolutionized at ISOLTRAP in 2007 by introducing a two-pulse Ramsey-type excitation scheme instead of one excitation pulse [[Kret07](#), [Geor07](#)]. This reduces the central-trough width and allows for a 10-fold gain in measurement time for similar precisions compared to the one-pulse ToF-ICR scheme. Time-of-flight spectra for both methods are compared for the same isotope $^{23}\text{Mg}^+$ and same total measurement time $T_{\text{RF}} = 600$ ms in [Fig. 2.4](#).

The main downside of the ToF-ICR technique is the scanning approach. In order to reach high precision, several hundred ions are necessary to obtain one full spectrum even though only ions excited around ν_c are actually contributing to the determination of the ion's true cyclotron frequency. While pursuing for evermore exoticness, the high number of required ions in the mass determination poses a problem. Furthermore, the technique doesn't allow for high-resolving power. The intrinsically Fourier-limited mass-resolving power $R_{\text{ToF-ICR}}$ of the technique [[Boll90](#)] $R_{\text{ToF-ICR}} = \frac{m}{\Delta m} = \frac{\nu}{\Delta \nu} \propto \nu_c T_{\text{RF}}$ is directly proportional to the measurement time T_{RF} and never exceeds the one of an MRTof-MS for short-lived species (see [Fig. 2.8](#)). Thus, low-lying isomeric states which can be found, among others, in the cadmium chain (see [Ch. 3.3](#)) cannot be resolved and only a mixture of states can be measured.

This technique was used for all publications (see [Ch. 3](#)) in this dissertation during which the best relative precision ever achieved at ISOLTRAP of $\delta m/m = 9 \times 10^{-10}$ was reached in the publication presented in [Ch. 3.1](#).

2.3.2 The PI-ICR Technique

To overcome ToF-ICR's downsides of low resolving power and high number of required ions, S. Eliseev *et al.* at SHIPTRAP developed a non-scanning, phase-sensitive PTMS technique [[Elis13a](#), [Elis14a](#)]. In the so-called phase-imaging ion-cyclotron-resonance (PI-ICR) technique, a radial frequency is determined by measuring the total phase φ_{tot} of a trapped ion in a Penning trap in a measurement time t_{acc} . This total phase φ_{tot} ,

$$\varphi_{\text{tot}} = 2\pi \cdot n + \varphi_i, \quad (2.9)$$

consists of $n \in \mathbb{N}_0$ integer turns and an additional phase $\varphi_i \in [0, 2\pi[$.

The radial frequency ν_i then results from:

$$\nu_i = \frac{\varphi_{\text{tot}}}{t_{\text{acc}}} = \frac{2\pi \cdot n + \varphi_i}{t_{\text{acc}}}. \quad (2.10)$$

Since the cyclotron frequency in a Penning trap $\nu_c = \nu_+ + \nu_-$ can be derived from the sum of the two radial motions ν_+ and ν_- , PI-ICR is perfectly suited to determine the ion's true cyclotron frequency in a Penning trap.

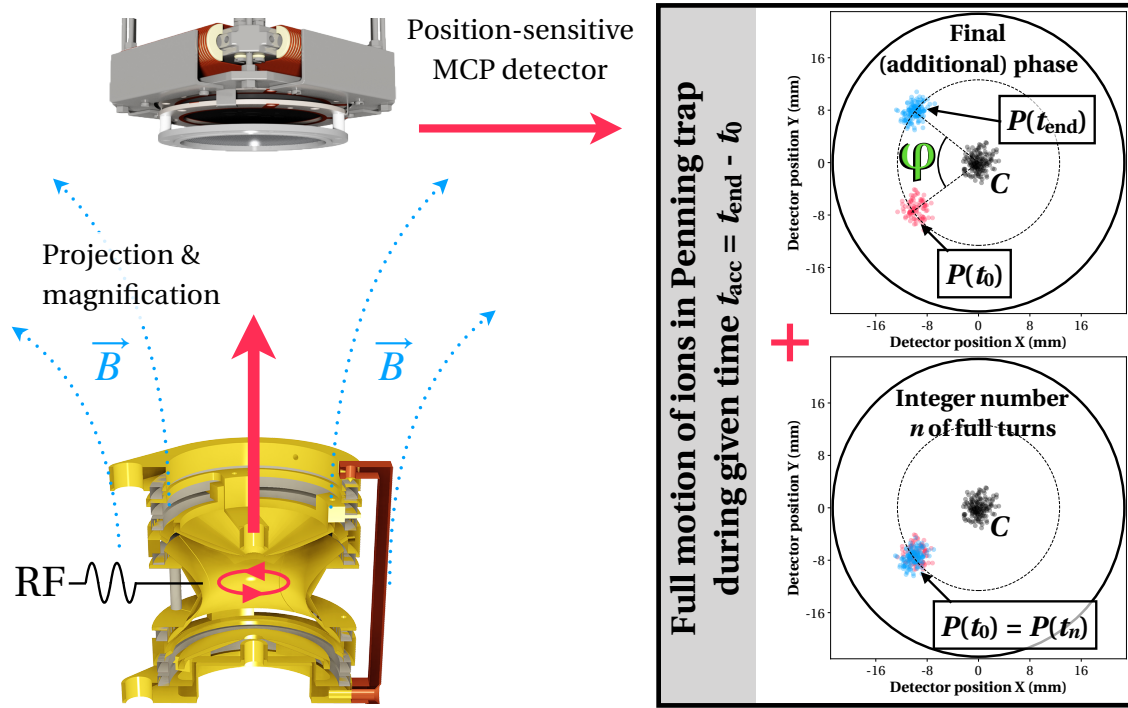


Figure 2.7: Schematic diagram of the PI-ICR technique. *Left:* Illustration of the excitation and ejection procedure using a hyperbolic Penning trap and a position-sensitive MCP detector outside the homogeneous part of the magnetic field \vec{B} . *Right:* Principle of the total-phase calculation.

PI-ICR is based on a destructive ion-motion projection onto a position-sensitive MCP detector in order to display/measure the total phase inside the Penning trap. The technique uses the magnetic field gradient between the trap and the MCP detector to magnify the motion without influencing its relative positions. This is shown in [Fig. 2.7](#). While the number of turns n proportionally increases with t_{acc} , n can be counted for any t_{acc} by stepwise increasing t_{acc} and starting with very low n . The additional phase φ_i at the final t_{acc} can be calculated as the polar angle between the ion's position P for $t = t_0$ and $t = t_{\text{acc}}$. The vertex is given by the center of the circular motion, in the following just referred to as center or C . Since the determination of n is based on integer counting, the statistical uncertainty rests upon the determination of the additional phase φ_i . Hence, increasing t_{acc} reduces the uncertainty of the measurement in a non-Fourier-limited manner.

Each position is gained in a destructive measurement. Repeated measurements for each position (so-called "spots") decrease the uncertainty on the 2D maximum likelihood fit which is used to derive the exact position. This measurement principle is applied to both radial eigenfrequencies separately, by minimizing the amplitude of the other respectively via dipolar excitation (see [Ch. 2.3](#)) on one of the ring electrode's segments (indicated by "RF" in [Fig. 2.7](#)). The real cyclotron frequency of the ion of interest is derived from:

$$\nu_c = \nu_+ + \nu_- = \frac{2\pi n_+ + \varphi_+}{2\pi t_{\text{acc}}} + \frac{2\pi n_- + \varphi_-}{2\pi t_{\text{acc}}} = \frac{2\pi(n_+ + n_-) + \varphi_{\text{final}}}{2\pi t_{\text{acc}}}. \quad (2.11)$$

Hence the measurement of the cyclotron frequency in a Penning trap can be reduced to three measurement steps:

1. The center C of the radial motions by minimizing the amplitudes of both radial eigenfrequencies ν_+ and ν_-
2. The final projection at $t = t_{\text{acc}}$ at ν_+ by minimizing the amplitude of ν_-
3. The final projection at $t = t_{\text{acc}}$ at ν_- by minimizing the amplitude of ν_+

The final phase φ_{final} can then be calculated by the polar angle between the spot in step two and three as the preparation for both is exactly the same (see [Fig. 5](#) in [\[Elis14a\]](#) for a detailed description of the ion preparation).

It is important to note, that in PI-ICR – unlike in ToF-ICR – *every single ion* contributes to the actual determination of the cyclotron frequency. In an upcoming publication [\[Moug20\]](#) we demonstrated the successful mass determination of very-low-yield (~ 20 ions/hour) isotopes at a $\delta m/m = 10^{-9}$ level of precision for as little as 5 ions per spot. This is a clear advantage and the main reason for the multifold reduction in measurement time compared to ToF-ICR.

The second advantage lies in the ultra-high resolving power of the new technique. Ions of different masses moving in a Penning trap undergo a similar time-of-flight separation in the radial plane as ions trapped in an MRToF-MS. As shown in [Fig. 2.8](#), the mass resolving power R ,

$$R \equiv \frac{t_i}{2 \cdot \Delta t} \triangleq \frac{\nu_c}{2 \cdot \Delta \nu_c} \triangleq \frac{\varphi_{\text{tot}}}{2 \cdot \Delta \varphi} \quad (2.12)$$

with MRToF trapping time t_i , MRToF peak FWHM Δt , ToF-ICR cyclotron frequency ν_c , ToF-ICR resonance trough width $\Delta \nu_c$, PI-ICR total phase φ_{tot} , and PI-ICR spot width $\Delta \varphi$, of PI-ICR is actually higher than ISOLTRAP's MRToF-MS at any trapping time. However the MRToF-MS's high dynamic range still justifies

the use of this technique. High mass-resolving powers are crucial to resolve low-lying (< 500 keV) isomeric states as shown in [Kart20, also see Ch. 3.3]. In an earlier attempt in 2016 [Atan16] using ToF-ICR, the aforementioned isomeric states could not be resolved and thus, the mass of a mixed state of ground and isomeric species was observed. In the first two ISOLTRAP PI-ICR publications a very high mass-resolving power $R \sim 10^6$ - 10^7 was reached in only $t \sim 10^2$ - 10^3 ms trapping time. [Kart19b, Kart20, also see Ch. 3.2, Ch. 3.3]

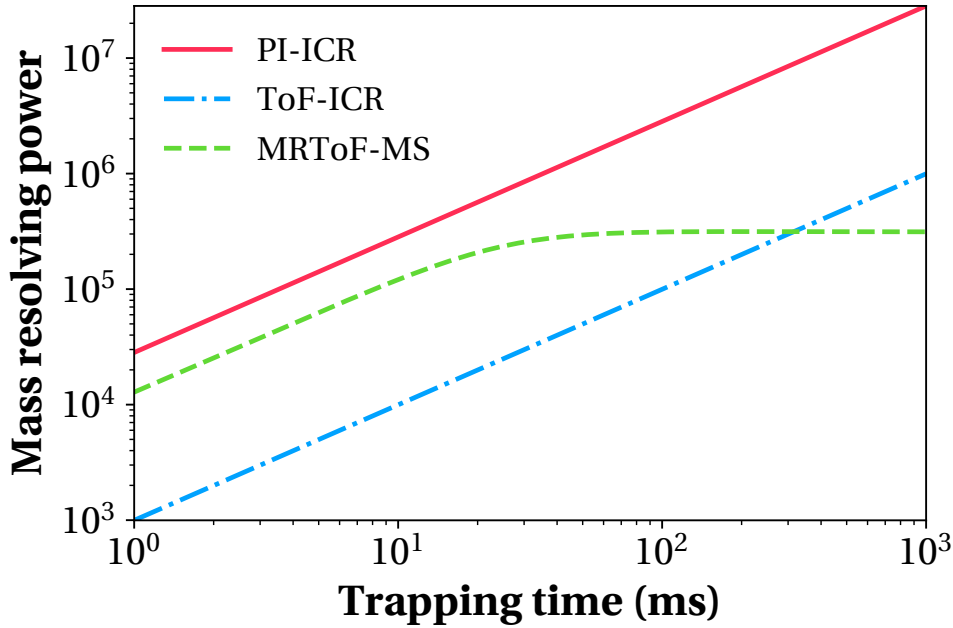


Figure 2.8: Mass-resolving power as function of the trapping time for ISOLTRAP's MRTof-MS and ISOLTRAP's precision Penning trap using ToF-ICR and PI-ICR.

Within the scope of this thesis, a Python based analysis software was written. It allows a full PI-ICR data analysis including the reconstruction of raw PI-ICR data, fitting of PI-ICR position information using unbinned, 2D maximum likelihood estimation and calculation of the cyclotron frequency using the pattern 1/2 measurement scheme, and the determination of a frequency ratio between a measurement ion and a reference ion. The pattern 1/2 measurement scheme allows for a direct determination of ν_c and is described in detail in [Elis14a]. Additionally, the code allows for the analysis of isomeric states separated in pattern 2 (see Ch. 3.3). The code was published on Github under the MIT license [Kart19d] and was used so far for the analysis of data in [Kart19b, Kart20, Moug20].

2.4 The ISOLTRAP Experiment

With its over 30 years of existence, the high-precision mass spectrometer ISOLTRAP [Mukh08, Krei13, Lunn17] is one of the longest running experiments at CERN. Since the first publication dating back to 1986, over 180 publications have followed in its history.

The experimental setup is depicted in Fig. 2.9. It consists of a horizontal and a vertical section. Each contains two traps with different purposes. The singly charged cation beam enters at an energy of 30-50 keV. There is the option to use radioactive beam, so-called "on-line" beam, from the ISOLDE facility. There is also the option to use beam from ISOLTRAP's so-called "off-line" ion source. This source also provides the cations used for the reference measurements. It hosts an alkali-ion source (stable potassium, rubidium and cesium cations) and is currently upgraded with an additional laser-ablation ion source to produce, among others, carbon clusters. These will be used in 2020 to perform extensive systematic studies of the measurement traps and the new measurement schemes implemented since the last systematic studies performed in 2003 [Kell03].

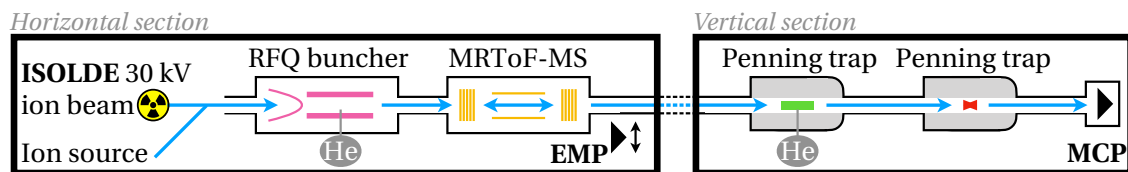


Figure 2.9: Schematic cross section of the ISOLTRAP experiment. *Left:* Horizontal section containing of an ion-source platform, the connection to radioactive ISOLDE beam, a radio-frequency-quadrupole (RFQ, purple) buncher filled with pure helium (He) gas, and an MRToF-MS (yellow) with an electron multiplier (EMP) detector. *Right:* Vertical section containing a linear preparation Penning trap (green) filled with pure He gas, a hyperbolic precision Penning trap (red) and a position-sensitive micro-channel plate (MCP) detector.

The continuous beam first enters into a segmented, linear Paul trap (also known as radio-frequency quadrupole (RFQ) buncher; purple) [Herf01], which is filled with high-purity helium gas for cooling and bunching. The ion bunch is subsequently injected into the MRToF-MS (yellow) [Wolf12, Wolf13b]. Here, mass measurements for very short-lived species ($t_{1/2} < 60$ ms) can be performed using an electron multiplier (EMP) particle detector and a fast timing card. For longer-lived species the trap is used as a mass separator. The purified beam is then bend into the vertical section and injected into the linear preparation Penning trap (green). It is filled with pure helium gas for further cooling. [Sava91] This step was

found to be crucial for the PI-ICR technique as optimal starting conditions (i.e., straight and centered injection into the precision Penning trap) are necessary for PI-ICR to work optimally. The beam finally arrives in the hyperbolic precision Penning trap (red) where mass measurements can be performed destructively using a position-sensitive MCP detector and the well-established one-[Gräf80] and two-pulse [Kret07, Geor07] ToF-ICR techniques or the recently implemented PI-ICR technique [Elis13a, Elis14a].

An alternative description can be found on ISOLTRAP's new website [Kart19f] which has been fully redesigned as part of this thesis.

2.4.1 Statistical and Systematic Uncertainties

The better precision an experiment can achieve, the more sensitive it gets to systematic uncertainties. The following list summarizes experimental and analysis techniques for PTMS in order to account for systematic shifts/uncertainties at ISOLTRAP down to a $\sim 10^{-9}$ level of precision. Further details can be found in [Kell03] and in an upcoming publication about the systematic studies at ISOLTRAP performed with a carbon-cluster source during CERN's long shutdown (LS2) in 2019/2020.

- From Eq. (2.6) one notices that the statistical uncertainty in the mass determination is based on the statistical uncertainty in the cyclotron-frequency determination. In both, ToF-ICR and PI-ICR, the statistical uncertainty is based on three factors: First, the number of detected ions of interest being limited by the production and ionization rate at ISOLDE (see Ch. 2.1) and the transport and purification efficiency to the measurement trap. Second, the purity of the beam. Hereby, the MRToF-MS for isobaric contaminants and PI-ICR for isomeric contaminants provide excellent tools for beam purification. And third, the width of the resonance in ToF-ICR or the number n of integer turns in PI-ICR (see Eq (2.11)), scaling both inversely proportional with the measurement time. All these factors are not really in the hand of the experimentator after optimal preparation since they heavily depend on the given ISOLDE yield for the species of interest, the given amount of beam time at ISOLDE and the half-life of the species limiting the measurement time. Relative systematic uncertainties as low as $\delta m/m = 9 \times 10^{-10}$ [Kart19a] are routinely achieved.
- The strongest external contribution in PTMS are fluctuations in the magnetic field which have a direct influence on the cyclotron frequency (see Eq. (2.6)).

This can be overcome by measuring alternating spectra of the ion of interest and a well-known reference ion faster than non-linear fluctuations of the magnetic field (typically ~ 15 min). Additionally, magnet-bore temperature and environment pressure, having strong influence on the magnetic field, are constantly logged at ISOLTRAP in order to detect inhomogeneous fluctuations during a measurement. With the publications in this thesis, the cyclotron-frequency-ratio evolution over time is now determined via a simultaneous polynomial fit of a subset of the cyclotron frequencies. This enhances the modeling of the evolution of magnetic-field drifts and therefore overcomes systematic uncertainties deriving from magnetic-field fluctuations. Details about this technique can be found in [Kart19a, Kart19b] and in the published analysis code [Kart19d].

- In addition to short-term fluctuations, the magnetic field of a superconductor shows a long-term drift which was measured to be $\delta\nu_c/\nu_c = 6.35 \times 10^{-11}$ T/min at ISOLTRAP [Kell03].
- So-called space-charge effects [Boll92] are systematic shifts in the cyclotron frequency due to Coulomb interactions by the presence of additional ions in a Penning trap. Hence the number of ions simultaneously trapped in the measurement Penning trap is intentionally kept at ~ 1 ion in the trap.
- Imperfections in the trap geometry lead to systematic shifts. The ion preparation is specifically designed such that measurement and reference ions are always taking the same flight path during a measurement and are therefore experiencing the same effects due to trap imperfections. In addition, a mass-dependent term was determined to be $\delta R/R = 1.6 \times 10^{-10} \times (m_{IOI} - m_{REF})/u$ with the atomic mass unit u [Kell03].
- A remaining uncertainty of $\delta R/R = 9 \times 10^{-9}$ was assigned due to a reduced χ^2 greater than one [Kell03]. This so-called "residual uncertainty" will be remeasured in the upcoming systematic studies since it is not applicable anymore due to a full dismantling of the vertical as well as horizontal part of setup since the last studies.
- During an analysis, many different cuts in the space domain, time-of-flight domain, number of ions per ejection (so-called "z-class"), as well as fit models can be tested. Correlation with magnet-bore temperature, environment pressure and reference spectra taken regularly can be searched for. Also mass-dependent effects (so-called "internal sandwiches") and decay-curves can be studied.

3 Publications

This thesis was composed as a cumulative dissertation in agreement with the regulations of the Department of Physics and Astronomy of Heidelberg University. The following chapter comprises three publications in internationally acclaimed peer-reviewed journals, which have already been published or are accepted for publication. The author holds the first authorship for all three publications.

The thesis describes the successful transition from the well-established ToF-ICR technique to the next-generation Penning-trap technique PI-ICR at ISOLTRAP. As such, the following publications connect via the revolution of the measurement method, demonstrating unprecedented resolving power and precision. The discovered physics results are of utmost importance for the field of nuclear physics and demonstrate the vastness of opportunities the new technique has to offer.

The first section presents ISOLTRAP's most precise (ToF-ICR) mass values ever published with a precision $\delta m/m = 9 \times 10^{-10}$ in the case of ^{21}Na . The Q -values of the measured mirror nuclei decays, namely $^{21}\text{Na} \rightarrow ^{21}\text{Ne}$ and $^{23}\text{Mg} \rightarrow ^{23}\text{Na}$, were used to calculate the corrected $\mathcal{F}t$ -value of these transitions. This value is used to calculate an experimental V_{ud} -element of the CKM quark-mixing matrix. Its unitarity can be tested, which is an integral part of the Standard Model.

The second section presents ISOLTRAP's first publication using the PI-ICR technique. In only ~ 4 hrs measurement time, a relative mass precision $\delta m/m = 1.4 \times 10^{-9}$ and a mass resolving power $m/\Delta m$ exceeding 1×10^7 in only 1 s trapping time were reached for ^{131}Cs . These values constitute the main improvements of the new technique, allowing measurements with ~ 25 times shorter measurement time at similar or better levels of precision and much higher resolving power. Additionally, the new measurement improves the uncertainty on the ground-to-ground-state Q_{EC} -value by a factor 25 precluding the $^{131}\text{Cs} \rightarrow ^{131}\text{Xe}$ pair as a feasible candidate for the direct determination of the ν_e mass.

In the third section, first high-resolution data using PI-ICR are presented, providing the first measurement of the low-lying isomeric states in ^{129}Cd and their ordering. These results shed light on the evolution of the $N = 82$ shell gap below the proton-magic number $Z = 50$ and suggest a substantial weakening of the $N = 82$ shell gap. Additionally, the first measurement of ^{132}Cd is presented, confirming the phenomenon of mutually enhanced magicity at ^{132}Sn .

3.1 Publication 1: Mirror Nuclei

Authors:

Jonas Karthein, Dinko Atanasov, Klaus Blaum, Martin Breitenfeldt, Vira Bondar, Sebastian George, Leendert Hayen, David Lunney, Vladimir Manea, Maxime Mougeot, Dennis Neidherr, Lutz Schweikhard, Nathal Severijns, Andree Welker, Frank Wienholtz, Robert Wolf, Kai Zuber

Publication status:

Published 15 July 2019

Journal reference:

Karthein, J. et al. Phys. Rev. C **100**, 015502 (2019).

Digital object identifier:

10.1103/PhysRevC.100.015502

Authors' contributions:

DA, KB, MB, DL, VM, DN, LS, FW, RW, and KZ were involved in the proposal for the experiment. DA, MB, VM, MM, NS, AW, and FW carried out the experiment. JK performed the first and final analysis with second analyses by VB and SG. JK and LH performed the theoretical calculations. JK, KB, VB, SG, LH, VM, MM, and NS were involved in the discussion of the results. NS wrote the introduction and JK wrote the remaining parts about the experiment, analysis, discussion, conclusion, and outlook and prepared all figures. The manuscript was reviewed critically before and after submission by all authors.

Abstract:

We report on high-precision Q_{EC} values of the $^{21}\text{Na} \rightarrow ^{21}\text{Ne}$ and $^{23}\text{Mg} \rightarrow ^{23}\text{Na}$ mirror β transitions from mass measurements with ISOLTRAP at ISOLDE/CERN. A precision of $\delta m/m = 9 \times 10^{-10}$ and $\delta m/m = 1.5 \times 10^{-9}$ was reached for the masses of ^{21}Na and ^{23}Mg , respectively. We reduce the uncertainty of the Q_{EC} values by a factor five, making them the most precise experimental input data for the calculation of the corrected $\mathcal{F}t$ -value of these mixed Fermi/Gamow-Teller transitions. For the $^{21}\text{Na} \rightarrow ^{21}\text{Ne}$ Q_{EC} value, a 2.3σ deviation from the literature Q_{EC} -value was found.

Q_{EC} -value determination for $^{21}\text{Na} \rightarrow ^{21}\text{Ne}$ and $^{23}\text{Mg} \rightarrow ^{23}\text{Na}$ mirror-nuclei decays using high-precision mass spectrometry with ISOLTRAP at the CERN ISOLDE facility

J. Karthein,^{1,2,*} D. Atanasov,^{2,†} K. Blaum,² M. Breitenfeldt,¹ V. Bondar,^{3,‡} S. George,² L. Hayen,³ D. Lunney,⁴ V. Manea,^{1,†} M. Mougeot,^{4,§} D. Neidherr,⁵ L. Schweikhard,⁶ N. Severijns,³ A. Welker,^{1,7} F. Wienholtz,^{1,6} R. N. Wolf,^{2,||} and K. Zuber⁷

¹CERN, Route de Meyrin, 1211 Genève, Switzerland

²Max-Planck-Institut für Kernphysik, 69117 Heidelberg, Germany

³KU Leuven, Instituut voor Kern- en Stralingsfysica, 3001 Leuven, Belgium

⁴CSNSM-IN2P3-CNRS, Université Paris-Sud, 91405 Orsay, France

⁵GSI Helmholtzzentrum für Schwerionenforschung, 64291 Darmstadt, Germany

⁶Universität Greifswald, Institut für Physik, 17487 Greifswald, Germany

⁷Technische Universität Dresden, 01069 Dresden, Germany



(Received 2 April 2019; published 15 July 2019)

We report on high-precision Q_{EC} values of the $^{21}\text{Na} \rightarrow ^{21}\text{Ne}$ and $^{23}\text{Mg} \rightarrow ^{23}\text{Na}$ mirror β transitions from mass measurements with ISOLTRAP at the CERN ISOLDE facility. A precision of $\delta m/m = 9 \times 10^{-10}$ and $\delta m/m = 1.5 \times 10^{-9}$ was reached for the masses of ^{21}Na and ^{23}Mg , respectively. We reduce the uncertainty of the Q_{EC} values by a factor of 5, making them the most precise experimental input data for the calculation of the corrected $\mathcal{F}t$ value of these mixed Fermi and Gamow-Teller transitions. For the $^{21}\text{Na} \rightarrow ^{21}\text{Ne}$ Q_{EC} value, a 2.3σ deviation from the literature Q_{EC} value was found.

DOI: [10.1103/PhysRevC.100.015502](https://doi.org/10.1103/PhysRevC.100.015502)

I. INTRODUCTION

After more than five decades of experiments determining half-lives, Q_{EC} values, and branching ratios for a set of 14 superallowed Fermi β transitions, a very robust data set has been obtained, leading to an impressive 2×10^{-4} precision on the weighted average corrected $\mathcal{F}t$ value for these transitions [1]. The constancy of these corrected $\mathcal{F}t$ values confirms the conserved vector current (CVC) hypothesis [2] and provides a very precise value for the dominant V_{ud} *up-down* quark-mixing matrix element [1]. Together with the V_{us} and V_{ub} matrix elements, the unitarity of the Cabibbo-Kobayashi-Maskawa (CKM) quark-mixing matrix [3] is now confirmed at the 5.5×10^{-4} precision level [1], thereby providing strong

constraints on several types of new physics beyond the Standard Model [4–6].

The uncertainty on the weighted averaged $\mathcal{F}t$ value for the superallowed Fermi transitions is mainly determined by the theoretical uncertainty on the nucleus-independent radiative correction, Δ_R [7]. Addressing this again to improve its theoretical uncertainty by at least a factor of 2 to 3 would be highly desirable and would allow for major progress in searches for new physics via the CKM-unitarity condition.

Meanwhile, progress from the experimental side is continuously ongoing. Input data for the $\mathcal{F}t$ values of well-known superallowed Fermi transitions are being cross checked and further improved. In addition, with production means at radioactive beam facilities steadily improving, the set of transitions of interest is being extended as well [1]. Finally, it would be of interest to obtain a precise value of V_{ud} from further types of β transitions. This would not only allow cross checking the validity of small theoretical corrections but, if sufficiently precise, would also contribute to further reducing the uncertainty of the V_{ud} value.

The β decay of the free neutron requires no nuclear structure-related corrections and would thus in part provide an independent check on the value of V_{ud} . This requires the determination of the neutron lifetime and of the ratio of the axial vector to vector coupling constants g_A/g_V . Significant progress in the determination of the neutron lifetime has been made over the past decade [5,6]. The ratio g_A/g_V , traditionally extracted from the electron-emission asymmetry parameter, A , faces a similar problem [8]. However, the most recent and also most precise results, obtained from independent measurements, all seem to converge to a common value [5,6].

It was pointed out that also the superallowed mirror β transitions in isospin doublets could contribute to further

*Corresponding author: jonas.karthein@cern.ch. This publication comprises part of the Ph.D. thesis of J. Karthein, enrolled at the Ruprecht-Karls-Universität Heidelberg.

[†]Present address: KU Leuven, Instituut voor Kern- en Stralingsfysica, 3001 Leuven, Belgium.

[‡]Present address: ETH Zürich, 8092 Zürich, Switzerland.

[§]Present address: Max-Planck-Institut für Kernphysik, 69117 Heidelberg, Germany.

^{||}Present address: ARC Center of Excellence for Engineered Quantum Systems, School of Physics, The University of Sydney, NSW 2006, Australia.

Published by the American Physical Society under the terms of the [Creative Commons Attribution 4.0 International](https://creativecommons.org/licenses/by/4.0/) license. Further distribution of this work must maintain attribution to the author(s) and the published article's title, journal citation, and DOI.

improving the precision on V_{ud} [9]. Moreover, such transitions could provide important cross checks for the calculation of the isospin impurity correction, δ_C [10]. In the past decade, many measurements leading to more precise $\mathcal{F}t$ values for such transitions have been performed. In addition, all theoretical contributions necessary to obtain the corrected $\mathcal{F}t$ values with a precision at the 10^{-4} level—for sufficiently precise experimental input data—have been provided [53]. However, similar to the case of the neutron lifetime, these mixed Fermi–Gamow–Teller transitions require the determination of the ratio of the axial vector to vector part in the decay. For the mirror β transitions, this mixing ratio has traditionally been extracted from the β -particle emission-asymmetry parameter, A , the β -neutrino correlation coefficient, a , and the neutrino-asymmetry parameter, B . As reaching high precision in β -decay correlation measurements is not straightforward, in most cases the precision on the mixing ratio determines the precision of V_{ud} [9,11]. The most precise results for V_{ud} from mirror β transitions have been obtained for ^{19}Ne [12] and ^{37}K [13]. The weighted average of the transitions for which data are available, i.e., $V_{ud} = 0.9730(14)$ [5], is still about seven times less precise than the value from the superallowed Fermi transitions [1].

With the advancement of recent radioactive ion beam facilities, intense ^{21}Na and ^{23}Mg beams of high purity are now relatively easy to obtain. Hence, the mirror β transitions of these two nuclei are ideal cases to further improve the value of V_{ud} from mirror β transitions. When the proposal for the experiments reported here was submitted to the ISOLDE and Neutron Time-of-Flight Committee (INTC) at CERN [14], the Q_{EC} value of both isotopes were the second-largest fractional contribution to their $\mathcal{F}t$ values. New measurements were reported since by TITAN [15] and LEBIT [16]. The data presented in this work constitutes the most precise results for the Q_{EC} values of these two isotopes to date. From the three experimental input data to the $\mathcal{F}t$ values, the Q_{EC} value now contributes the smallest fraction of the uncertainty for both isotopes and provides thus strong motivation for improved measurements of the other quantities.

II. EXPERIMENT AND ANALYSIS

The sodium, neon, and magnesium isotopes discussed in the present article were produced at the ISOLDE facility at CERN [17]. There, a proton beam of up to $2\ \mu\text{A}$ at an energy of 1.4 GeV from CERN’s Proton-Synchrotron booster is impinged on a silicon carbide target [18] to produce the desired isotopes. The target was heated up to $2000\ ^\circ\text{C}$ to allow the release of the produced isotopes via thermal diffusion and effusion. In order to enable reacceleration to 30 keV and magnetic mass separation using the general-purpose separator (GPS), the sodium and neon nuclides were ionized using the recently developed versatile arc discharge and laser ion source (VADLIS) [19,20] in its electron-impact ionization mode. The magnesium ions were selectively ionized using ISOLDE’s resonant ionization laser ion source (RILIS) [21] while the VADLIS was used in a special surface-ion suppressing mode [20,22].

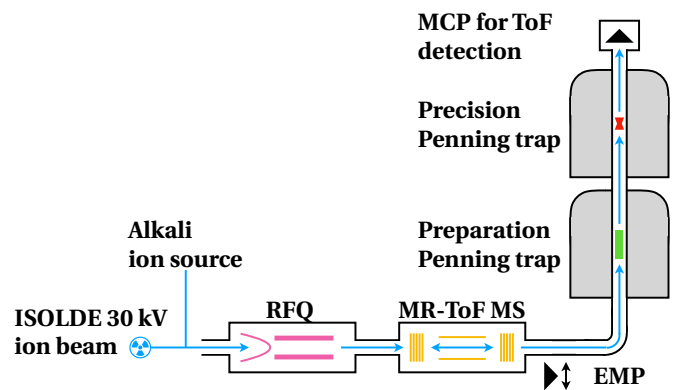


FIG. 1. Schematic overview of the ISOLTRAP setup. On-line beam from the CERN ISOLDE facility or off-line beam from ISOLTRAP’s offline source enters to the left to go through a sequence of four ion traps: a linear radio-frequency Paul trap (RFQ, pink), a multi-reflection time-of-flight (MR-ToF, yellow) device, and two Penning traps (green, red). For particle detection and time-of-flight measurements, a secondary electron multiplier (EMP) ion detector and a micro-channel plate (MCP) ion detector are used.

The high-precision mass spectrometer ISOLTRAP [23–25], schematically depicted in Fig. 1, includes a linear radio-frequency Paul trap (RFQ), a multireflection time-of-flight (MR-ToF) device, and two Penning traps. The continuous on-line beam from ISOLDE or from the off-line alkali ion source arrives at ISOLTRAP’s RFQ (see the purple part in Fig. 1) cooler and buncher [26], which accumulates, bunches, and cools the continuous beam in a 1.9×10^{-3} mbar helium buffer-gas environment for 20 ms. The bunched beam is then extracted from the RFQ and its energy is adjusted to 3.2 keV using a pulsed drift cavity. The ions are then injected in the MR-ToF mass spectrometer-separator (MS) [27,28] (see the yellow part in Fig. 1). The latter is the first trap which can be used for high-precision mass determination and ion identification. In order to inject (eject) ions into (from) the MR-ToF MS, a so-called lift cavity situated between the trapping electrodes is switched to ground [29,30]. This reduces the kinetic energy of the ions to be lower (higher) than the electrostatic trapping potential created by the mirror electrodes. Inside the MR-ToF MS, the ion bunch was reflected between 1000 and 2000 times, corresponding to a trapping time of ≈ 15 to 25 ms and extending its flight path accordingly. Therefore, ions with the same kinetic energy $E_{\text{kin}} = q_i U = m_i v_i^2 / 2$ (charge q_i , acceleration voltage U , and velocity v_i) and different masses m_i are separated for the same flight path since the mean flight time t_i

$$t_i = \alpha \sqrt{m_i / q} + \beta \quad (1)$$

is proportional to their mass-over-charge ratio (α and β are calibration constants of the ToF system). After ejection, the ions were detected using a secondary electron multiplier (EMP) ion detector (see Fig. 2). Once a sufficient time-of-flight separation is achieved, the ions of interest (IOI) were selected by properly timing the potential change of the in-trap lift [31]. In Fig. 2, the achieved mass-resolving power R was on the order of $R = t_i / (2 \times \text{FWHM}_i) \approx 10^5$ (with the mean

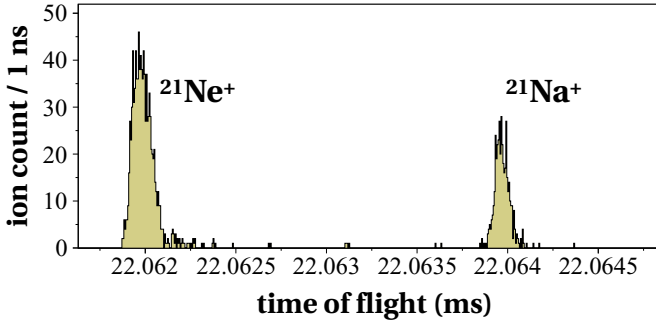


FIG. 2. Typical time-of-flight spectrum using laser ionization (for details, see text), here shown for 80 summed spectra of $A = 21$ after 2000 revolutions in ISOLTRAP’s MR-ToF MS.

time of flight t_i and the full width at half maximum $FWHM_i$ of the time-of-flight distribution).

The purified beam from the MR-ToF MS then enters the helium buffer-gas-filled preparation Penning trap where the ions are further cooled and purified [32]. Finally, the IOIs are transferred to the precision Penning trap where the high-precision mass measurements are performed by determining the ions’ cyclotron frequency ν_c

$$\nu_c = \frac{1}{2\pi} \frac{q_i}{m_i} B \quad (2)$$

with the charge-to-mass ratio q_i/m_i and the magnetic field strength B . The detection techniques used in this work were the single-excitation-pulse time-of-flight ion cyclotron resonance (ToF-ICR) [33] and the two-pulse Ramsey-type ToF-ICR [34,35]. In both cases, a quadrupolar excitation frequency, applied to the trap’s segmented ring electrode, is scanned. This couples the two radial eigenmotions of the trapped particles. If the excitation frequency equals the cyclotron frequency of the trapped ion ensemble, their time of flight after ejection to a detector is shorter [33].

In the case of the $A = 21$ system, 30 spectra pairs of subsequent reference-IOI measurements were taken while 19 were taken for $A = 23$. In all cases, the Ramsey technique (Ramsey pattern: 50-500-50 ms, 100-1000-100 ms, and in case of $^{21}\text{Ne}^+$ even 200-2000-200 ms) was used in order to reduce the statistical uncertainty (see Table I). Over the duration of the beam time, the mass was switched four times on the ISOLDE mass separator to exclude systematic uncertainties deriving from the data acquisition at ISOLTRAP. Furthermore, trap parameters such as the capture time in the trap, the (magnetron) excitation amplitude, the injection

TABLE I. Summary for $^{21}\text{Na}^+$ and $^{23}\text{Mg}^+$ showing the number of Ramsey-type spectra taken, the estimated production yield at ISOLDE, the half-lives [36], the reference ion for cyclotron frequency ratio determination, the measured cyclotron frequency ratio r , and the measured Q_{EC} values in comparison to the ones published by LEBIT for ^{21}Na [16] and by TITAN for ^{23}Mg [15].

Isotope	N_{spectra}	Yield (s^{-1})	$T_{1/2}$ (s)	Ref.	Ratio r	Q_{EC} (keV)	
						This work	Literature
$^{21}\text{Na}^+$	30	6×10^6	22.422(10)	$^{21}\text{Ne}^+$	1.0001813796(9)	3546.902(18)	3547.11(9)
$^{23}\text{Mg}^+$	19	1×10^8	11.317(11)	$^{23}\text{Na}^+$	1.0001894144(15)	4056.182(32)	4056.35(16)

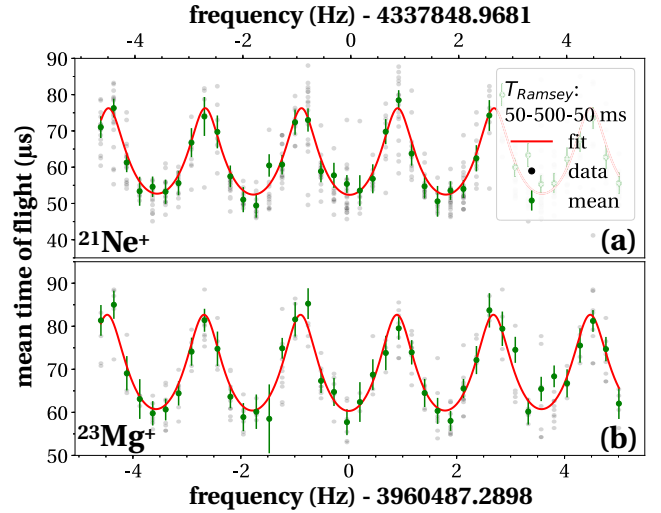


FIG. 3. Typical Ramsey-type ion-cyclotron resonances, here shown for $^{21}\text{Ne}^+$ and for $^{23}\text{Mg}^+$ after a total of 600 ms measurement time (Ramsey pattern: 50-500-50 ms) in ISOLTRAP’s precision Penning trap. For each frequency bin, the mean of the recorded, unbinned time-of-flight distribution (black) and its associated standard deviation is depicted in green. The red line represents a least squares fit to the expected line shape [37].

voltage, and transport parameters from the preparation trap to the precision trap were varied consistently for both the reference and IOI. With respect to these changes, no statistically significant deviation was observed. Finally, comparison spectra were taken using the well-established single-pulse ToF-ICR technique. A typical Ramsey-type ToF-ICR spectra for $^{21}\text{Ne}^+$ and $^{23}\text{Mg}^+$ at an excitation time of 50 ms per pulse and a waiting time of 500 ms is shown in Fig. 3.

The time-of-flight spectra were fitted using the well-established analysis software EVA [38] while cross checking additionally selected spectra with a customized analysis software based on ROOT [39]. During the evaluation of the data, the impact of varying the time-of-flight-selection window was systematically investigated. It was found to be well below the statistical uncertainty of the measurement, which can be explained by the purity of the spectra (see Fig. 2). Therefore, the window was kept the same for all measurements. A z -class analysis [38], i.e., an evaluation of the data with respect to the number of ions inside the Penning trap for a given measurement cycle, could not be performed due to the intentionally low count rate of about one ion per cycle. Three independent analyses of the whole dataset following

the procedure described in Ref. [38] were carried out in order to confirm the robustness of the result with respect to the subjective choices made by the evaluators.

From alternating cyclotron-frequency measurements between the IOI and the reference nucleus, one can determine the ratio

$$r = \frac{\nu_{c,\text{ref}}}{\nu_{c,\text{IOI}}} \quad (3)$$

in order to eliminate systematic uncertainties, e.g., coming from temporal variations of the magnetic field B . The well-established calculation procedure uses a linearly interpolated $\nu_{c,\text{ref}}$ between the two closest measured cyclotron frequencies of the reference ion at the time of the measurement of the IOI. The final ratio value is then calculated as the weighted mean of all individual ratios. In the case of the present measurement series, the reference isotope is the daughter nucleus of the corresponding β decay and the ion of interest is the mother nucleus. This allows direct determination of the Q_{EC} value from the frequency ratio r while minimizing systematic uncertainties:

$$Q_{\text{EC}} = (r - 1)(m_{\text{ref,lit}} - m_e)c^2, \quad (4)$$

with the literature mass for the reference atom $m_{\text{ref,lit}}$, the electron mass m_e [40], and the speed of light c .

In addition, the fitting technique described in Ref. [41] which uses a polynomial fit to simultaneously model the temporal evolution of the cyclotron frequency measurements of the mother and daughter nucleus was used. The result of this fit is shown in Fig. 4, where a fifth-order polynomial function was fitted to a subset of measured cyclotron frequencies for both decay partners of mass $A = 21$. The proportionality factor between the fit functions represents the cyclotron-frequency ratio for the whole measurement series between the two masses. Therefore, the fluctuations of the measured cyclotron frequencies $\nu_i(t)$ can be described with a polynomial function $f(t)$ and the frequency ratio of Eq. (3):

$$\nu_{\text{IOI}}(t) = f(t) \quad (5)$$

$$\nu_{\text{ref}}(t) = r\nu_{\text{IOI}} = rf(t). \quad (6)$$

The degree of the polynomial function describes the dominant effects leading to a change in cyclotron frequency over time. For the presented data, it is determined using the degree of the continuously measured magnet's bore temperature fluctuation during the measurement time. The final ratios are calculated as the weighted mean of the fitted subsets. In addition, correlations between fit parameters were calculated and found to be insignificant.

The polynomial fitting technique and the linear interpolation analysis techniques agree well within one combined σ . Following the description in Ref. [38], the mass-dependent effect, the ion production process, the magnetic-field drift, and ISOLTRAP's absolute residual systematic uncertainty were considered. The mass-dependent effect of isobars in this mass range is more than one order of magnitude smaller than the statistical uncertainty and is thus negligible. For each pair, the production process and the experimental conditions were kept constant to avoid any systematic effects. Furthermore, the magnetic-field drift is taken into account by the polynomial

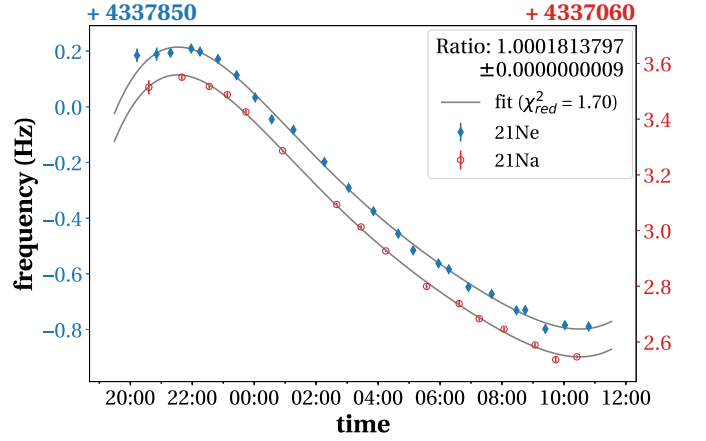


FIG. 4. Cyclotron-frequency-ratio determination using a simultaneous polynomial fit for a subset of measured cyclotron frequencies (including error bars) of $^{21}\text{Ne}^+$ and $^{21}\text{Na}^+$.

fitting. The results of the data analysis are summarized in Table I. In the case of the $^{21}\text{Na} \rightarrow ^{21}\text{Ne}$ transition, a 2.3σ deviation from the literature Q_{EC} value, which is dominated by the value reported in Ref. [16], was found.

III. DISCUSSION

With the measured Q_{EC} value, one can calculate the mirror-nuclei $\mathcal{F}t^{\text{mirror}}$ value

$$\mathcal{F}t^{\text{mirror}} = f_V t (1 + \delta'_R) (1 + \delta_{\text{NS}}^V - \delta_C^V) \quad (7)$$

using the nucleus-dependent radiative corrections, δ'_R and δ_{NS}^V , and the isospin-symmetry-breaking correction δ_C^V calculated in Ref. [53]. The vector parts of the statistical-rate functions f_V were calculated using our new Q_{EC} values and the formalism described in Ref. [42]. The corrected mirror-nuclei $\mathcal{F}t_0^{\text{mirror}}$ value can then be calculated according to the relation

$$\mathcal{F}t_0^{\text{mirror}} = \mathcal{F}t^{\text{mirror}} \left(1 + \frac{f_A}{f_V} \rho^2 \right), \quad (8)$$

where ρ is the Fermi and Gamow-Teller mixing ratio while f_A/f_V is the ratio of the axial to vector statistical rate functions. The latter was calculated using the formalism of Ref. [42] and the results of shell model calculations performed with “universal” sd (USDB) interaction (in a full sd valence space) and the β -spectrum generator (BSG) nuclear shell-model code [43].

For the $^{21}\text{Na} \rightarrow ^{21}\text{Ne}$ transition the Fermi–Gamow-Teller mixing ratio $\rho = -0.714(7)$ was calculated according to

$$\rho = \pm \frac{\sqrt{3 - 3a_{\text{SM}}}}{\sqrt{1 + 3a_{\text{SM}}}}, \quad (9)$$

using the β -neutrino asymmetry coefficient a_{SM} from Ref. [44]. The sign of ρ can be derived from the aforementioned shell-model calculations. For ^{23}Mg , there has not yet been a measurement which allows the calculation of

TABLE II. Calculated vector part of the statistical-rate function f_V , mirror-nuclei $\mathcal{F}t^{\text{mirror}}$ value, and V_{ud} element of the CKM matrix for ^{21}Na and ^{23}Mg . For details, see text.

Isotope	f_V	f_A/f_V	$\mathcal{F}t^{\text{mirror}}$ (s)	V_{ud}
^{21}Na	170.710(6)	1.0170(17)	4071(4)	0.9715(34)
^{23}Mg	378.51(2)	1.0195(20)	4724(14)	N/A

ρ . The partial half-lives t

$$t = t_{1/2} \left(\frac{1 + P_{EC}}{BR} \right) \quad (10)$$

were calculated using the half-lives $t_{1/2}$ and branching ratios BR given in Refs. [45–47] and in Ref. [53] for ^{21}Na and ^{23}Mg , respectively. For both transitions, the correction for the competing electron-capture process P_{EC} was taken from Ref. [53].

The V_{ud} element of the CKM matrix

$$V_{ud} = \sqrt{\frac{K}{\mathcal{F}t_0^{\text{mirror}} G_F^2 C_V^2 (1 + \Delta_R^V)}} \quad (11)$$

can finally be calculated using $K/(\hbar c)^6 = 2\pi^3 \ln(2) \hbar (m_e c^2)^{-5} = 8120.276(5) \times 10^{10} \text{ GeV}^4 \text{ s}$, the fundamental weak interaction coupling constant $G_F/(\hbar c)^3 = 1.16639(1) \times 10^5 \text{ GeV}^2$, the conserved vector current (CVC) constant $C_V = 1$ (assuming that the CVC hypothesis is correct; see, e.g., Ref. [1]), and the transition-independent correction $\Delta_R^V = 0.02361(38)^1$ [53]. The results are summarized in Table II. In Fig. 5, a comparison with five other transitions for which a V_{ud} value can be experimentally determined is presented. A comparison between the average V_{ud} value extracted from these mixed Fermi–Gamow-Teller transitions and that extracted using the superallowed transitions [48] is also shown in Fig. 5.

The weighted mean of the V_{ud} values for all displayed mirror-nuclei transitions results to $\bar{V}_{ud} = 0.9727(14)$, which is about seven times less precise than the $\bar{V}_{ud} = 0.97420(21)$ [48] of the superallowed transitions. Even though we improved the precision on the Q_{EC} value for the $^{21}\text{Na} \rightarrow ^{21}\text{Ne}$ transition by a factor of 5, we did not significantly improve the uncertainty on the V_{ud} value for this transition.

Figure 6 presents the relative uncertainties attributed to each experimental and theoretical input factor that contributes

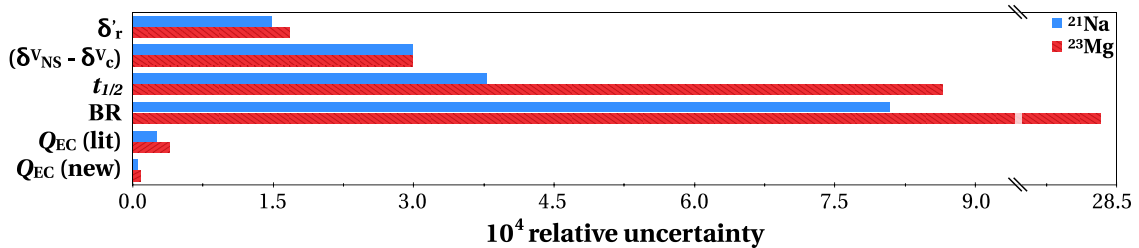


FIG. 6. Comparison of the relative uncertainty contributions to the $\mathcal{F}t^{\text{mirror}}$ value: the nucleus-dependent radiative corrections, δ'_r , and $\delta^{V_{NS}}$, the isospin-symmetry-breaking corrections δ^{V_C} , the half-lives, the branching ratios BR, and the Q_{EC} values from Ref. [16] for ^{21}Na (blue), from Ref. [15] for ^{23}Mg (red), as well as from this work. For details, see text.

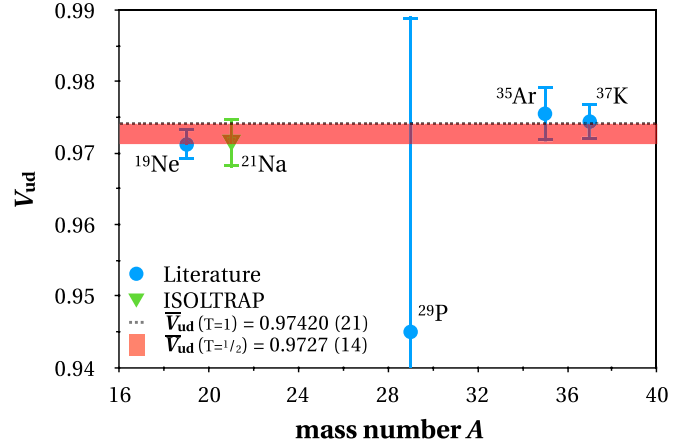


FIG. 5. Comparison between different mirror-nuclei V_{ud} values: ^{19}Ne [49], ^{29}P [16], ^{35}Ar [9], ^{37}K [13] (blue), our new value for ^{21}Na (green), the weighted mean V_{ud} value of all values (red = two σ band), and the mean V_{ud} value for the superallowed transitions [48] (gray = two σ band).

to the final $\mathcal{F}t^{\text{mirror}}$ values. Our new measurements of the ^{21}Na and ^{23}Mg Q_{EC} values have such a small relative uncertainty that they do not contribute much to a reduction of the final uncertainty of the $\mathcal{F}t^{\text{mirror}}$ values and therefore of the V_{ud} value that can be extracted for ^{21}Na . As a result, our measurements reinforce the motivation for the other experimental quantities, in particular the branching ratios BR and the half-lives $t_{1/2}$, to be measured with significantly improved precision. Furthermore, in the case of ^{23}Mg , a β -asymmetry or β -neutrino correlation measurement would allow the calculation of an additional mirror-nuclei V_{ud} value.

IV. CONCLUSION AND OUTLOOK

This publication presented high-precision Q_{EC} values of the $^{21}\text{Na} \rightarrow ^{21}\text{Ne}$ and $^{23}\text{Mg} \rightarrow ^{23}\text{Na}$ mirror β transitions with ISOLTRAP at the CERN ISOLDE facility. Precisions of $\delta m/m = 9 \times 10^{-10}$ and $\delta m/m = 1.5 \times 10^{-9}$ were reached for the masses of ^{21}Na and ^{23}Mg , respectively. We reduced the uncertainty of the Q_{EC} values by a factor of 5, making them the most precise experimental input data for the calculation of the corrected $\mathcal{F}t$ value of these mixed Fermi and Gamow-Teller transitions and strongly reinforces the motivation for

improved measurements of the branching ratios BR and the half-lives $t_{1/2}$.

Yet lower uncertainties on Q_{EC} values are now reachable with the recently implemented phase-imaging ion-cyclotron-resonance technique [50], which has already been applied to the case of $^{163}\text{Ho} \rightarrow ^{163}\text{Dy}$ [51].

Note added. Recently, a new transition-independent correction value was published [52]. However, since this value has shifted significantly from previous values and since additionally it is breaking the CKM unitarity, we decided to use the one from Ref. [53].

ACKNOWLEDGMENTS

We thank the ISOLDE technical group and the ISOLDE Collaboration for their professional assistance. We acknowledge support by the Max Planck Society, the German Federal Ministry of Education and Research (BMBF) (Grants No. 05P12HGCI1, No. 05P12HGFNE, and No. 05P15ODCIA), the French IN2P3, the Flemish FWO, and the European Union's Horizon 2020 research and innovation programme (Grant No. 654002). Jonas Karthein acknowledges support by a Wolfgang Gentner Ph.D. scholarship from the BMBF (Grant No. 05E12CHA).

-
- [1] J. C. Hardy and I. S. Towner, *Phys. Rev. C* **91**, 025501 (2015).
- [2] R. P. Feynman and M. Gell-Mann, *Phys. Rev.* **109**, 193 (1958).
- [3] M. Tanabashi *et al.* (Particle Data Group), *Phys. Rev. D* **98**, 030001 (2018).
- [4] K. K. Vos, H. W. Wilschut, and R. G. E. Timmermans, *Rev. Mod. Phys.* **87**, 1483 (2015).
- [5] M. González-Alonso, O. Naviliat-Cuncic, and N. Severijns, *Prog. Part. Nucl. Phys.* **104**, 165 (2019).
- [6] A. Czarnecki, W. J. Marciano, and A. Sirlin, *Phys. Rev. Lett.* **120**, 202002 (2018).
- [7] W. J. Marciano and A. Sirlin, *Phys. Rev. Lett.* **96**, 032002 (2006).
- [8] M. A.-P. Brown, E. B. Dees, E. Adamek, B. Allgeier, M. Blatnik, T. J. Bowles, L. J. Broussard, R. Carr, S. Clayton, C. Cude-Woods, S. Currie, X. Ding, B. W. Filippone, A. García, P. Geltenbort, S. Hasan, K. P. Hickerson, J. Hoagland, R. Hong, G. E. Hogan, A. T. Holley, T. M. Ito, A. Knecht, C.-Y. Liu, J. Liu, M. Makela, J. W. Martin, D. Melconian, M. P. Mendenhall, S. D. Moore, C. L. Morris, S. Nepal, N. Nouri, R. W. Pattie, A. Pérez Galván, D. G. Phillips, R. Picker, M. L. Pitt, B. Plaster, J. C. Ramsey, R. Rios, D. J. Salvat, A. Saunders, W. Sondheim, S. J. Seestrom, S. Sjue, S. Slutsky, X. Sun, C. Swank, G. Swift, E. Tatar, R. B. Vogelaar, B. Vorn Dick, Z. Wang, J. Wexler, T. Womack, C. Wrede, A. R. Young, and B. A. Zeck (UCNA Collaboration), *Phys. Rev. C* **97**, 035505 (2018).
- [9] O. Naviliat-Cuncic and N. Severijns, *Phys. Rev. Lett.* **102**, 142302 (2009).
- [10] I. S. Towner and J. C. Hardy, *Phys. Rev. C* **82**, 065501 (2010).
- [11] N. Severijns and O. Naviliat-Cuncic, *Phys. Scr.* **2013**, 014018 (2013).
- [12] F. P. Calaprice, S. J. Freedman, W. C. Mead, and H. C. Vantine, *Phys. Rev. Lett.* **35**, 1566 (1975).
- [13] B. Fenker, A. Gorelov, D. Melconian, J. A. Behr, M. Anholm, D. Ashery, R. S. Behling, I. Cohen, I. Craiciu, G. Gwinner, J. McNeil, M. Mehlman, K. Olchanski, P. D. Shidling, S. Smale, and C. L. Warner, *Phys. Rev. Lett.* **120**, 062502 (2018).
- [14] M. Breitenfeldt and N. Severijns, Q values of mirror transitions for fundamental interaction studies, Technical Report No. CERN-INTC-2013-003, INTC-P-369, CERN, Geneva, Switzerland, 2013.
- [15] B. E. Schultz, M. Brodeur, C. Andreoiu, A. Bader, A. Chaudhuri, U. Chowdhury, A. T. Gallant, A. Grossheim, R. Klawitter, A. A. Kwiatkowski, K. G. Leach, A. Lennarz, T. D. Macdonald, J. Lassen, H. Heggen, S. Raeder, A. Teigelhöfer, and J. Dilling, *Phys. Rev. C* **90**, 012501(R) (2014).
- [16] M. Eibach, G. Bollen, M. Brodeur, K. Cooper, K. Gulyuz, C. Izzo, D. J. Morrissey, M. Redshaw, R. Ringle, R. Sandler, S. Schwarz, C. S. Sumithrarachchi, A. A. Valverde, and A. C. C. Villari, *Phys. Rev. C* **92**, 045502 (2015).
- [17] M. J. G. Borge and K. Blaum, *J. Phys. G: Nucl. Part. Phys.* **45**, 010301 (2018).
- [18] E. Hagebø, P. Hoff, O. Jonsson, E. Kugler, J. Omtvedt, H. Ravn, and K. Steffensen, *Nucl. Instrum. Methods Phys. Res., Sect. B* **70**, 165 (1992).
- [19] R. Kirchner and E. Roeckl, *Nucl. Instrum. Methods* **139**, 291 (1976).
- [20] Y. Martinez Palenzuela, B. A. Marsh, J. Ballof, R. Catherall, K. Chrysalidis, T. E. Cocolios, B. Crepieux, T. Day Goodacre, V. N. Fedosseev, M. H. Huysse, P. B. Larmonier, J. P. Ramos, S. Rothe, J. D. Smith, T. Stora, P. Van Duppen, and S. Wilkins, *Nucl. Instrum. Methods Phys. Res., Sect. B* **431**, 59 (2018).
- [21] V. Fedosseev, K. Chrysalidis, T. D. Goodacre, B. Marsh, S. Rothe, C. Seiffert, and K. Wendt, *J. Phys. G: Nucl. Part. Phys.* **44**, 084006 (2017).
- [22] T. Day Goodacre, J. Billowes, R. Catherall, T. Cocolios, B. Crepieux, D. Fedorov, V. Fedosseev, L. Gaffney, T. Giles, A. Gottberg, K. Lynch, B. Marsh, T. Mendonça, J. Ramos, R. Rossel, S. Rothe, S. Sels, C. Sotty, T. Stora, C. Van Beveren, and M. Veinhard, *Nucl. Instrum. Methods Phys. Res., Sect. B* **376**, 39 (2016).
- [23] M. Mukherjee, D. Beck, K. Blaum, G. Bollen, J. Dilling, S. George, F. Herfurth, A. Herlert, A. Kellerbauer, H. J. Kluge, S. Schwarz, L. Schweikhard, and C. Yazidjian, *Eur. Phys. J. A* **35**, 1 (2008).
- [24] D. Lunney (ISOLTRAP collaboration), *J. Phys. G: Nucl. Part. Phys.* **44**, 064008 (2017).
- [25] S. Kreim, D. Atanasov, D. Beck, K. Blaum, C. Böhm, C. Borgmann, M. Breitenfeldt, T. Cocolios, D. Fink, S. George, A. Herlert, A. Kellerbauer, U. Köster, M. Kowalska, D. Lunney, V. Manea, E. Minaya Ramirez, S. Naimi, D. Neidherr, T. Nicol, R. Rossel, M. Rosenbusch, L. Schweikhard, J. Stanja, F. Wienholtz, R. Wolf, and K. Zuber, *Nucl. Instrum. Methods Phys. Res., Sect. B* **317**, 492 (2013).
- [26] F. Herfurth, J. Dilling, A. Kellerbauer, G. Bollen, S. Henry, H.-J. Kluge, E. Lamour, D. Lunney, R. Moore, C. Scheidenberger, S. Schwarz, G. Sikler, and J. Szerypo, *Nucl. Instrum. Methods Phys. Res., Sect. A* **469**, 254 (2001).
- [27] R. Wolf, M. Eritt, G. Marx, and L. Schweikhard, *Hyperfine Interact.* **199**, 115 (2011).
- [28] R. Wolf, F. Wienholtz, D. Atanasov, D. Beck, K. Blaum, C. Borgmann, F. Herfurth, M. Kowalska, S. Kreim, Y. A.

- Litvinov, D. Lunney, V. Manea, D. Neidherr, M. Rosenbusch, L. Schweikhard, J. Stanja, and K. Zuber, *Int. J. Mass Spectrom.* **349–350**, 123 (2013).
- [29] R. Wolf, G. Marx, M. Rosenbusch, and L. Schweikhard, *Int. J. Mass Spectrom.* **313**, 8 (2012).
- [30] R. Wolf, D. Beck, K. Blaum, C. Böhm, C. Borgmann, M. Breitenfeldt, F. Herfurth, A. Herlert, M. Kowalska, S. Kreim, D. Lunney, S. Naimi, D. Neidherr, M. Rosenbusch, L. Schweikhard, J. Stanja, F. Wienholtz, and K. Zuber, *Nucl. Instrum. Methods Phys. Res., Sect. A* **686**, 82 (2012).
- [31] F. Wienholtz, S. Kreim, M. Rosenbusch, L. Schweikhard, and R. Wolf, *Int. J. Mass Spectrom.* **421**, 285 (2017).
- [32] G. Savard, S. Becker, G. Bollen, H.-J. Kluge, R. Moore, T. Otto, L. Schweikhard, H. Stolzenberg, and U. Wiess, *Phys. Lett. A* **158**, 247 (1991).
- [33] G. Gräff, H. Kalinowsky, and J. Traut, *Z. Phys. A* **297**, 35 (1980).
- [34] M. Kretzschmar, in *Trapped Charged Particles and Fundamental Physics*, edited by D. H. E. Dubin, AIP Conf. Proc. No. 457 (American Institute of Physics, New York, 1999), pp. 242–251.
- [35] S. George, S. Baruah, B. Blank, K. Blaum, M. Breitenfeldt, U. Hager, F. Herfurth, A. Herlert, A. Kellerbauer, H.-J. Kluge, M. Kretzschmar, D. Lunney, R. Savreux, S. Schwarz, L. Schweikhard, and C. Yazidjian, *Phys. Rev. Lett.* **98**, 162501 (2007).
- [36] G. Audi, F. G. Kondev, M. Wang, W. Huang, and S. Naimi, *Chin. Phys. C* **41**, 030001 (2017).
- [37] M. König, G. Bollen, H.-J. Kluge, T. Otto, and J. Szerypo, *Int. J. Mass Spectrom. Ion Phys.* **142**, 95 (1995).
- [38] A. Kellerbauer, K. Blaum, G. Bollen, F. Herfurth, H.-J. Kluge, M. Kuckein, E. Sauvan, C. Scheidenberger, and L. Schweikhard, *Eur. Phys. J. D* **22**, 53 (2003).
- [39] I. Antcheva, M. Ballintijn, B. Bellenot, M. Biskup, R. Brun, N. Buncic, P. Canal, D. Casadei, O. Couet, V. Fine, L. Franco, G. Ganis, A. Gheata, D. G. Maline, M. Goto, J. Iwaszkiewicz, A. Kreshuk, D. M. Segura, R. Maunder, L. Moneta, A. Naumann, E. Offermann, V. Onuchin, S. Panacek, F. Rademakers, P. Russo, and M. Tadel, *Comput. Phys. Commun.* **180**, 2499 (2009).
- [40] S. Sturm, F. Köhler, J. Zatorski, A. Wagner, Z. Harman, G. Werth, W. Quint, C. H. Keitel, and K. Blaum, *Nature (London)* **506**, 467 (2014).
- [41] D. Fink, J. Barea, D. Beck, K. Blaum, C. Böhm, C. Borgmann, M. Breitenfeldt, F. Herfurth, A. Herlert, J. Kotila, M. Kowalska, S. Kreim, D. Lunney, S. Naimi, M. Rosenbusch, S. Schwarz, L. Schweikhard, F. Šimkovic, J. Stanja, and K. Zuber, *Phys. Rev. Lett.* **108**, 062502 (2012).
- [42] L. Hayen, N. Severijns, K. Bodek, D. Rozpedzik, and X. Mougeot, *Rev. Mod. Phys.* **90**, 015008 (2018).
- [43] L. Hayen and N. Severijns, *Comp. Phys. Comm.* **240**, 152 (2019).
- [44] P. A. Vetter, J. R. Abo-Shaer, S. J. Freedman, and R. Maruyama, *Phys. Rev. C* **77**, 035502 (2008).
- [45] P. D. Shidling, R. S. Behling, B. Fenker, J. C. Hardy, V. E. Jacob, M. Mehlman, H. I. Park, B. T. Roeder, and D. Melconian, *Phys. Rev. C* **98**, 015502 (2018).
- [46] J. Grinyer, G. F. Grinyer, M. Babo, H. Bouzomita, P. Chauveau, P. Delahaye, M. Dubois, R. Frigot, P. Jardin, C. Leboucher, L. Maunoury, C. Seiffert, J. C. Thomas, and E. Traykov, *Phys. Rev. C* **91**, 032501(R) (2015).
- [47] P. Finlay, A. T. Laffoley, G. C. Ball, P. C. Bender, M. R. Dunlop, R. Dunlop, G. Hackman, J. R. Leslie, A. D. MacLean, D. Miller, M. Moukaddam, B. Olaizola, N. Severijns, J. K. Smith, D. Southall, and C. E. Svensson, *Phys. Rev. C* **96**, 025501 (2017).
- [48] J. C. Hardy and I. S. Towner, [arXiv:1807.01146v1](https://arxiv.org/abs/1807.01146v1).
- [49] L. J. Broussard, H. O. Back, M. S. Boswell, A. S. Crowell, P. Dendooven, G. S. Giri, C. R. Howell, M. F. Kidd, K. Jungmann, W. L. Kruithof, A. Mol, C. J. G. Onderwater, R. W. Pattie, P. D. Shidling, M. Sohani, D. J. van der Hoek, A. Rogachevskiy, E. Traykov, O. O. Versolato, L. Willmann, H. W. Wilschut, and A. R. Young, *Phys. Rev. Lett.* **112**, 212301 (2014).
- [50] S. Eliseev, K. Blaum, M. Block, A. Dörr, C. Droese, T. Eronen, M. Goncharov, M. Höcker, J. Ketter, E. M. Ramirez, D. A. Nesterenko, Y. N. Novikov, and L. Schweikhard, *Appl. Phys. B* **114**, 107 (2014).
- [51] S. Eliseev, K. Blaum, M. Block, S. Chenmarev, H. Dorrer, C. E. Düllmann, C. Enss, P. E. Filianin, L. Gastaldo, M. Goncharov, U. Köster, F. Lautenschläger, Y. N. Novikov, A. Rischka, R. X. Schüssler, L. Schweikhard, and A. Türler, *Phys. Rev. Lett.* **115**, 062501 (2015).
- [52] C.-Y. Seng, M. Gorchtein, H. H. Patel, and M. J. Ramsey-Musolf, *Phys. Rev. Lett.* **121**, 241804 (2018).
- [53] N. Severijns, M. Tandecki, T. Phalet, and I. S. Towner, *Phys. Rev. C* **78**, 055501 (2008).

3.2 Publication 2: Neutrino Mass

Authors:

Jonas Karthein, Dinko Atanasov, Klaus Blaum, Sergey Eliseev, Pavel Filianin, David Lunney, Vladimir Manea, Maxime Mougeot, Dennis Neidherr, Yuri Novikov, Lutz Schweikhard, Andree Welker, Frank Wienholtz, Kai Zuber

Publication status:

Published 12 June 2019

Journal reference:

Karthein, J. et al. *Hyperfine Interact.* **240**, 61 (2019).

Digital object identifier:

10.1007/s10751-019-1601-z

Authors' contributions:

DA, KB, SE, PF, DL, VM, DN, YN, LS, AW, FW, and KZ were involved in the proposal for the experiment. JK, DA, KB, SE, DL, VM, MM, DN, YN, LS, AW, FW, and KZ were involved in the letter of intent for the experiment. JK, DA, SE, VM, MM, and FW carried out the experiment. JK performed the first and final analysis with second analyses by VM. JK performed the theoretical calculations. JK, KB, PF, DL, VM, MM, and LS were involved in the discussion of the results. JK wrote the first draft of the article and prepared all figures. The manuscript was then reviewed critically before and after submission by all authors.

Abstract:

A high-precision measurement of the $^{131}\text{Cs} \rightarrow ^{131}\text{Xe}$ ground-to-ground-state electron-capture Q_{EC} -value was performed using the ISOLTRAP mass spectrometer at ISOLDE/CERN. The novel PI-ICR technique allowed to reach a relative mass precision $\delta m/m = 1.4 \times 10^{-9}$. A mass resolving power $m/\Delta m$ exceeding 1×10^7 was obtained in only 1 s trapping time. Allowed electron-capture transitions with sub-keV or lower decay energies are of high interest for the direct determination of the ν_e mass. The new measurement improves the uncertainty on the ground-to-ground-state Q_{EC} -value by a factor 25 precluding the $^{131}\text{Cs} \rightarrow ^{131}\text{Xe}$ pair as a feasible candidate for the direct determination of the ν_e mass.

Direct decay-energy measurement as a route to the neutrino mass

J. Karthein · D. Atanasov* · K. Blaum ·
S. Eliseev · P. Filianin · D. Lunney ·
V. Manea* · M. Mougeot† · D. Neidherr ·
Y. Novikov · L. Schweikhard · A. Welker ·
F. Wienholtz · K. Zuber

Received: January 29, 2019 / Accepted: May 14, 2019

Abstract A high-precision measurement of the $^{131}\text{Cs} \rightarrow ^{131}\text{Xe}$ ground-to-ground-state electron-capture Q_{EC} -value was performed using the ISOLTRAP mass spectrometer at ISOLDE/CERN. The novel PI-ICR technique allowed to reach a relative mass precision $\delta m/m$ of $1.4 \cdot 10^{-9}$. A mass resolving power $m/\Delta m$ exceeding $1 \cdot 10^7$ was obtained in only 1 s trapping time. Allowed electron-capture transitions with sub-keV or lower decay energies are of high interest for the direct determination of the ν_e mass. The new measurement improves the uncertainty on the ground-to-ground-state Q_{EC} -value by a factor 25 precluding the $^{131}\text{Cs} \rightarrow ^{131}\text{Xe}$ pair as a feasible candidate for the direct determination of the ν_e mass.

Keywords PI-ICR · β -decay · neutrino mass · high-precision mass spectrometry

* Current address: KU Leuven, Instituut voor Kern- & Stralingsfysica, 3001 Leuven, Belgium

† Current address: Max-Planck-Institut für Kernphysik, 69117 Heidelberg, Germany

This article contains data from the Ph.D thesis work of Jonas Karthein, enrolled at Heidelberg University, Germany. Corresponding author: jonas.karthein@cern.ch

J. Karthein · V. Manea · A. Welker · F. Wienholtz
CERN, Route de Meyrin, 1211 Genève, Switzerland

J. Karthein · K. Blaum · S. Eliseev · P. Filianin
Max-Planck-Institut für Kernphysik, 69117 Heidelberg, Germany

D. Atanasov · A. Welker · K. Zuber
Technische Universität Dresden, 01062 Dresden, Germany

D. Lunney · M. Mougeot
CSNSM-IN2P3-CNRS, Université Paris-Sud, 91400 Orsay, France

D. Neidherr
GSI Helmholtzzentrum für Schwerionenforschung, 64291 Darmstadt, Germany

Y. Novikov
Department of Physics, St Petersburg State University, St Petersburg 198504, Russia

Y. Novikov
Petersburg Nuclear Physics Institute, 188300 St Petersburg, Russia

L. Schweikhard · F. Wienholtz
Physikalisches Institut, Universität Greifswald, 17489 Greifswald, Germany

1 Introduction

The determination of the neutrino rest mass is of broad interest not only in nuclear physics but also in the fields of particle and astrophysics. On the most fundamental level, the existence of a non-zero neutrino mass is not explained by the standard model. However, abundant experimental evidence by the observation of neutrino oscillations has been found in the last decades, which requires a neutrino mass and mixing. Hence, a detailed study of different neutrino properties and interactions evolved as a powerful tool in the search for the fundamental theory beyond the standard model. [1, 2] A very feasible approach for the determination of the electron-neutrino mass lies in the investigation of electron-capture (EC) reactions with energies of a few keV or lower. Here, the only particle emitted is the neutrino itself. Therefore, the smaller the decay energy of these transitions, the higher the sensitivity to the neutrino rest mass. Such transitions are found in allowed EC-transitions to excited nuclear states in the daughter nucleus.

Electron and nuclear excitation energies are typically known to sub-keV precision. Unfortunately, the ground state masses of the decay pairs are, in most cases, known with uncertainties well above 1 keV and thus constitute the main contribution to the uncertainty of decay energies. Presently, only Penning-trap mass spectrometry (PTMS) is capable of providing mass measurements with sub-keV uncertainties. In recent years, a combination of PTMS and cryogenic microcalorimetry (MMC) [3] has proven to be a very successful combination for investigating the β^- -decay in ^{187}Re and the electron capture in ^{163}Ho [4]. Several other transitions have been subsequently suggested as possible candidates for neutrino physics research - the electron-capture of ^{131}Cs to the $E^* = 364.490(4)$ keV [5] excited state in ^{131}Xe being one example.

2 Experiment and analysis

The measurement was performed with the high-precision Penning-trap mass spectrometer ISOLTRAP [6, 7, 8] located at CERN's radioactive ion beam facility ISOLDE [9]. There, isotopes are produced in nuclear reactions in a thick target, induced by a 1.4 GeV proton beam. In the present case a uranium-carbide target was used. After surface ionization, the beam was accelerated to 50 keV, magnetically separated for the ion of interest in ISOLDE's HRS separator and transported to the ISOLTRAP setup.

The ISOLTRAP apparatus, depicted in Fig. 1, consists of a sequence of four ion traps. The continuous $^{131}\text{Cs}^+$ beam from ISOLDE, as well as the $^{133}\text{Cs}^+$ beam from ISOLTRAP's offline alkali ion source in the case of reference mass, is first accumulated in a radio-frequency quadrupole (RFQ) trap [10], where it is cooled and bunched for 10 ms using ultra-pure helium gas. Isobaric separation is subsequently performed using ISOLTRAP's multi-reflection time-of-flight (MR-ToF) device [11], in which trapped ions are reflected back and forth in order to extend their flight path to ~ 1 km (~ 28 ms). Not only has this device shown numerous times its suitability for the measurement of short-lived isotopes produced in min-

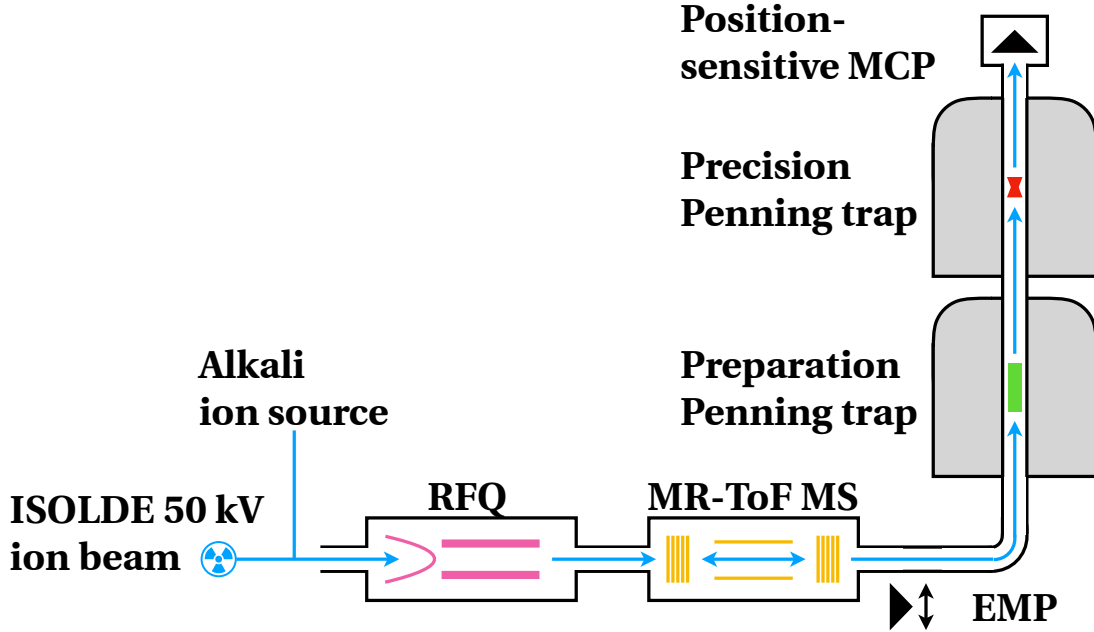


Fig. 1 Schematic overview of the ISOLTRAP mass spectrometer. Radioactive ion beams provided by ISOLDE or an offline alkali ion source at an energy of 50 keV are delivered. Inside the ISOLTRAP apparatus the beam is processed by a sequence of traps: a radio-frequency quadrupole (RFQ) cooler and buncher (pink), a multi-reflection time-of-flight (MR-ToF) mass separator/spectrometer (yellow), a preparation Penning trap (green) and a precision Penning trap (red). Furthermore, an electron multiplier (EMP) particle detector for ToF detection and a position-sensitive multi-channel plate (MCP) particle detector for position and ToF detection are shown. For further details, see text.

utes quantities [12, 13] but it has also proved itself to be a perfectly suitable tool for mass purification [14]. More specifically, in this experiment a mass resolving power $R = m/\Delta m = t/(2 \cdot \Delta t)$ (where t is the mean of the time-of-flight distribution and Δt its full width at half maximum) in excess of $1.1 \cdot 10^5$ was achieved. The purified beam is then transported to the helium buffer-gas-filled preparation Penning trap for further cooling and purification following the well-established mass-selective centering technique [15]. Ultimately, the ions arrive in the precision Penning trap where high-precision mass determination is accomplished by measuring the ion's cyclotron frequency ν_c

$$\nu_c = \frac{1}{2\pi} \cdot \frac{q_i}{m_i} \cdot B \quad (1)$$

with the charge-to-mass ratio q_i/m_i and the magnetic field strength B . All detection techniques currently available at the ISOLTRAP setup - namely the single pulse time-of-flight ion-cyclotron-resonance (ToF-ICR) mass spectrometry (MS) [16], the two-pulse Ramsey-type ToF-ICR MS [17] and the recently developed phase-imaging ion-cyclotron-resonance (PI-ICR) MS [18, 19] - were all used in the presented experiment.

In both ToF-ICR techniques an excitation frequency is scanned, i.e. the excitation frequency is varied from one experimental cycle to the next, and the ion's time of flight (ToF) to a multi-channel plate detector after ejection from the trap is measured. This ToF has a minimum at the cyclotron frequency. A typical Ramsey-type ToF-ICR scan for $^{131}\text{Cs}^+$ is shown in Fig. 2 for an excitation time of 100 ms per

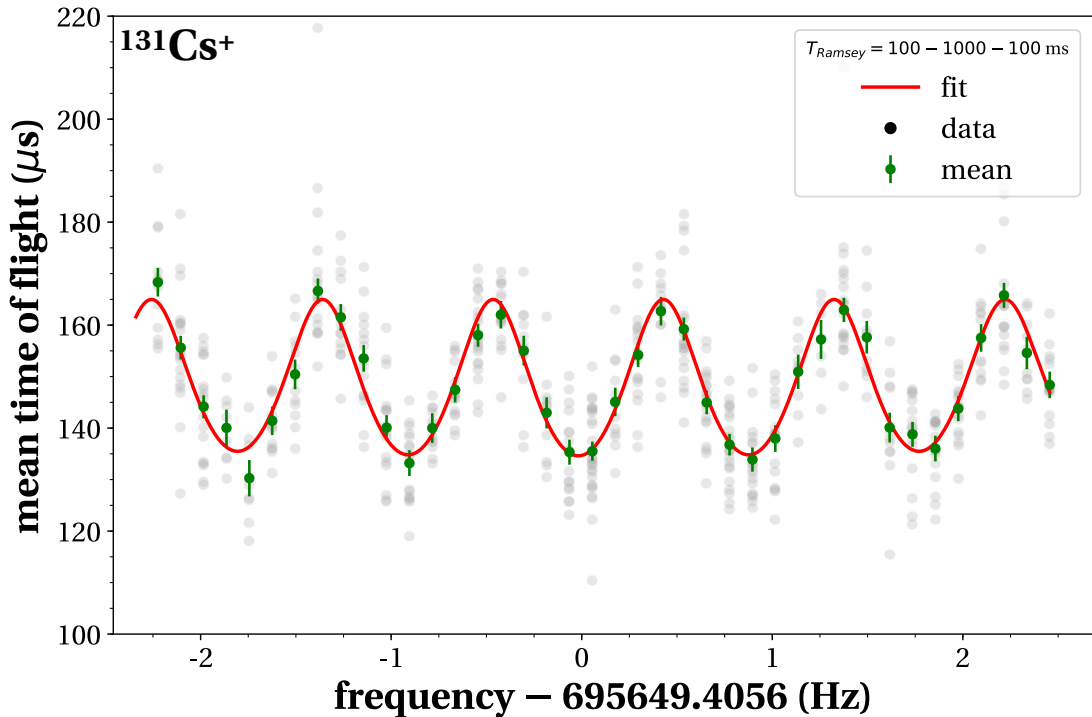


Fig. 2 Typical Ramsey-type ToF-ICR spectrum of $^{131}\text{Cs}^+$ with an excitation time of 100 ms per pulse and 1000 ms waiting time. Individual, repeated ToF measurements are shown in black without any analysis cuts, thus demonstrating the purity of the beam injected inside the precision Penning trap. The mean of the unbinned ToF distribution per scan step with its standard deviation as error bar and the fitted theoretical line shape are represented in green and red respectively [16]. For further details, see text.

pulse and a "waiting time" of 1000 ms between the pulses. There, the individual, repeated ToF measurements per scan step is shown in black. The green data points represent the mean of the unbinned ToF distribution per scan step with its standard deviation as error bar. The red line represents a least squares fit of the theoretical line shape to the mean ToF distributions [16].

In addition to the well-established ToF-ICR techniques, the new non-scanning approach to PTMS, namely PI-ICR, has been applied. This method allows the determination of radial ion frequencies by determining the full phase $\phi_{\text{tot}} = 2\pi n + \phi$ in a given accumulation time t_{acc} , consisting of an integer number $n \in \mathbb{N}_0$ of full turns plus an additional phase ϕ which is measured. The radial frequency then results as $\nu_i = (2\pi n + \phi)/(2\pi t_{\text{acc}})$. Since the cyclotron frequency in a Penning trap $\nu_c = \nu_+ + \nu_-$ is equal to the sum of its radial eigenfrequencies $\nu_{+/-}$, the technique is perfectly suited for PTMS allowing a frequency determination at the same or better precision as ToF-ICR techniques with ~ 25 times shorter measurement time [19].

A typical PI-ICR detector image for $^{131}\text{Cs}^+$ is shown in Fig. 2: The dots represent repeated position projections (so called spots) from the Penning trap to a position-sensitive detector. In this case, the frequency determination was performed according to the pattern 1/2 (in Fig. 3 referred to as **P1/P2**) measurement scheme described in [19] which allows for a direct determination of ν_c . The achieved

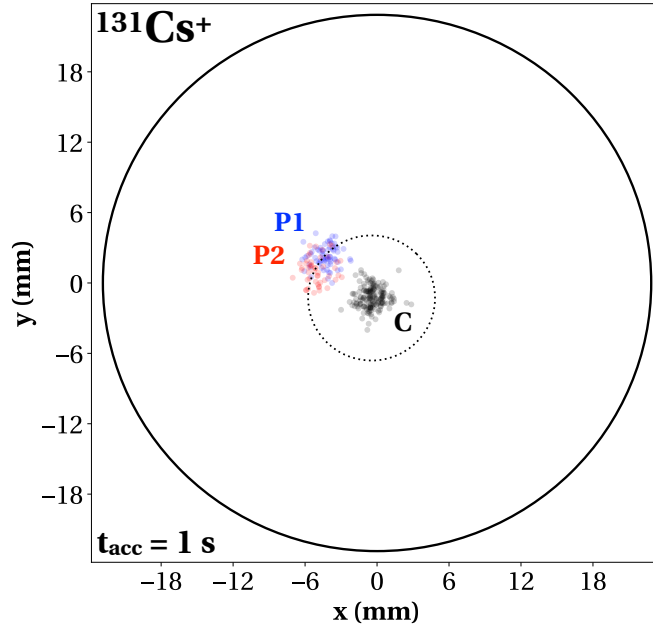


Fig. 3 Typical PI-ICR detector image for $^{131}\text{Cs}^+$ with a center spot **C** and two overlapping spots **P1/P2** for $t_{\text{acc}} = 1$ s, resolving power $R = \phi_{\text{tot}}/(2 \cdot \Delta\phi) = 1 \cdot 10^7$. For further details, see text and Ref. [19].

resolving power R in case of Fig. 3 was $R = \phi_{\text{tot}}/(2 \cdot \Delta\phi) = 1 \cdot 10^7$ with the total accumulated phase ϕ_{tot} after $t_{\text{acc}} = 1$ s and the spot's FWHM in terms of angle $\Delta\phi$. The analysis was performed with a custom-designed analysis software (for details see Ref. [20]) based on Python and ROOT [21]. The analysis was independently performed with a LabView analysis software developed by the SHIPTRAP collaboration [19] and agrees within uncertainties.

The determination of the cyclotron frequency ratio $r = \nu_{c,\text{ioi}}/\nu_{c,\text{ref}}$ between all measured cyclotron frequency values $\nu_{c,\text{ioi}}$ of the ion of interest (in this case $^{131}\text{Cs}^+$) of all three measurement methods and the reference ion values $\nu_{c,\text{ref}}$ (in this case $^{133}\text{Cs}^+$) is performed by simultaneously fitting a polynomial function $p(t)$ to both data sets [22]:

$$\nu_{c,\text{ioi}} = p(t) \quad (2)$$

$$\nu_{c,\text{ref}} = r \cdot \nu_{c,\text{ioi}} = r \cdot p(t). \quad (3)$$

The polynomial fit function describes the temporal evolution of the cyclotron frequencies while the proportionality between the two fits is exactly the cyclotron frequency ratio r . The ground-to-ground state Q_{EC} -value can be directly expressed following the relation:

$$Q_{\text{EC}} = (r - 1) \cdot (m_{\text{ref,lit}} - m_e), \quad (4)$$

where $m_{\text{ref,lit}}$ is the literature mass of the reference ion (here taken from AME16 [23]) and m_e [24] is the electron mass. Figure 4 shows all individual cyclotron frequency measurements of $^{131}\text{Cs}^+$ and $^{133}\text{Cs}^+$ over time. In addition, the polynomial fits are shown. As one can see, all PTMS detection methods used in this publication are in good agreement. Moreover, the weighted mean of all individual

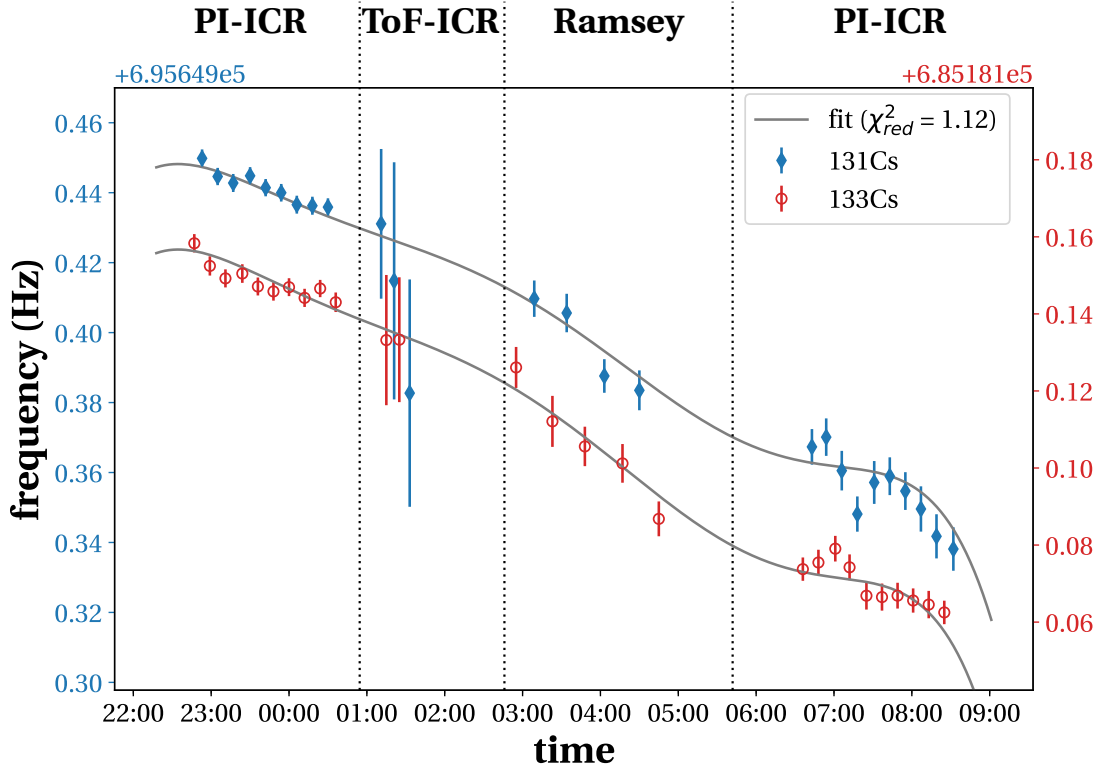


Fig. 4 Simultaneous polynomial fits of the four data sets as well as of all cyclotron frequency data for $^{131}\text{Cs}^+$ and $^{133}\text{Cs}^+$. For further details, see text.

cyclotron frequency ratios for neighboring, alternating frequency measurements of $^{131}\text{Cs}^+$ and $^{133}\text{Cs}^+$ was calculated [25] and agrees with the polynomial method described above. The final frequency ratio yields $r_{\text{final}} = 0.9849517704(14)$. The uncertainty of the combination of all PI-ICR data is $\delta\nu_c/\nu_c = 1.4 \cdot 10^{-9}$.

In addition to the statistical uncertainty derived from the fit, a careful analysis of the systematic uncertainties which are not covered by the polynomial fit was performed. These include considering fit parameter correlations, where off-axis elements in the correlation matrix were negligibly small. The fluctuation of the individual frequencies after applying different fit cuts was systematically studied. They were found to be well within the statistical uncertainty on the individual frequency, proving the purity of the beam. Since the ion rate was purposely kept below one ion per measurement cycle, a z-class analysis, i.e. reducing the number of detected ions per cycle and therefore in the trap itself, did not have to be performed. The data was corrected for ISOLTRAP's mass-dependent shift (relative shift: $7 \cdot 10^{-10}$) due to the difference in mass between the ion of interest and the reference ion as described in Ref. [25, 26]. The residual systematic uncertainty of ISOLTRAP [25] was not taken into account due to the fact that both the ion of interest and the reference were prepared, injected and measured in identical conditions, hence probing the same volume of the precision trap.

Table 1 presents the obtained ground-to-ground-state decay energy Q_{EC} as well as the allowed $(Q_{\text{EC}} - E^*)$ -value of interest to the $E^* = 364.490(4)$ keV [5] state in ^{131}Xe with their associated uncertainties. The decay-energy of the allowed EC-

Table 1 Comparison of the measured mass excess, the measured released energy Q_{EC} of the electron-capture-pair ground-to-ground-state decay of $^{131}\text{Cs} \rightarrow ^{131}\text{Xe}$, the released energy ($Q_{\text{EC}} - E^*$) for this electron-capture-pair in terms of ground-to-excited-state decay of $^{131}\text{Cs} \rightarrow ^{131}\text{Xe}^*$, the latter one corrected for the binding energy B of captured L - and M -shell electrons ($Q_{\text{EC}} - E^* - B$) and the final uncertainty compared to literature [5, 23]. For further details, see text.

(keV)	ME	Q_{EC}	$Q_{\text{EC}} - E^*$	$Q_{\text{EC}} - E^* - B_L$	$Q_{\text{EC}} - E^* - B_M$	unc.
Literature	-88059	355	-10	-15	-11	5
ISOLTRAP	-88055.56	358.00	-6.49	-11.95	-7.64	0.17

transition has to be corrected for the binding energy B of captured electrons ($Q_{\text{EC}} - E^* - B$) to the L -shell-electron ($B(L-e^-) = 5.453 \text{ keV}$ [27, 28]) and to the M -shell-electron ($B(M-e^-) = 1.1487 \text{ keV}$ [27, 28]). It is worth mentioning, that the ^{131}Xe literature mass is dominated by a high-precision measurement from SHIPTRAP using the PI-ICR technique [29].

With the refined uncertainty, the ground-to-excited-state value ($Q_{\text{EC}} - E^*$) = $-6.49(17) \text{ keV}$ appears undoubtedly negative. This translates to the excited state $^{131}\text{Xe}^*$ being higher in energy than the parent ground state in ^{131}Cs , thus prohibiting this $^{131}\text{Cs} \rightarrow ^{131}\text{Xe}^*$ transition and excluding it as a suitable candidate for the determination of the electron-neutrino mass.

3 Conclusion

High-precision mass measurements of the ^{131}Cs using established time-of-flight ion-cyclotron-resonance (ToF-ICR) mass spectrometry (MS) as well as the recently developed phase-imaging ion-cyclotron-resonance (PI-ICR) detection technique was performed with ISOLTRAP/CERN. We were able to demonstrate the successful implementation of PI-ICR at ISOLTRAP with a high resolving power of $1 \cdot 10^7$ for 1 s single-measurement time, a statistical uncertainty of only $1.4 \cdot 10^{-9}$ in ~ 4 hrs of beam time and a very good agreement with our well-established ToF-ICR measurement techniques (see Fig. 4). The obtained Q_{EC} -value agrees with the value found in literature. However, the refined precision allows now to exclude this electron-capture transition as a possible candidate for the determination of the neutrino mass.

Thus the PI-ICR technique appears very promising to tackle even more challenging cases such as ^{134}Ce , ^{159}Dy and ^{175}Hf [30, 31], the decay energy of which must be determined at a sub-100 eV level of precision.

Acknowledgements We thank the ISOLDE technical group and the ISOLDE Collaboration for their professional help. We acknowledge support by the Max Planck Society, the German Federal Ministry of Education and Research (BMBF) (05P12HGCI1, 05P12HGFNE, and 05P15ODCIA), the French IN2P3, the ExtreMe Matter Institute (EMMI) at GSI, and the European Union’s Horizon 2020 research and innovation programme (654002). Jonas Karthein acknowledges the support by a Wolfgang Gentner Ph.D scholarship of the BMBF (05E12CHA).

References

1. Bellini, G. *et al.* Neutrino Oscillations. *Adv. High En. Phys.* **2014**, 1 (2014).
2. Giunti, C. and Studenikin, A. Neutrino electromagnetic interactions: A window to new physics. *Rev. Mod. Phys.* **87**, 531 (2015).
3. Ranitzsch, O. *et al.* Development of Metallic Magnetic Calorimeters for High Precision Measurements of Calorimetric 187 Re and 163 Ho Spectra. *J. Low Temp. Phys.* **167**, 1004 (2012).
4. Eliseev, S. *et al.* Direct Measurement of the Mass Difference of 163 Ho and 163 Dy Solves the Q-Value Puzzle for the Neutrino Mass Determination. *Phys. Rev. Lett.* **115**, 062501 (2015).
5. Khazov, Y.U. *et al.* Nuclear Data Sheets for $A = 131$. *Nuclear Data Sheets* **107**, 2715 (2006).
6. Lunney, D. (on behalf of the ISOLTRAP Collaboration). Extending and refining the nuclear mass surface with ISOLTRAP. *J. Phys. G* **44**, 064008 (2017).
7. Kreim, S. *et al.* Recent exploits of the ISOLTRAP mass spectrometer. *Nucl. Instr. Meth. B* **317**, 492 (2013).
8. Mukherjee, M. *et al.* ISOLTRAP: An on-line Penning trap for mass spectrometry on short-lived nuclides. *Eu. Phys. J.* **35**, 1 (2008).
9. Borge, M.J.G. and Blaum, K. Focus on Exotic Beams at ISOLDE: A Laboratory Portrait. *J. Phys. G* **45**, 010301 (2018).
10. Herfurth, F. *et al.* A linear radiofrequency ion trap for accumulation, bunching, and emittance improvement of radioactive ion beams. *Nucl. Instr. Meth. A* **469**, 254 (2001).
11. Wolf, R.N. *et al.* ISOLTRAP's multi-reflection time-of-flight mass separator/spectrometer. *Int. J. Mass Spectr.* **349-350**, 123 (2013).
12. Mougeot, M. *et al.* Precision Mass Measurements of 58-63 Cr: Nuclear Collectivity Towards the $N = 40$ Island of Inversion. *Phys. Rev. Lett.* **120**, 232501 (2018).
13. Wienholtz, F. *et al.* Masses of exotic calcium isotopes pin down nuclear forces. *Nature* **498**, 346 (2013).
14. Wienholtz, F. *et al.* Mass-selective ion ejection from multi-reflection time-of-flight devices via a pulsed in-trap lift. *Int. J. Mass Spectr.* **421**, 285 (2017).
15. Savard, G. *et al.* A new cooling technique for heavy ions in a Penning trap. *Phys. Lett. A* **158**, 247 (1991).
16. König, M. *et al.* Quadrupole excitation of stored ion motion at the true cyclotron frequency. *Int. J. Mass Spectr. and Ion Processes* **142**, 95 (1995).
17. George, S. *et al.* Ramsey Method of Separated Oscillatory Fields for High-Precision Penning Trap Mass Spectrometry. *Phys. Rev. Lett.* **98**, 162501 (2007).
18. Eliseev, S. *et al.* Phase-Imaging Ion-Cyclotron-Resonance Measurements for Short-Lived Nuclides. *Phys. Rev. Lett.* **110**, 082501 (2013).
19. Eliseev, S. *et al.* A phase-imaging technique for cyclotron-frequency measurements. *Appl. Phys. B* **114**, 107 (2014).
20. Karthein, J. *Precision mass measurements using the Phase-Imaging Ion-Cyclotron-Resonance detection technique* - Master thesis - Ruprecht-Karls-Universität Heidelberg, 2017.
21. Antcheva, I. *et al.* ROOT — A C++ framework for petabyte data storage, statistical analysis and visualization. *Comp. Phys. Comm.* **180**, 2499 (2009).

22. Fink, D. *et al.* Q Value and Half-Lives for the Double- β -Decay Nuclide Pd 110. *Phys. Rev. Lett.* **108**, 062502 (2012).
23. Wang, M. *et al.* The AME2016 atomic mass evaluation (II). Tables, graphs and references. *Chin. Phys. C* **41**, 030003 (2017).
24. Sturm, S. *et al.* High-precision measurement of the atomic mass of the electron. *Nature* **506**, 467 (2014).
25. Kellerbauer, A. *et al.* From direct to absolute mass measurements: A study of the accuracy of ISOLTRAP. *Eu. Phys. J. D* **22**, 53 (2003).
26. Welker, A. *et al.* Precision electron-capture energy in ^{202}Pb and its relevance for neutrino mass determination. *Eu. Phys. J.* **53**, 153 (2017)
27. Cardona, M. and Ley, L. editors. *Photoem. Solids I* 26 (1978).
28. NIST X-ray Photoelectron Spectroscopy (XPS) Database, Version 3.5.
29. Nesterenko, D. A. *et al.* Direct determination of the atomic mass difference of Re 187 and Os 187 for neutrino physics and cosmochronology. *Phys. Rev. C* **90**, 042501 (2014).
30. Eliseev, S. *et al.* Proposal to the ISOLDE and Neutron Time-of-Flight Committee: Search for β -transitions with the lowest decay energy for a determination of the neutrino mass. Technical report, CERN, 2014.
31. Karthein, J. *et al.* Letter of Intent to the ISOLDE and Neutron Time-of-Flight Committee. Technical report, CERN, 2017.

3.3 Publication 3: *N*-rich Cadmium

Authors:

Vladimir Manea*, Jonas Karthein*, Dinko Atanasov, Michael Bender, Klaus Blaum, Thomas E. Cocolios, Sergey Eliseev, Alexander Herlert, Jason D. Holt, Wenjia Huang, Yuri Litvinov, David Lunney, Javier Menendez, Maxime Mougeot, Dennis Neidherr, Lutz Schweikhard, Achim Schwenk, Johannes Simonis, Andree Welker, Frank Wienholtz, Kai Zuber

*VM and JK share the first authorship for equal contributions to this work.

Publication status:

Accepted 07 January 2020

Journal reference:

Manea, V. & Karthein, J. *et al.* Phys. Rev. Lett. **124**, 092502 (2020).

Digital object identifier:

[10.1103/PhysRevLett.124.092502](https://doi.org/10.1103/PhysRevLett.124.092502)

Authors' contributions:

VM, JK, DA, KB, TC, AH, YL, DL, MM, DN, LS, AW, FW, and KZ were involved in the proposal or addendum for the experiment. VM, JK, DA, KB, TC, AH, WH, YL, MM, DN, AW and FW carried out the experiment. VM performed the first and final analysis for the MRTof and ToF-ICR datasets and JK performed the first and final analysis for the PI-ICR datasets. Second analyses were carried out by VM, JK, DA, and SE. JK, MB, JH, JM, AS, and JS performed the theoretical calculations. VM, JK, KB, DL, MM, LS and AS were involved in the discussion of the results. VM and JK wrote the first draft of the article and prepared all figures. MB and JH each wrote a paragraph describing details about their theoretical calculations. The manuscript was then reviewed critically before and after submission by all authors.

Abstract:

We probe the $N = 82$ nuclear shell closure by mass measurements of neutron-rich cadmium isotopes with the ISOLTRAP spectrometer at ISOLDE-CERN. The new mass of ^{132}Cd offers the first value of the $N = 82$, two-neutron shell gap below $Z = 50$ and confirms the phenomenon of mutually enhanced magicity at ^{132}Sn . Using the recently implemented phase-imaging ion-cyclotron-resonance method, the ordering of the low-lying isomers in ^{129}Cd and their energies were determined. The new experimental findings are used to test large-scale shell-model, mean-field and beyond-mean-field calculations, as well as the *ab initio* valence-space in-medium similarity renormalization group.

First Glimpse of the $N = 82$ Shell Closure below $Z = 50$ from Masses of Neutron-Rich Cadmium Isotopes and Isomers

V. Manea^{1,2,3,*}, J. Karthein^{1,2,†}, D. Atanasov^{4,‡}, M. Bender⁵, K. Blaum⁶, T. E. Cocolios³, S. Eliseev², A. Herlert⁶, J. D. Holt⁷, W. J. Huang^{8,§}, Yu. A. Litvinov⁹, D. Lunney⁸, J. Menéndez^{10,11}, M. Mougeot^{8,‡}, D. Neidherr⁹, L. Schweikhard¹², A. Schwenk^{13,14,2}, J. Simonis^{15,13,14}, A. Welker^{1,4}, F. Wienholtz^{1,12,||} and K. Zuber⁴

¹CERN, 1211 Geneva 23, Switzerland

²Max-Planck-Institut für Kernphysik, 69117 Heidelberg, Germany

³Instituut voor Kern—en Stralingsfysica, Katholieke Universiteit Leuven, B-3001 Leuven, Belgium

⁴Technische Universität Dresden, 01069 Dresden, Germany

⁵IP2I Lyon, CNRS/IN2P3, Université de Lyon, Université Claude Bernard Lyon 1, F-69622 Villeurbanne, France

⁶FAIR GmbH, 64291 Darmstadt, Germany

⁷TRIUMF, 4004 Wesbrook Mall, Vancouver, BC V6T 2A3, Canada

⁸CSNSM-IN2P3-CNRS, Université Paris-Sud, 91406 Orsay, France

⁹GSI Helmholtzzentrum für Schwerionenforschung GmbH, 64291 Darmstadt, Germany

¹⁰Center for Nuclear Study, The University of Tokyo, 113-0033 Tokyo, Japan

¹¹Department de Física Quàntica i Astrofísica, Universitat de Barcelona, 08028 Barcelona, Spain

¹²Institut für Physik, Universität Greifswald, 17487 Greifswald, Germany

¹³Institut für Kernphysik, Technische Universität Darmstadt, 64289 Darmstadt, Germany

¹⁴ExtreMe Matter Institute EMMI, GSI Helmholtzzentrum für Schwerionenforschung GmbH, 64291 Darmstadt, Germany

¹⁵Institut für Kernphysik and PRISMA Cluster of Excellence, Johannes Gutenberg-Universität, 55099 Mainz, Germany



(Received 13 September 2019; accepted 7 January 2020; published 5 March 2020)

We probe the $N = 82$ nuclear shell closure by mass measurements of neutron-rich cadmium isotopes with the ISOLTRAP spectrometer at ISOLDE-CERN. The new mass of ^{132}Cd offers the first value of the $N = 82$, two-neutron shell gap below $Z = 50$ and confirms the phenomenon of mutually enhanced magicity at ^{132}Sn . Using the recently implemented phase-imaging ion-cyclotron-resonance method, the ordering of the low-lying isomers in ^{129}Cd and their energies are determined. The new experimental findings are used to test large-scale shell-model, mean-field, and beyond-mean-field calculations, as well as the *ab initio* valence-space in-medium similarity renormalization group.

DOI: 10.1103/PhysRevLett.124.092502

The so-called magic numbers of protons and neutrons are associated with large energy gaps in the effective single-particle spectrum of the nuclear mean field [1], revealing shell closures. As such, they are intimately connected to the nuclear interaction and represent essential benchmarks for nuclear models.

Experiments with light radioactive beams have shown that shell closures at $N = 8, 20$, and 28 are substantially weakened when the number of protons in the nuclear system is reduced (see [2,3] for a review). New but weaker shell closures have also been found, e.g., $N = 32$ and 34 [4–7]. In the shell model, this evolution results from the interplay between the monopole part of the valence-space

nucleon-nucleon interaction that determines the single-particle spectrum and multipole forces that induce correlations [8]. Starting from realistic nuclear forces, the study of closed-shell nuclei provides benchmarks for microscopic calculations of valence-space Hamiltonians, with their many-body contributions [9–13]. Despite extensive work, significantly less is known for heavier nuclei, in particular for the magic $N = 82$.

The doubly magic nature of ^{132}Sn (with 50 protons and 82 neutrons) was reconfirmed recently [14,15]. But below $Z = 50$ the orbitals occupied by the Fermi-level protons change, as does the proton-neutron interaction, which drives shell evolution. This means that without data for nuclides with $Z < 50$ and $N \approx 82$, any predictions for the $N = 82$ shell gap are rather uncertain. While decay-spectroscopy [16–18], laser-spectroscopy [19], and mass-spectrometry [20,21] studies have been performed for the neutron-rich cadmium isotopes, the energies of the low-lying isomers in ^{129}Cd and the $N = 82$ two-neutron shell gap remain unknown.

Published by the American Physical Society under the terms of the Creative Commons Attribution 4.0 International license. Further distribution of this work must maintain attribution to the author(s) and the published article's title, journal citation, and DOI. Funded by the Max Planck Society.

The $A \approx 130$ r -process abundance peak has long been considered an indication of a persistent $N = 82$ shell gap in various models. However, recent studies of r -process nucleosynthesis have underlined the importance of fission recycling in certain scenarios, in which the $A = 130$ abundance peak is primarily determined by the fission-fragment distribution of r -process actinides [22,23].

In this Letter, we present the first direct determination of the $N = 82$ shell gap for $Z < 50$ with mass measurements of exotic cadmium isotopes and isomers between ^{124}Cd and ^{132}Cd . We exploit all mass-measurement techniques of the ISOLTRAP spectrometer, including the phase-imaging ion-cyclotron-resonance (PI-ICR) method [24–26]. The data are interpreted in comparison to the large-scale shell model and to new calculations made with a beyond-mean-field (BMF) approach [27,28], as well as the *ab initio* valence-space in-medium similarity renormalization group (VS-IMSRG) [12,29–33].

The cadmium isotopes were produced at CERN’s ISOLDE facility [34] by neutron-induced fission in a uranium-carbide target. The neutrons were produced by 1.4-GeV protons accelerated by CERN’s Proton Synchrotron Booster and impinging on a tungsten rod, which reduced contaminants from proton-induced reactions [35]. The neutral products diffused from the $\approx 2000^\circ\text{C}$ target into a hot tantalum cavity where the resonance-ionization laser ion source [36] was used to produce singly charged cadmium ions. A cold quartz line [37] greatly suppressed surface ionized cesium and barium contaminants.

The beam was accelerated to 50 keV, mass separated by the ISOLDE High Resolution Separator and transported to ISOLTRAP for accumulation in a segmented, linear radio-frequency quadrupole cooler and buncher [38]. The ion bunch was then injected into the multireflection time-of-flight mass spectrometer (MR-TOF MS) [39] where the cadmium ions were separated from contaminants with a resolving power of $\approx 10^5$. The separated ions were either detected using a secondary electron multiplier for mass measurements, or purified [40] and transported to a tandem Penning-trap system, composed of a preparation trap for beam cooling and further purification [41,42] and a precision trap for measurements.

In this Letter, the masses of $^{131,132}\text{Cd}$ were determined with the MR-TOF MS (see Fig. 1) using a two-parameter calibration formula and hence requiring two reference measurements, as described in [5]. Its short measurement time of only about 27 ms and direct ion counting made it the method of choice for the most exotic isotopes. Considering only singly charged ions, the mass $m_{i,x}$ of the ion of interest is related to the masses $m_{i,1}$ and $m_{i,2}$ of two reference ions by $m_{i,x}^{1/2} = C_{\text{TOF}}\Delta_{\text{ref}} + \frac{1}{2}\Sigma_{\text{ref}}$, with $\Delta_{\text{ref}} = m_{i,1}^{1/2} - m_{i,2}^{1/2}$, $\Sigma_{\text{ref}} = m_{i,1}^{1/2} + m_{i,2}^{1/2}$ and $C_{\text{TOF}} = (2t_x - t_1 - t_2)/[2(t_1 - t_2)]$. The quantities t_x , t_1 , and t_2 are the TOFs, measured in the same conditions, of the ions of mass

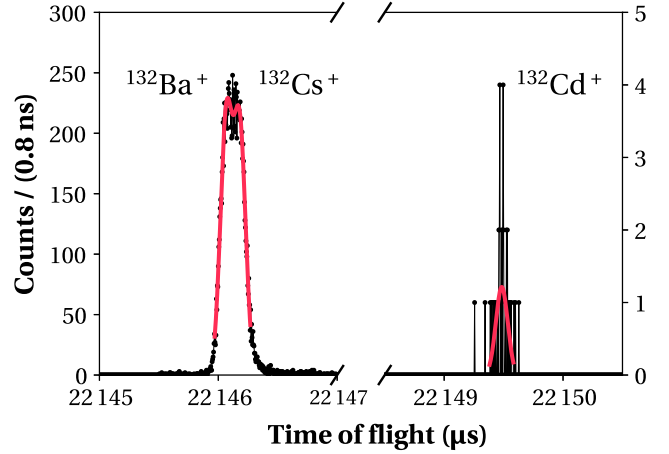


FIG. 1. MR-TOF spectrum (after 800 revolutions) of $^{132}\text{Cd}^+$ along with isobaric ions ($^{132}\text{Ba}^+$ and $^{132}\text{Cs}^+$), with fits (in red) to Gaussian line shapes.

$m_{i,x}$, $m_{i,1}$, and $m_{i,2}$, respectively, with $m_{i,1}$ an isobar of the ion of interest.

The masses of the other studied cadmium isotopes were determined with the precision Penning trap, allowing typically a higher precision and resolving power than the MR-TOF MS, by measuring their cyclotron frequency (as singly charged ions) in the trap, $\nu_{c,x} = qB/(2\pi m_{i,x})$ (where q is in our case the elementary charge and B is the trap’s magnetic-field induction) [43]. The atomic mass m_x can then be determined as $m_x = r_{\text{ref},x}(m_{\text{ref}} - m_e) + m_e$, where m_e is the electron mass and $r_{\text{ref},x} = \nu_{c,\text{ref}}/\nu_{c,x}$ is the measured cyclotron-frequency ratio between a singly charged reference ion of atomic mass m_{ref} and the ion of interest. The binding energy of the electron, neglected in the atomic-mass formula, is orders of magnitude smaller than the statistical uncertainty.

Penning-trap measurements of $^{124,126,128,131}\text{Cd}$ were performed with the time-of-flight ion-cyclotron-resonance (TOF-ICR) method [44], including Ramsey-type excitations [45,46].

For $^{127,129}\text{Cd}$ the beam was a mixture of ground and isomeric state ($J = 3/2^+$ and $J = 11/2^-$) which in a prior attempt could not be separated by a long-excitation TOF-ICR measurement [20] due to the short half-lives. In this Letter, we used instead the recently developed PI-ICR method [24,25], by which a radial frequency is determined from the phase “accumulated” by the circular ion motion in the trap in a given time t_{acc} , using its projection on a position-sensitive microchannel-plate detector (MCP). In PI-ICR MS one performs three ion-position measurements: (1) the center of the radial ion trajectory by ejection without preparing a radial motion, (2) for ions prepared on a cyclotron orbit (at frequency ν_+) after evolving for t_{acc} , (3) for ions prepared on a magnetron orbit (at frequency ν_-), after evolving for the same t_{acc} . The cyclotron frequency is

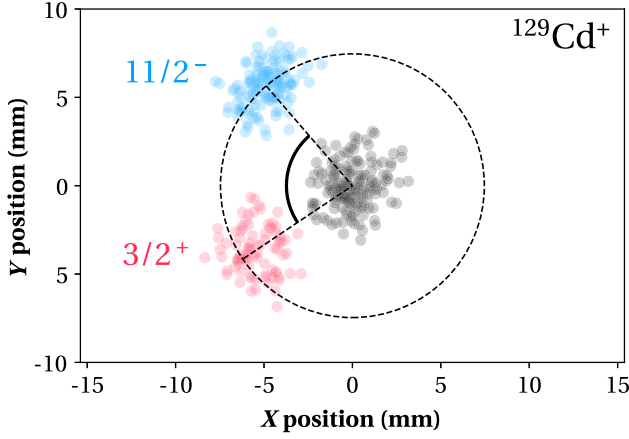


FIG. 2. PI-ICR ion projection image of $^{129}\text{Cd}^+$ with center ion spot measured separately (in black) and the $11/2^-$ (blue) and $3/2^+$ states (red) separated by the marked angle after 106-ms phase accumulation at the modified cyclotron frequency.

then given by $\nu_c = [2\pi(n_+ + n_-) + \phi]/(2\pi t_{\text{acc}})$, where n_+ and n_- are the number of integer rotations performed by the ions in steps (2) and (3), respectively, while ϕ is the angle between the ion positions measured in the two steps [24,25].

In the second step of the PI-ICR measurement, a resolving power of about 2×10^6 was achieved in only 106 ms, allowing a clear separation of the two states as illustrated in Fig. 2 for $^{129}\text{Cd}^+$. Their individual masses could thus be determined.

The experimental results of this work are summarized in Table I. During the ^{132}Cd measurements the yield of (stable) $^{132}\text{Ba}^+$ remained constant, while a gradual increase in the yield of (radioactive) $^{132}\text{Cs}^+$ was observed. The data set for ^{132}Cd was thus split, depending on which isobaric reference dominated, resulting in two independent C_{TOF} values. In

this case, as well as for ^{131}Cd , the weighted averages of the new mass-excess values are used for the figures.

The analysis of the TOF-ICR measurements followed the procedure in [49]. For the MR-TOF MS spectra, Gaussian distributions were fit to the data (double-Gaussian for the $^{132}\text{Ba}^+ / ^{132}\text{Cs}^+$ double peak) by the binned maximum-likelihood method. When statistically significant, shifts of the C_{TOF} values from changing the fit range, data binning and number of ions simultaneously stored in the MR-TOF MS were included in the total uncertainty.

For the PI-ICR measurements, the unbinned maximum-likelihood fit of the ion-spot positions was performed using 2D Gaussian distributions. The effect of the number of ions simultaneously stored in the trap was studied and, for the analysed data set, was within statistical uncertainties. The mass-dependent shift and systematic uncertainty from [49] were quadratically added to the total uncertainty.

The spin assignments for the measured states in ^{127}Cd and ^{129}Cd are based on the fact that the high-spin isomers were systematically produced with higher yields, corroborated by a laser-spectroscopy study of cadmium isotopes performed at ISOLDE [19] with the same production mechanism, where the yield ratios were determined for $^{127,129}\text{Cd}$. We conclude that the excited $11/2^-$ state in ^{127}Cd becomes the ground state in ^{129}Cd . The 283(12)-keV excitation energy obtained for ^{127}Cd agrees with the TITAN result using highly charged ions [21]. The 343(8)-keV excitation energy of the $3/2^+$ state in ^{129}Cd is a new value.

In a simple picture, the $3/2^+$ and $11/2^-$ states in ^{129}Cd are formed by the odd neutron occupying the $d_{3/2}$ and $h_{11/2}$ orbitals, respectively, and allow probing the evolution of the two states with proton number. This is shown in Fig. 3, where neutron binding energies, calculated as in [2] for the low-lying states in the even Z , $N = 81$ and $N = 83$ isotones are plotted as a function of Z . For $Z = 48$ they are obtained from this Letter. One notices the larger slope of

TABLE I. Frequency ratio ($r = \nu_{c,\text{ref}}/\nu_c$), time-of-flight ratio (C_{TOF}) and mass excess of the cadmium isotopes measured in this work. Mass excesses from the literature ([21] for ^{127}Cd , [20] for ^{129}Cd and AME2016 [47] for the rest) are given as well (# indicates extrapolated values). The masses of the reference ions used in the evaluation are from AME2016 [47]. Experimental half-lives are taken from [48] (and [18] for ^{127}Cd). The yields, where available, are order-of-magnitude estimates of ion intensities on the ISOLDE central beam line. Values between parentheses are total (statistical plus systematic) uncertainties.

A	J^π	Half-life (s)	Yield (Ions/s)	Method	References	Ratio r or C_{TOF}	Mass excess (keV)	
							This Letter	Literature
124	0^+	1.25(2)		TOF-ICR	$^{133}\text{Cs}^+$	$r = 0.932\,374\,318\,6(432)$	-76692.4(5.4)	-76701.7(3.0)
126	0^+	0.513(6)		TOF-ICR	$^{133}\text{Cs}^+$	$r = 0.947\,458\,558\,1(503)$	-72249.8(6.2)	-72256.8(2.5)
127	$3/2^+$	$0.45(\frac{12}{8})$	5×10^4	PI-ICR	$^{133}\text{Cs}^+$	$r = 0.955\,011\,112\,2(922)$	-68737(11)	-68743.4(5.6)
	$11/2^-$	0.36(4)	1×10^5			$r = 0.955\,013\,397\,2(435)$	-68453.8(5.4)	-68460.1(4.7)
128	0^+	0.246(2)	8×10^4	TOF-ICR	$^{133}\text{Cs}^+$	$r = 0.962\,547\,502(114)$	-67225(14)	-67242(7)
129	$11/2^-$	0.152(6)	1×10^4	PI-ICR	$^{133}\text{Cs}^+$	$r = 0.970\,104\,817\,5(432)$	-63122.1(5.4)	-63058(17)
	$3/2^+$	0.147(3)	5×10^3			$r = 0.970\,107\,588\,6(450)$	-62779.1(5.6)	
131	$7/2^-$	0.098(2)	3×10^2	TOF-ICR	$^{133}\text{Cs}^+$	$r = 0.985\,217\,426(252)$	-55167(31)	-55220(100)
				MR-TOF MS	$^{131}\text{Cs}^+, ^{133}\text{Cs}^+$	$C_{\text{TOF}} = 0.482\,316\,6(126)$	-55238(24)	
132	0^+	0.082(4)	5	MR-TOF MS	$^{132}\text{Ba}^+, ^{133}\text{Cs}^+$	$C_{\text{TOF}} = 0.459\,215\,6(773)$	-50499(72)	-50260
					$^{132}\text{Cs}^+, ^{133}\text{Cs}^+$	$C_{\text{TOF}} = 0.460\,420(118)$	-50386(110)	

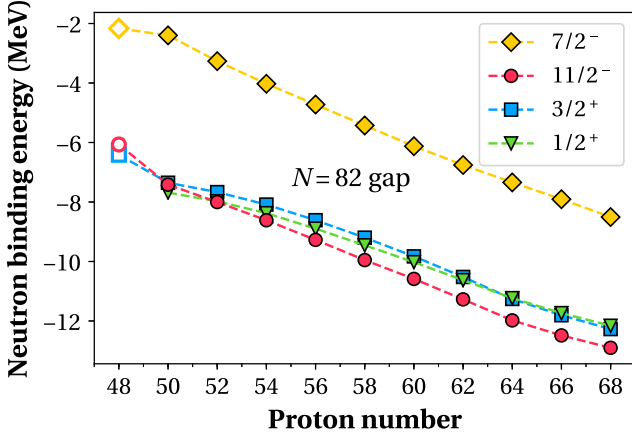


FIG. 3. Neutron binding energies of the low-lying nuclear states of the $N = 81$ ($J^\pi = 1/2^+, 3/2^+, 11/2^-$) and $N = 83$ ($J^\pi = 7/2^-$) isotones. Experimental data are taken from [48,50] and this Letter (open symbols).

the $11/2^-$ states, which changes more abruptly for $Z < 50$, suggesting a stronger, attractive monopole proton-neutron interaction for the high-spin state.

Figure 4 shows the difference in energy between the $3/2^+$ and $11/2^-$ states for the odd cadmium isotopes. Shell-model calculations assuming a closed ^{132}Sn ($\text{jj}45\text{pn}$ [51,52] and NA-14 [16–18,53]) or allowing cross-shell excitations (EPQQM [54]) predict the $11/2^-$ state to become the ground state in ^{129}Cd . For EPQQM, obtaining the correct prediction required enhancing the monopole interaction between the $\pi g_{9/2}$ and $\nu h_{11/2}$ orbits [55].

The mass of ^{132}Cd allows addressing a broader range of models via the $N = 82$ two-neutron shell gap $\Delta_{2n}(Z, N) = S_{2n}(Z, N) - S_{2n}(Z, N + 2)$ (where S_{2n} is the two-neutron separation energy), a quantity involving only even nuclei

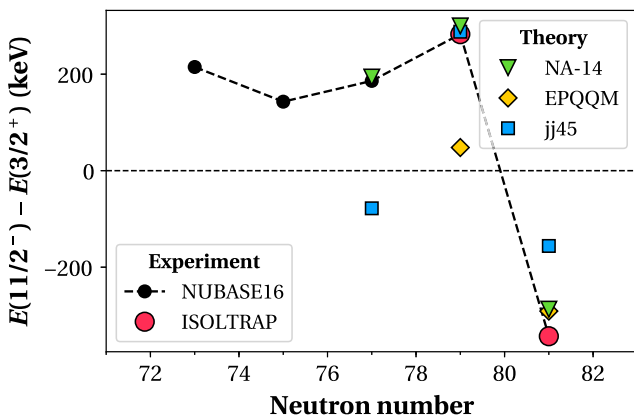


FIG. 4. Energy difference between the $J = 11/2^-$ and $J = 3/2^+$ states in the odd cadmium isotopes. Experimental data from [48] and this Letter are compared to theoretical calculations (EPQQM [54], NA-14 [18,53], $\text{jj}45\text{pn}$ [51] using NUSHELLX [52]).

and the first such value below the doubly magic ^{132}Sn . This gap is shown as a function of Z in Fig. 5, with the new data (full circle) revealing a peak at the proton magic number $Z = 50$. This phenomenon called “mutually enhanced magicity” [56,57] is known from other doubly magic nuclei and was explained by a BMF calculation using the SLy4 Skyrme interaction, within a symmetry-restored generator coordinate method (GCM) [27,28]. In this Letter, we show that this enhancement manifests also for ^{132}Sn . The BMF calculations were extended to $Z = 46$ and describe the peak at $Z = 50$. By contrast, results obtained with SLy4 just at the mean-field level (SLy4-MF) fail to reproduce the peak. It is by BMF correlations that the $N = 80, 84$ isotones gain binding with respect to $N = 82$, lowering the empirical shell gap, while for $Z = 50$ the closed proton shell maintains the high gap value. The same failure to produce the peak in more basic mean-field calculations is also found when using other interactions. Figure 5 illustrates this for the nonrelativistic HFB31 [58] and UNEDF0 [59] Skyrme interactions and the relativistic DD-ME δ [60]. Calculations with HFB31 include a collective-energy correction for BMF effects, which slightly enhances Δ_{2n} around $Z = 50$. While the peak is qualitatively described by BMF correlations, the size of the drop of Δ_{2n} below $Z < 50$ is not reproduced by any of these calculations.

We also present VS-IMSRG calculations of ground- and two-neutron separation energies of cadmium, tin, and tellurium isotopes across the $N = 82$ shell gap. For details on the VS-IMSRG decoupling to derive the valence-space Hamiltonian, we refer to Refs. [12,29–33]. When this *ab initio* valence-space Hamiltonian is diagonalized (here with the shell-model code ANTOINE [8]) some subset of eigenvalues of the full Hamiltonian should be reproduced

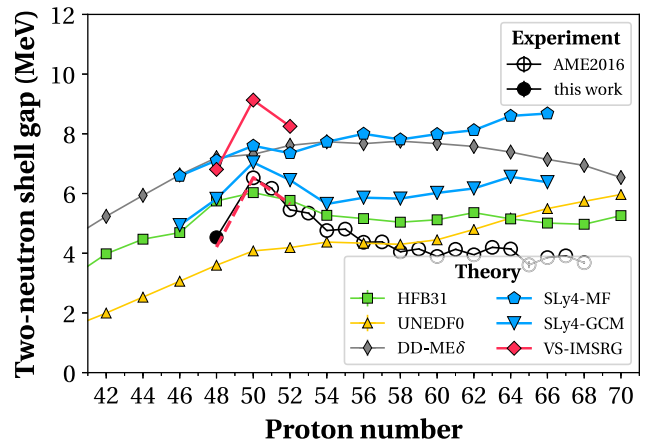


FIG. 5. Experimental two-neutron shell gap of the $N = 82$ isotones from the AME2016 [47] and this Letter compared to predictions of different calculations (for details, see text). The dashed line corresponds to the VS-IMSRG results shifted to match the $Z = 50$ value.

when no IMSRG approximations are made. In this Letter, we use the IMSRG(2) approximation, where all induced operators are truncated at the two-body level, typically giving binding energies closer than 1% to full-space *ab initio* results [12]. We begin from the 1.8/2.0(EM) chiral interaction of Refs. [61,62], used successfully throughout the medium- to heavy-mass region [13,63,64]. For heavier systems, achieving convergence with respect to the $E_{3\max}$ cut on 3N matrix elements is however a key limitation. The resulting Δ_{2n} values are presented in Fig. 5. The calculations overestimate data by almost 3 MeV, but are not fully converged with respect to the 3N matrix elements included, here up to $E_{3\max} = 18$ excitations in a harmonic oscillator basis. In contrast, the relative trend of Δ_{2n} , which is safely converged up to ~ 50 keV, is well described. This is illustrated by the dashed lines in Fig. 5, which show the IMSRG results translated to match the Δ_{2n} value at $Z = 50$.

In summary, we have measured the masses of neutron-rich cadmium isotopes and isomers across the $N = 82$ shell closure. The PI-ICR technique allowed establishing the inversion of the $11/2^-$ and $3/2^+$ states in ^{129}Cd , showing that the $h_{11/2}$ neutron orbital is key for the evolution of the $N = 82$ shell gap towards $Z = 40$. The trend of the $N = 82$ shell gap was determined below $Z = 50$ with the mass of ^{132}Cd , showing a large drop, which confirms the mutually enhanced magicity of ^{132}Sn . A BMF model reproduces the effect, but underestimates its size, whereas the VS-IMSRG approach shows an offset to experiment, but describes it qualitatively.

V. M. and J. K. contributed equally to this work. We thank D. T. Yordanov for the helpful communication regarding the spin assignment in ^{129}Cd and R. Stroberg for fruitful discussions on the VS-IMSRG framework. We thank the ISOLDE technical group and the ISOLDE Collaboration for their support and the excellent quality of the neutron-rich beams. We acknowledge support by the Max-Planck Society, the German Federal Ministry of Education and Research (BMBF, Contracts No. 05P12HGCI1, No. 05P12HGFNE, No. 05P15ODCIA, No. 05P15HGCIA, No. 05P18HGCIA, and No. 05P18RDFN1), the European Union 7th framework through ENSAR2 (Contract No. 262010), the French IN2P3 and FWO Vlaanderen (Belgium). J. K. and A. W. acknowledge support by a Wolfgang Gentner Ph.D. Scholarship of the BMBF (05E15CHA). W. J. H. acknowledges the support by the China Scholarship Council (Grant No. 201404910496). J. M. acknowledges support from the JSPS KAKENHI Grant No. 18K03639, MEXT as Priority issue on post-K computer (Elucidation of the fundamental laws and evolution of the universe), Joint Institute for Computational Fundamental Science (JICFuS), the CNS-RIKEN joint project for large-scale nuclear structure calculations, and the Ramón y Cajal program RYC-2017-22781 of the Spanish Ministry of Science, Innovation and Universities.

*Corresponding author.

vladimir.manea@cern.ch

†This article contains data from the Ph.D. thesis work of Jonas Karthein, enrolled at the Ruprecht-Karls-Universität Heidelberg.

‡Present address: CERN, 1211 Geneva 23, Switzerland.

§Present address: Max-Planck-Institut für Kernphysik, 69117 Heidelberg, Germany.

||Present address: Institut für Kernphysik, Technische Universität Darmstadt, 64289 Darmstadt, Germany.

- [1] M. G. Mayer and J. H. D. Jensen, *Elementary Theory of Nuclear Shell Structure* (Wiley, New York, 1955).
- [2] O. Sorlin and M.-G. Porquet, *Prog. Part. Nucl. Phys.* **61**, 602 (2008).
- [3] R. Kanungo, *Phys. Scr.* **T152**, 014002 (2013).
- [4] A. Huck, G. Klotz, A. Knipper, C. Miehé, C. Richard-Serre, G. Walter, A. Poves, H. L. Ravn, and G. Marguier, *Phys. Rev. C* **31**, 2226 (1985).
- [5] F. Wienholtz *et al.*, *Nature (London)* **498**, 346 (2013).
- [6] D. Steppenbeck *et al.*, *Nature (London)* **502**, 207 (2013).
- [7] S. Michimasa *et al.*, *Phys. Rev. Lett.* **121**, 022506 (2018).
- [8] E. Caurier, G. Martínez-Pinedo, F. Nowacki, A. Poves, and A. P. Zuker, *Rev. Mod. Phys.* **77**, 427 (2005).
- [9] T. Otsuka, T. Suzuki, J. D. Holt, A. Schwenk, and Y. Akaishi, *Phys. Rev. Lett.* **105**, 032501 (2010).
- [10] K. Hebeler, J. Holt, J. Menéndez, and A. Schwenk, *Annu. Rev. Nucl. Part. Sci.* **65**, 457 (2015).
- [11] G. Hagen, G. R. Jansen, and T. Papenbrock, *Phys. Rev. Lett.* **117**, 172501 (2016).
- [12] S. R. Stroberg, A. Calci, H. Hergert, J. D. Holt, S. K. Bogner, R. Roth, and A. Schwenk, *Phys. Rev. Lett.* **118**, 032502 (2017).
- [13] T. D. Morris, J. Simonis, S. R. Stroberg, C. Stumpf, G. Hagen, J. D. Holt, G. R. Jansen, T. Papenbrock, R. Roth, and A. Schwenk, *Phys. Rev. Lett.* **120**, 152503 (2018).
- [14] D. Rosiak *et al.*, *Phys. Rev. Lett.* **121**, 252501 (2018).
- [15] C. Gorges *et al.*, *Phys. Rev. Lett.* **122**, 192502 (2019).
- [16] J. Taprogge *et al.*, *Phys. Lett. B* **738**, 223 (2014).
- [17] J. Taprogge *et al.*, *Phys. Rev. C* **91**, 054324 (2015).
- [18] C. Lorenz *et al.*, *Phys. Rev. C* **99**, 044310 (2019).
- [19] D. T. Yordanov, D. L. Balabanski, J. Bieroń, M. L. Bissell, K. Blaum, I. Budinčević, S. Fritzsche, N. Frömmgen, G. Georgiev, C. Geppert, M. Hammen, M. Kowalska, K. Kreim, A. Krieger, R. Neugart, W. Nörtershäuser, J. Papuga, and S. Schmidt, *Phys. Rev. Lett.* **110**, 192501 (2013).
- [20] D. Atanasov *et al.*, *Phys. Rev. Lett.* **115**, 232501 (2015).
- [21] D. Lascar *et al.*, *Phys. Rev. C* **96**, 044323 (2017).
- [22] S. Goriely, J. L. Sida, J. F. Lemaître, S. Panebianco, N. Dubray, S. Hilaire, A. Bauswein, and H. T. Janka, *Phys. Rev. Lett.* **111**, 242502 (2013).
- [23] D. Martin, A. Arcones, W. Nazarewicz, and E. Olsen, *Phys. Rev. Lett.* **116**, 121101 (2016).
- [24] S. Eliseev, K. Blaum, M. Block, C. Droese, M. Goncharov, E. Minaya Ramirez, D. A. Nesterenko, Y. N. Novikov, and L. Schweikhard, *Phys. Rev. Lett.* **110**, 082501 (2013).
- [25] S. Eliseev, K. Blaum, M. Block, A. Dörr, C. Droese, T. Eronen, M. Goncharov, M. Höcker, J. Ketter, E. M. Ramirez, D. A. Nesterenko, Y. N. Novikov, and L. Schweikhard, *Appl. Phys. B* **114**, 107 (2014).

- [26] J. Karthein, D. Atanasov, K. Blaum, S. Eliseev, P. Filianin, D. Lunney, V. Manea, M. Mougeot, D. Neidherr, Y. Novikov, L. Schweikhard, A. Welker, F. Wienholtz, and K. Zuber, *Hyperfine Interact.* **240**, 61 (2019).
- [27] M. Bender, G. F. Bertsch, and P.-H. Heenen, *Phys. Rev. C* **73**, 034322 (2006).
- [28] M. Bender, G. F. Bertsch, and P.-H. Heenen, *Phys. Rev. C* **78**, 054312 (2008).
- [29] K. Tsukiyama, S. K. Bogner, and A. Schwenk, *Phys. Rev. C* **85**, 061304(R) (2012).
- [30] S. K. Bogner, H. Hergert, J. D. Holt, A. Schwenk, S. Binder, A. Calci, J. Langhammer, and R. Roth, *Phys. Rev. Lett.* **113**, 142501 (2014).
- [31] T. D. Morris, N. M. Parzuchowski, and S. K. Bogner, *Phys. Rev. C* **92**, 034331 (2015).
- [32] S. R. Stroberg, H. Hergert, J. D. Holt, S. K. Bogner, and A. Schwenk, *Phys. Rev. C* **93**, 051301(R) (2016).
- [33] S. R. Stroberg, S. K. Bogner, H. Hergert, and J. D. Holt, *Ann. Rev. Nucl. Part. Sci.* **69**, 307 (2019).
- [34] M. J. G. Borge and K. Blaum, *J. Phys. G* **45**, 010301 (2018).
- [35] U. Köster, *Eur. Phys. J. A* **15**, 255 (2002).
- [36] V. Fedosseev, L.-E. Berg, D. Fedorov, D. Fink, O. Launila, R. Losito, B. Marsh, R. Rossel, S. Rothe, M. Seliverstov, A. Sjödin, and K. Wendt, *Rev. Sci. Instrum.* **83**, 02A903 (2012).
- [37] E. Bouquerel, R. Catherall, M. Eller, J. Lettry, S. Marzari, and T. Stora, *Nucl. Instrum. Methods Phys. Res., Sect. B* **266**, 4298 (2008).
- [38] F. Herfurth, J. Dilling, A. Kellerbauer, G. Bollen, S. Henry, H.-J. Kluge, E. Lamour, D. Lunney, R. B. Moore, C. Scheidenberger, S. Schwarz, G. Sikler, and J. Szerypo, *Nucl. Instrum. Methods Phys. Res., Sect. A* **469**, 254 (2001).
- [39] R. N. Wolf, F. Wienholtz, D. Atanasov, D. Beck, K. Blaum, C. Borgmann, F. Herfurth, M. Kowalska, S. Kreim, Y. A. Litvinov, D. Lunney, V. Manea, D. Neidherr, M. Rosenbusch, L. Schweikhard, J. Stanja, and K. Zuber, *Int. J. Mass Spectrom.* **349–350**, 123 (2013).
- [40] F. Wienholtz, S. Kreim, M. Rosenbusch, L. Schweikhard, and R. N. Wolf, *Int. J. Mass Spectrom.* **421**, 285 (2017).
- [41] H. Raimbault-Hartmann, D. Beck, G. Bollen, M. König, H.-J. Kluge, E. Scharf, J. Stein, S. Schwarz, and J. Szerypo, *Nucl. Instrum. Methods Phys. Res., Sect. B* **126**, 378 (1997).
- [42] G. Savard, S. Becker, G. Bollen, H.-J. Kluge, R. B. Moore, T. Otto, L. Schweikhard, H. Stolzenberg, and U. Wiess, *Phys. Lett. A* **158**, 247 (1991).
- [43] K. Blaum, *Phys. Rep.* **425**, 1 (2006).
- [44] M. König, G. Bollen, H.-J. Kluge, T. Otto, and J. Szerypo, *Int. J. Mass Spectrom.* **142**, 95 (1995).
- [45] S. George, S. Baruah, B. Blank, K. Blaum, M. Breitenfeldt, U. Hager, F. Herfurth, A. Herlert, A. Kellerbauer, H.-J. Kluge, M. Kretzschmar, D. Lunney, R. Savreux, S. Schwarz, L. Schweikhard, and C. Yazidjian, *Phys. Rev. Lett.* **98**, 162501 (2007).
- [46] S. George, K. Blaum, F. Herfurth, A. Herlert, M. Kretzschmar, S. Nagy, S. Schwarz, L. Schweikhard, and C. Yazidjian, *Int. J. Mass Spectrom.* **264**, 110 (2007).
- [47] M. Wang, G. Audi, F. G. Kondev, W. J. Huang, S. Naimi, and X. Xu, *Chin. Phys. C* **41**, 030003 (2017).
- [48] G. Audi, F. G. Kondev, M. Wang, W. J. Huang, and S. Naimi, *Chin. Phys. C* **41**, 030001 (2017).
- [49] A. Kellerbauer, K. Blaum, G. Bollen, F. Herfurth, H.-J. Kluge, M. Kuckein, E. Sauvan, C. Scheidenberger, and L. Schweikhard, *Eur. Phys. J. D* **22**, 53 (2003).
- [50] M. Bhat, in *Nuclear Data for Science and Technology*, Research Reports in Physics, edited by S. Qaim (Springer Berlin Heidelberg, 1992), pp. 817–821, data extracted using the NNDC On-Line Data Service from the ENSDF database (<http://nndc.bnl.gov>), file revised as of 01.09.2019.
- [51] M. Hjorth-Jensen, T. T. S. Kuo, and E. Osnes, *Phys. Rep.* **261**, 125 (1995).
- [52] B. A. Brown and W. D. M. Rae, *Nucl. Data Sheets* **120**, 115 (2014).
- [53] C. Lorenz and D. Rudolph (private communication).
- [54] H.-K. Wang, K. Kaneko, Y. Sun, Y.-Q. He, S.-F. Li, and J. Li, *Phys. Rev. C* **95**, 011304(R) (2017).
- [55] H.-K. Wang, Y. Sun, H. Jin, K. Kaneko, and S. Tazaki, *Phys. Rev. C* **88**, 054310 (2013).
- [56] N. Zeldes, T. Dumitrescu, and H. Köhler, *Nucl. Phys. A* **399**, 11 (1983).
- [57] K.-H. Schmidt, and D. Vermeulen, in *AMCO-6*, edited by J. A. Nolen and W. Benenson (Springer, Boston, 1980), p. 119.
- [58] S. Goriely, N. Chamel, and J. M. Pearson, *Phys. Rev. C* **93**, 034337 (2016).
- [59] M. Kortelainen, T. Lesinski, J. Moré, W. Nazarewicz, J. Sarich, N. Schunck, M. V. Stoitsov, and S. Wild, *Phys. Rev. C* **82**, 024313 (2010).
- [60] A. V. Afanasjev and S. E. Agbemava, *Phys. Rev. C* **93**, 054310 (2016).
- [61] K. Hebeler, S. K. Bogner, R. J. Furnstahl, A. Nogga, and A. Schwenk, *Phys. Rev. C* **83**, 031301(R) (2011).
- [62] J. Simonis, K. Hebeler, J. D. Holt, J. Menéndez, and A. Schwenk, *Phys. Rev. C* **93**, 011302(R) (2016).
- [63] J. Simonis, S. R. Stroberg, K. Hebeler, J. D. Holt, and A. Schwenk, *Phys. Rev. C* **96**, 014303 (2017).
- [64] J. D. Holt, S. R. Stroberg, A. Schwenk, and J. Simonis, [arXiv:1905.10475](https://arxiv.org/abs/1905.10475).

4 Discussion & Outlook

The publications presented in [Ch. 3](#) demonstrated the successful transition of the high-precision mass spectrometer ISOLTRAP to the next-generation Penning-trap mass spectrometry technique PI-ICR. The findings in this cumulative thesis pave the way for high-precision mass spectrometry on radionuclides with unprecedented resolving power in new areas of the nuclear chart.

4.1 Mirror Nuclei

The first publication [[Kart19a](#)] presents the highest relative mass precision ever achieved at ISOLTRAP using the well-established Ramsey-type ToF-ICR technique. This result constitutes the sixth-best relative mass precision ever achieved on a short-lived species with half-lives $t_{1/2} < 1$ hr [[Audi17](#), [Wang17](#)]. Better relative mass precisions were, to our best knowledge, only reached for ^{34}Cl , ^{20}F , ^{14}O , ^{116}In , and ^{41}Sc [[Audi17](#), [Wang17](#)]. In order to achieve such a superior result, comprehensive studies were performed to reduce, on the one hand, the statistical uncertainties and, on the other hand, the systematic uncertainties. An increased number of measurements accomplished the former. In the case of $^{21}\text{Na}/^{21}\text{Ne}$, 30 spectra pairs were taken while 19 were taken in the case of $^{23}\text{Mg}/^{23}\text{Na}$. This amount of spectra is exceptionally numerous for mass measurements on a radioactive species since the measurement time at RIB facilities is precious.

Moreover, the cyclotron frequency ratio determination (see [Eq. \(2.7\)](#)) was improved significantly. In order to eliminate time-dependent systematic shifts in the mass measurement originating from magnetic-field fluctuations (e.g., caused by temporal fluctuations), a cyclotron frequency ratio measurement of a reference ion and the ion of interest at the same point in time is required. Since the ToF-ICR technique does not allow for simultaneous measurement of both species, an alternating measurement scheme is performed with a period of time, shorter than non-linear fluctuations of the magnetic field (i.e., ~ 15 min). So far, the method of choice for the cyclotron frequency measurement estimation of the reference ion at the exact point in time of the IOI measurement was based on a linear extrapolation of the two neighboring reference measurements in time. This procedure, however, fails to make use of the information about the entire temporal evolution of the B -field via the continuously logged temperature of the environment.

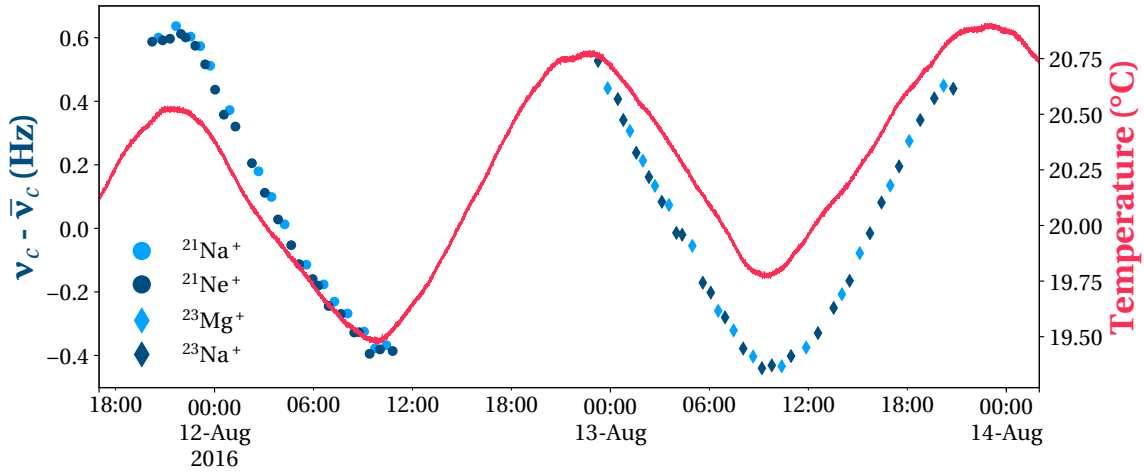


Figure 4.1: Normalized cyclotron-frequency subsets of the whole dataset's mean frequency (with uncertainties) of $^{21}\text{Na}/^{21}\text{Ne}$ and $^{23}\text{Mg}/^{23}\text{Na}$, respectively, using the alternating measurement scheme. The absolute frequency shifts over time are compared to the magnet's bore temperature, directly influencing the superconducting magnetic field of the precision Penning trap, and thus the ion's cyclotron frequency in the trap.

Modeling the temporal evolution of the B -field (as shown in [Fig. 4.1](#)) with a simultaneous polynomial fit of cyclotron frequencies of both species (e.g., see Eq. (5) and [Fig. 4](#) in [Ch. 3.1](#), or Eq. (2) and [Fig. 4](#) in [Ch. 3.2](#)) thus results in an up to 20% reduced statistical uncertainty on the frequency ratio for the same dataset, compared to the previous technique. The polynomial degree of the fit function is varied around the degree of temperature fluctuation and chosen based on which fit produces the closest resulting reduced χ^2 to one (e.g., see [Fig. 4.1](#)). A vanishing systematic uncertainty was accomplished by applying the well-established preparation procedure described in [Ch. 2.4.1](#). A specific focus was given to the elimination of the increased contamination due to enhanced charge-exchange of the noble gas $^{21}\text{Ne}^+$ with the buffer gas in the RFQ and preparation Penning trap.

The resulting masses measured with this technique were used to calculate the Q_{EC} -values of the EC-decays $^{21}\text{Na} \rightarrow ^{21}\text{Ne}$ and $^{23}\text{Mg} \rightarrow ^{23}\text{Na}$. Along with branching ratios and half-lives as experimental input values, and theoretical isospin-symmetry-breaking and nucleus dependent radiative correction terms, new $\mathcal{F}t$ -values for these mirror nuclei were calculated. Our new results reduced the uncertainty on the literature values by a factor of five, making them by far the most precise experimental input value for these $\mathcal{F}t$ -values and providing a motivation for the other quantities to be measured with a much-improved precision. In the case of the $^{21}\text{Na} \rightarrow ^{21}\text{Ne}$ Q_{EC} -value, a deviation of over 2σ from the literature value was found. This deviation could be explained by contamination in previous experi-

ments due to charge-exchange of the ^{21}Ne noble gas. In our experiment, specific care was taken to eliminate any contamination, which could induce systematic shifts.

In the case of $^{21}\text{Na} \rightarrow ^{21}\text{Ne}$, a new V_{ud} -element of the CKM-matrix was calculated, since a β - ν -asymmetry coefficient was already measured (which was not the case for $^{23}\text{Mg} \rightarrow ^{23}\text{Na}$). The new value agrees with the standard model and allows, with values of ^{19}Ne , ^{29}P , ^{35}Ar , and ^{37}K , for a reduced independent V_{ud} -element value based on mirror nuclei: $\bar{V}_{\text{ud}} = 0.9727(14)$. The new value is only seven times less precise than the value of superallowed transitions, which is the current most precise experimental determination of the V_{ud} -element: $\bar{V}_{\text{ud}} = 0.97420(21)$ [Hard18].

With the successful implementation of PI-ICR, even higher precisions in shorter measurement times are now in reach, as shown for the Q_{EC} -value measurement of the long-lived $^{163}\text{Ho} \rightarrow ^{163}\text{Dy}$ decay [Elis15]. Additionally, the technique allows in-trap purification due to its supreme resolving power, making it the technique of choice for future mass measurements of radioisotopes at the highest precisions. Furthermore, the current temperature fluctuations of $\Delta T > 1.25$ °C (see Fig. 4.1) will be reduced in 2020 by installing an active temperature stabilization of the magnet's bore as well as all sensitive power supplies. This procedure will further reduce possible sources of systematic shifts and result in even smaller measurement uncertainties, as already successfully demonstrated at the PENTATRAP experiment [Repp12].

Note: During the writing process of this thesis, we realized that equation (4) in the publication could no longer be approximated at this level of precision without accounting for ionization energies. Hence the formula changes to:

$$Q_{\text{EC}} = (r - 1)(m_{\text{ref,lit}} - m_e)c^2 + r E_{i,\text{ref}} - E_{i,\text{IOI}}, \quad (4.1)$$

with the cyclotron-frequency ratio r (see Eq. (2.7)), the literature mass of the reference ion $m_{\text{ref,lit}}$, the electron mass m_e [Stur14], the speed of light c , and the ionization energies for the reference atom and atom of interest, $E_{i,\text{ref}}$ and $E_{i,\text{IOI}}$, respectively. The Q_{EC} -values for $^{21}\text{Na} \rightarrow ^{21}\text{Ne}$ and $^{23}\text{Mg} \rightarrow ^{23}\text{Na}$ in Tab. 1 of the publication thus change by 17 eV and 3 eV to 3546.919(18) keV and 4056.179(32) keV, respectively, using ionization energies from NIST [NIST20]. Based on the Q_{EC} -value for the $^{21}\text{Na} \rightarrow ^{21}\text{Ne}$ decay, the f_V -value in Tab. 2 changes to 170.714(6). The essence of the paper, namely the calculated $\mathcal{F}t$ -values and the resulting V_{ud} -element of the CKM quark-mixing matrix, is not affected due to dominating uncertainties in the other relevant quantities. The corrections were submitted to *Phys. Rev. C* and will be visible shortly in the on-line version of the article.

4.2 Neutrino Mass

With publication [Kart19b], ISOLTRAP's first measurement using the state-of-the-art Penning-trap measurement technique PI-ICR was presented. In only 4 hrs of measurement time, a competitive precision of $\delta m/m = 1.4 \times 10^{-9}$ and resolving power $m/\Delta m$ exceeding 1×10^7 was achieved. Based on the mass measurement, the ground-to-ground-state Q_{EC} -value (see Ch. 1.2.2) of this EC-decay was calculated to be $Q_{\text{EC}}(^{131}\text{Cs} \rightarrow ^{131}\text{Xe}) = 358.00(17)$ keV, reducing the uncertainty on the literature value by a factor of 25. After comparison with different possible excited atomic states in the decay daughter $^{131}\text{Xe}^*$, ^{131}Cs is undoubtedly lower in energy than $^{131}\text{Xe}^*$, hence prohibiting the $^{131}\text{Cs} \rightarrow ^{131}\text{Xe}^*$ decay. With the refined uncertainty, ^{131}Cs was thus precluded from the proposed list of possible neutrino-mass determination candidates [Elis14a, Kart17].

In this experiment, PI-ICR demonstrated enormous potential for the search of possible candidates for the determination of the neutrino mass. In a scheduled measurement campaign for 2020, the ISOLTRAP experiment will measure two further possible candidates, namely ^{159}Dy and ^{175}Hf . As detailed in the letter of intent for the upcoming experiment [Kart17], these isotopes promise to have vanishing ground-to-excited-state Q_{EC} -values at current precision levels, which is a requirement for the complementary MMC measurement (see Ch. 1.2.2). High precision measurements based on the new PI-ICR technique will shed light on both cases, and possibly provide crucial information for an improved upper limit on the ν_e mass.

4.3 *N*-rich Cadmium

The third publication [Kart20] presented the latest ISOLTRAP results of *N*-rich cadmium isotopes around the *N* = 82 shell gap. For this beam time, all available mass measurement techniques at ISOLTRAP were employed, including the PI-ICR technique. This technique allowed for the first time the spatial separation of low-lying isomeric states in $^{127,129}\text{Cd}$ with unprecedented resolution. In a novel comparison with recent laser-spectroscopy results at ISOLDE [Yord13], the spin-states were assigned uncovering a surprising change in the ordering of these states in ^{129}Cd . Compared to many lighter odd-cadmium isotopes, the $J^\pi = 11/2^-$ suddenly becomes the ground state in ^{129}Cd while the $J^\pi = 3/2^+$ state (i.e., the ground state in the lighter systems) becomes the isomer. This behavior could be reproduced by shell-model calculations with an increased attraction between the proton $g_{9/2}$ and neutron $h_{11/2}$ orbits (see Fig. 4 in Ch. 3.3).

Furthermore, the data allowed for a detailed study of the *N* = 82 shell gap strength, which will be explained in more detail in the following. Finally, the first mass measurement of ^{132}Cd using ISOLTRAP's MRTof-MS proved the doubly magic character (also known as mutually enhanced magicity) of ^{132}Sn and allowed for comprehensive comparison with state-of-the-art nuclear theory. Among others, valence-space in-medium similarity renormalization group (VS-IMSRG) *ab-initio* theoretical calculations with the most abundant valence space ever attempted were compared to the experimental values. The promising results raise hope for a better description of nuclear interactions based on chiral-effective interactions, also for heavy exotic elements.

In analogy to [Sorl08], the one-neutron separation energies for *N* = 82 and *N* = 83 and the *N* = 82 shell gap resulting from the subtraction of the former two is plotted in Fig. 4.2 in order to study the *N* = 82 shell strength. With the inclusion of ISOLTRAP's new results for *Z* = 48, significant improvement was achieved based on the first experimental data for *N* ~ 82 and *Z* < 50. These new mass values give the first experimental evidence for the so-called *N* = 82 shell quenching, which γ -spectroscopic results in ^{130}Cd already hinted at [Dill03]. Shell quenching describes the phenomenon, in which a "magic" shell configuration of enhanced nuclear stability weakens to the extent of no longer representing a closed nuclear shell.

The *N* = 82 shell is special among the neutron-shell gaps. It is extremely stable over a wide range of isotopes and produces, with seven stable isotopes, the most stable isotopes of any neutron shell. The top panel in Fig. 4.2 shows the strength of the

$N=82$ shell gap via the quantity $\Delta_{S_{1n}}(N=82) = S_{1n}(N=82)_{\text{GS}} - S_{1n}(N=83)_{\text{GS}}$. The gap is generally very high at ~ 4 MeV while showing a slightly enhanced strength for ^{146}Gd , closing the $g_{7/2}$ and $d_{5/2}$ proton orbits, and a strongly enhanced strength for the doubly magic ^{132}Sn , closing the $g_{9/2}$ proton orbit at $Z=50$.

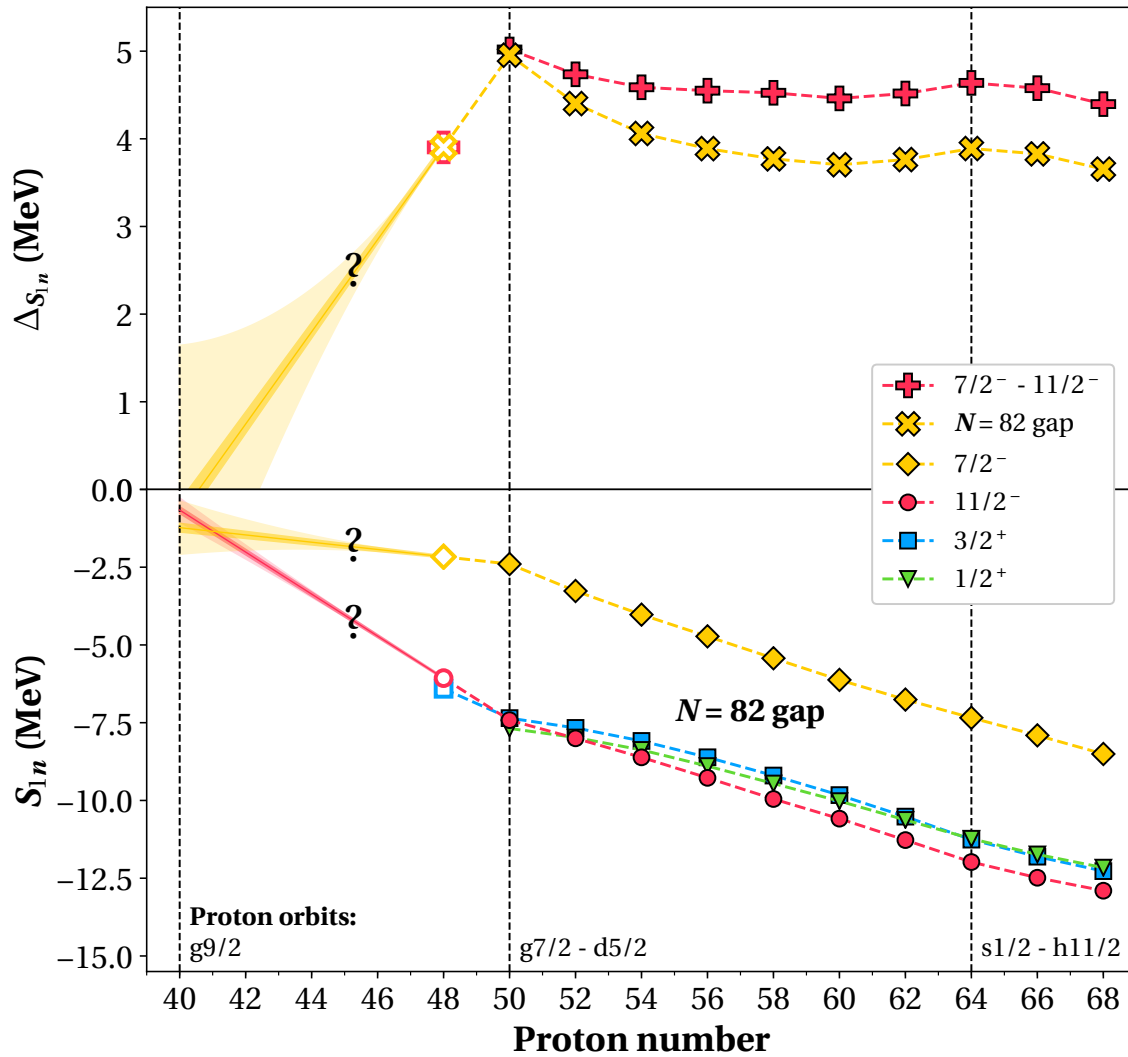


Figure 4.2: *Bottom:* One-neutron separation energies (S_{1n} , see Eq. (1.2)) calculated for three states $J^\pi = \{11/2^-, 3/2^+, 1/2^+\}$ for $N=82$ and the ground state (GS) $J^\pi = 7/2^-$ for $N=83$. *Top:* Resulting $N=82$ shell gap $\Delta_{S_{1n}}(N=82) = S_{1n}(N=82)_{\text{GS}} - S_{1n}(N=83)_{\text{GS}}$, which demonstrates the strength of the $N=82$ shell. *General:* The experimental data for $Z=48$ (unfilled marker) were taken from the publication discussed in Ch. 3.3 [Kart20], the ones for $Z=\{50-68\}$ (filled marker) were taken from the 2016 atomic-mass evaluation [Audi17, Wang17]. Linear extrapolations for $Z < 48$ and their 2σ band (solid lines and filled areas) are based on the experimental data for $Z=\{48, 50\}$. Quadratic extrapolations and their 2σ band (solid line and filled area with 80% transparency) are based on the linear trend for $Z=\{48, 50\}$ and the curvature for $Z=\{50-64\}$.

The interesting point here constitutes the gap strength for $Z < 50$, which allows for the study of the interaction of the proton $g_{9/2}$ orbit with neutrons filling the $N = 82$ shell gap. On the one hand, the cadmium data give proof for the doubly magic character of ^{132}Sn via its greatly enhanced strength. On the other hand, it also provides a first trend of the $N = 82$ shell gap for $Z < 50$ with the result of a substantial weakening of the $N = 82$ shell (i.e., shell quenching). A simple extrapolation shown in the figure indicates this trend. First, a linear extrapolation was performed based on the experimental data for $Z = \{48, 50\}$, and their associated uncertainties. From orbital evolution based on spectroscopic data, a curvature in the gap strength is to be expected [Sorl08]. Hence, a simple extrapolation based on the strong curvature for $Z = \{50-68\}$ towards the doubly magic ^{132}Sn is shown to provide a more realistic frame for possible directions of the $N = 82$ shell gap for $Z < 48$ and its strongly suggested weakening. This result is particularly vital since an experimental expansion towards $N \sim 82$ and $Z < 48$ seems unlikely due to production limitations at current RIB facilities. Next-generation facilities, like the facility for antiproton and ion research (FAIR; Darmstadt, Germany) [Henn05] and the facility for rare isotope beams (FRIB; East Lansing, USA) [Boll10], promise to deliver neutron-rich beams at higher yields over the next decade.

5 Summary

This dissertation demonstrated ISOLTRAP's transition to the next-generation Penning-trap mass spectrometry technique PI-ICR along with publications at unprecedented resolving powers and relative mass precisions. Within these findings, progress has been made in the following fields:

1. Q_{EC} -value for the $^{21}\text{Na} \rightarrow ^{21}\text{Ne}$ and $^{23}\text{Mg} \rightarrow ^{23}\text{Na}$ decays were measured using the well-established ToF-ICR technique accomplishing the highest precision ever reached at ISOLTRAP. For the former case, a new V_{ud} -element of the CKM quark-mixing matrix was calculated to be $V_{\text{ud}} = 0.9715(34)$. This value agrees with the standard model of particle physics and allows for a reduced independent V_{ud} -element value based on the mirror nuclei ^{19}Ne , ^{21}Na , ^{29}P , ^{35}Ar , and ^{37}K : $\bar{V}_{\text{ud}} = 0.9727(14)$. This new value is only seven times less precise than the value of superallowed transitions, which is the current most precise experimental determination of the V_{ud} -element.
2. In ISOLTRAP's first publication using the state-of-the-art Penning-trap measurement technique PI-ICR, a competitive precision of $\delta m/m = 1.4 \times 10^{-9}$ was achieved in only 4 hrs of measurement time. A new ground-to-ground-state Q_{EC} -value of this EC-decay was determined to be $Q_{\text{EC}}(^{131}\text{Cs} \rightarrow ^{131}\text{Xe}) = 358.00(17)$ keV, reducing the uncertainty on the literature value by a factor of 25 and precluding this decay as a possible candidate for the direct determination of the neutrino mass.
3. First spatial separation in $^{127,129}\text{Cd}$ using PI-ICR allowed for solving the ordering in the low-lying isomeric states in neutron-rich cadmium. Based on these results, the strength of the $N = 82$ shell gap was studied and found to show a substantial weakening for $Z < 50$ (= shell quenching). Furthermore, the first mass measurement of ^{132}Cd provided proof for the phenomenon of mutually enhanced magicity in ^{132}Sn . It also allowed for the test of state-of-the-art nuclear theories, paving the way for *ab-initio* calculations of heavy elements.

In summary, PI-ICR has shown extreme potential due to its superior resolving power, and a factor of ~25 faster measurement times compared to the well-established ToF-ICR technique while allowing for comparable or better relative mass precisions. Thus, PI-ICR is the key to the future success of the ISOLTRAP setup in uncovering new areas of the nuclear chart and possibly new physics.

Bibliography

- [Asto19] Aston, F. W. "The Constitution of the Elements". *Nature* **104**, 393–393 (1919).
- [Asto27] Aston, F. W. "Atoms and their Packing Fractions¹". *Nature* **120**, 956–959 (1927).
- [Atan15] Atanasov, D. et al. "Precision Mass Measurements of ¹²⁹⁻¹³¹Cd and Their Impact on Stellar Nucleosynthesis via the Rapid Neutron Capture Process". *Phys. Rev. Lett.* **115**, 232501 (2015).
- [Audi17] Audi, G. et al. "The NUBASE2016 evaluation of nuclear properties". *Chinese Phys. C* **41**, 030001 (2017).
- [Auge75] Auger, P. "The Auger effect". *Surf. Sci.* **48**, 1–8 (1975).
- [Ball19] J. Ballof (2019) private communication
- [Bamb15] C. Bambi, et al. "Introduction to Particle Cosmology". *Springer* 35–52. (2015, book)
- [Bile87] Bilenky, S. M. et al. "Massive neutrinos and neutrino oscillations". *Rev. Mod. Phys.* **59**, 671–754 (1987).
- [Blau06] Blaum, K. "High-accuracy mass spectrometry with stored ions". *Physics Reports* **425**, 1–78 (2006).
- [Blau13] Blaum, K. et al. "100 Years of Mass Spectrometry". *Int. J. Mass Spectrom.* **349–350**, 1–2 (2013).
- [Boll10] Bollen, G. "FRIB - Facility for Rare Isotope Beams." *AIP Conf. Proc.* **1224** (2010), 432–41.
- [Boll90] Bollen, G. et al. "The accuracy of heavy-ion mass measurements using time of flight-ion cyclotron resonance in a Penning trap". *J. Appl. Phys.* **68**, 4355–4374 (1990).
- [Boll92] Bollen, G. et al. "Resolution of nuclear ground and isomeric states by a Penning trap mass spectrometer". *Phys. Rev. C* **46**, R2140–R2143 (1992).
- [Borg18] Borge, M. J. G. & Blaum, K. "Focus on Exotic Beams at ISOLDE: A Laboratory Portrait". *J. Phys. G Nucl. Part. Phys.* **45**, 15–18 (2018).
- [Caki13] Cakirli, R. B. & Casten, R. F. "Nuclear binding and nuclear structure". *Int. J. Mass Spectrom.* **349–350**, 187–191 (2013).
- [Cath17] Catherall, R. et al. "The ISOLDE facility". *J. Phys. G Nucl. Part. Phys.* **44**, 094002 (2017).
- [Clar13] Clark, J. & Savard, G. "Precision masses for studies of the astrophysical r process". *Int. J. Mass Spectrom.* **349–350**, 81–86 (2013).

- [Coop56] Cooper, L. N. "Bound Electron Pairs in a Degenerate Fermi Gas". *Phys. Rev.* **104**, 1189–1190 (1956).
- [Cost35] Coster, D. & L. Kronig, R. De. "New type of auger effect and its influence on the x-ray spectrum". *Physica* **2**, 13–24 (1935).
- [Dill03] Dillmann, I. et al. "N = 82 Shell Quenching of the Classical R-Process "Waiting-Point" Nucleus 130Cd." *Phys. Rev. Lett.* **91**, 162503 (2003).
- [Eins05] Einstein, A. "Ist die Trägheit eines Körpers von seinem Energieinhalt abhängig?". *Ann. Phys.* **323**, 639–641 (1905).
- [Elis13a] Eliseev, S. et al. "Phase-imaging ion-cyclotron-resonance measurements for short-lived nuclides". *Phys. Rev. Lett.* **110**, 082501 (2013).
- [Elis13b] Eliseev, S. et al. "Penning-trap mass spectrometry for neutrino physics". *Int. J. Mass Spectrom.* **349–350**, 102–106 (2013).
- [Elis14a] Eliseev, S. et al. "A phase-imaging technique for cyclotron-frequency measurements". *Appl. Phys. B* **114**, 107–128 (2014).
- [Elis14b] Eliseev, S. et al. "Search for β -Transitions with the Lowest Decay Energy for a Determination of the Neutrino Mass". *Proposal to the ISOLDE and Neutron Time-of-Flight Committee* (2014).
- [Elis15] Eliseev, S. et al. "Direct Measurement of the Mass Difference of ^{163}Ho and ^{163}Dy Solves the Q-Value Puzzle for the Neutrino Mass Determination". *Phys. Rev. Lett.* **115**, 062501 (2015).
- [Erle19] Erlner, J. & Schott, M. "Electroweak precision tests of the Standard Model after the discovery of the Higgs boson". *Prog. Part. Nucl. Phys.* **106**, 68–119 (2019).
- [Eron13] Eronen, T. & Jokinen, A. "High-precision atomic mass measurements for a CKM unitarity test". *Int. J. Mass Spectrom.* **349–350**, 69–73 (2013).
- [Fedo17] Fedosseev, V. et al. "Ion beam production and study of radioactive isotopes with the laser ion source at ISOLDE". *J. Phys. G Nucl. Part. Phys.* **44**, 084006 (2017).
- [Fran08] Franzke, B. et al. "Mass and lifetime measurements of exotic nuclei in storage rings". *Mass Spectrom. Rev.* **27**, 428–469 (2008).
- [Gast17] Gastaldo, L. et al. "The electron capture in ^{163}Ho experiment - ECHO". *Eur. Phys. J. Spec. Top.* **226**, 1623–1694 (2017).
- [Geor07] George, S. et al. "Ramsey method of separated oscillatory fields for high-precision penning trap mass spectrometry". *Phys. Rev. Lett.* **98**, 162501 (2007).
- [Gräff80] Gräff, G. et al. "A direct determination of the proton electron mass ratio". *Zeit. Phys. A* **297**, 35–39 (1980).

- [Graw07] Grawe, H. et al. "Nuclear structure and astrophysics". *Rep. Prog. Phys.* **70**, 1525–1582 (2007).
- [Hann06] Hanneke, D. et al. "New Measurement of the Electron Magnetic Moment and the Fine Structure Constant." *Phys. Rev. Lett.* **100**, 120801 (2008).
- [Hard15] Hardy, J. C. & Towner, I. S. "Superaligned $0^+ \rightarrow 0^+$ nuclear β decays : 2014 critical survey , with precise results for V_{ud} and CKM unitarity". *Phys. Rev. C* **91**, 1–27 (2015).
- [Hard18] Hardy, J. C. & Towner, I. S. "Nuclear beta decays and CKM unitarity". *CIPANP2018* (2018, proceeding).
- [Haye19] Hayen, L. & Severijns, N. "Beta Spectrum Generator: High precision allowed β spectrum shapes". *Comp. Phys. Comm.* **240**, 152–164 (2019).
- [Henn05] Henning, W. "FAIR - An international accelerator facility for research with ions and antiprotons." *AIP Conf. Proc.* **773** (2005), 3–5.
- [Herf01] Herfurth, F. et al. "A linear radiofrequency ion trap for accumulation, bunching, and emittance improvement of radioactive ion beams". *Nucl. Inst. Meth. Phys. A* **469**, 254–275 (2001).
- [Kart17] Karthein, J. et al. "Search for β -Transitions with the Lowest Decay Energy for a Determination of the Neutrino Mass: Precision Q-Value Measurements Of ^{159}Dy and ^{175}Hf During the CERN Long Shutdown 2". *Letter of Intent to the ISOLDE and Neutron Time-of-Flight Committee* (2017).
- [Kart19a] Karthein, J. et al. " Q_{EC} -value determination for $^{21}\text{Na} \rightarrow ^{21}\text{Ne}$ and $^{23}\text{Mg} \rightarrow ^{23}\text{Na}$ mirror-nuclei decays using high-precision mass spectrometry with ISOLTRAP at the CERN ISOLDE facility". *Phys. Rev. C* **100**, 015502 (2019).
- [Kart19b] Karthein, J. et al. "Direct decay-energy measurement as a route to the neutrino mass". *Hyperfine Interact.* **240**, 61 (2019).
- [Kart19c] Karthein, J. (2019) isoltrap.web.cern.ch/
- [Kart19d] Karthein, J. (2019) github.com/jonas-ka/pi-icr-analysis
- [Kart19e] Karthein, J. (2019) github.com/jonas-ka/mr-tof-analysis
- [Kart19f] Karthein, J. (2019) github.com/jonas-ka/nuclear-chart-plotter
- [Kart20] Manea, M. & Karthein, J. et al. "First glimpse of the $N = 82$ shell closure below $Z = 50$ from masses of neutron-rich cadmium isotopes and isomers". *Phys. Rev. Lett* **124**, 092502 (2020).
- [Kell03] Kellerbauer, A. et al. "From direct to absolute mass measurements: A study of the accuracy of ISOLTRAP". *Eur. Phys. J. D* **22**, 53–64 (2003).

- [Koba73] Kobayashi, M. & Maskawa, T. "CP-Violation in the Renormalizable Theory of Weak Interaction." *Prog. Theo. Phys.* **49**, 652–57 (1973).
- [Köhl16] Köhler, F. et al. "Isotope Dependence of the Zeeman Effect in Lithium-like Calcium." *Nature Comm.* **7**, 10246 (2016).
- [Köst01] Köster, U. "ISOLDE target and ion source chemistry". *Radioch. Acta* **89**, 749–756 (2001).
- [Krei13] Kreim, S. et al. "Recent exploits of the ISOLTRAP mass spectrometer". *Nucl. Inst. Meth. Phys. B* **317**, 492–500 (2013).
- [Kret07] Kretschmar, M. "The Ramsey method in high-precision mass spectrometry with Penning traps: Theoretical foundations". *Int. J. Mass Spectrom.* **264**, 122–145 (2007).
- [Kret99] Kretschmar, M. "A quantum mechanical model of Rabi oscillations between two interacting harmonic oscillator modes and the interconversion of modes in a Penning trap". *AIP Conf. Proc.* **457**, 242–251 (1999).
- [Lunn17] Lunney, D. (on behalf of the ISOLTRAP Collaboration) "Extending and refining the nuclear mass surface with ISOLTRAP". *J. Phys. G Nucl. Part. Phys.* **44**, 064008 (2017).
- [Maye48] Mayer, M. G. "On Closed Shells in Nuclei". *Phys. Rev.* **74**, 235–239 (1948).
- [Moug18] Mougeot, M. et al. "Precision Mass Measurements of $^{58-63}\text{Cr}$: Nuclear Collectivity Towards the $N = 40$ Island of Inversion". *Phys. Rev. Lett.* **120**, 232501 (2018).
- [Moug20] Mougeot, M. et al. "The masses of $^{99-101}\text{In}$ " (preliminary title). *In preparation* (2020).
- [Mukh08] Mukherjee, M. et al. "ISOLTRAP: An on-line Penning trap for mass spectrometry on short-lived nuclides". *Eur. Phys. J. A* **35**, 1–29 (2008).
- [Münz13] Münzenberg, G. "Development of Mass Spectrometers from Thomson and Aston to Present." *Int. J. Mass Spectrom.* **349–350**, 9–18 (2013).
- [Naim10] Naimi, S. et al. "Critical-point boundary for the nuclear quantum phase transition near $A = 100$ from Mass measurements of $^{96,97}\text{Kr}$ ". *Phys. Rev. Lett.* **105**, 032502 (2010).
- [NIST20] Kramida, A. et al. "NIST Atomic Spectra Database" (ver. 5.7.1) [Online Feb. 2020]. *National Institute of Standards and Technology, Gaithersburg, MD.*
- [PDG18] Tanabashi, M. et al. (Particle Data Group) "Review of Particle Physics". *Phys. Rev. D* **98**, 030001 (2018).

- [Rain04] Rainville, S. et al. "An Ion Balance for Ultra-High-Precision Atomic Mass Measurements." *Science* **303**, 334–38 (2004).
- [Repp12] Repp, J. et al. "Pentatrap: A novel cryogenic multi-penning-trap experiment for high-precision mass measurements on highly charged ions." *Appl. Phys. B Lasers Opt.* **107** (2012), 983–96.
- [Riis13] Riisager, K. "Halos and related structures". *Phys. Scr.* **T152**, 014001 (2013).
- [Sava91] Savard, G. et al. "A new cooling technique for heavy ions in a Penning trap". *Phys. Lett. A* **158**, 247–252 (1991).
- [Scha13] Schatz, H. "Nuclear masses in astrophysics". *Int. J. Mass Spectrom.* **349–350**, 181–186 (2013).
- [Seve08] Severijns, N. et al. " $\mathcal{F}t$ -values of the $T = \frac{1}{2}$ mirror β transitions". *Phys. Rev. C* **78**, 1–14 (2008).
- [Smor19] Smorra, C. et al. "Direct limits on the interaction of antiprotons with axion-like dark matter". *Nature* **575**, 310–314 (2019).
- [Sorl08] Sorlin, O., & Porquet, M. G. "Nuclear Magic Numbers: New Features Far from Stability." *Prog. Part. Nucl. Phys.* **61**, 602–73 (2008).
- [Stur14] Sturm, S. et al. "High-precision measurement of the atomic mass of the electron". *Nature* **506**, 467–470 (2014).
- [Thom13] Thomson, J. "Rays of Positive Electricity and Their Application to Chemical Analyses". *Longmans, Green and Co.* (1913, book).
- [Wang17] Wang, M. et al. "The AME2016 atomic mass evaluation (II). Tables, graphs and references". *Chin. Phys. C* **41**, 030003 (2017).
- [Waut09] Wauters, F. et al. " β asymmetry parameter in the decay of ^{114}In ". *Phys. Rev. C* **80**, 2–6 (2009).
- [Welk17] Welker, A. et al. "Binding Energy of ^{79}Cu : Probing the Structure of the Doubly Magic ^{78}Ni from only One Proton Away". *Phys. Rev. Lett.* **119**, 192502 (2017).
- [Wien13] Wienholtz, F. et al. "Masses of exotic calcium isotopes pin down nuclear forces". *Nature* **498**, 346–349 (2013).
- [Wien17] Wienholtz, F. et al. "Mass-selective ion ejection from multi-reflection time-of-flight devices via a pulsed in-trap lift". *Int. J. Mass Spectrom.* **421**, 285–293 (2017).
- [Wien19] Wienholtz, F. et al. "Improved Stability of Multi-Reflection Time-of-Flight Mass Spectrometers through Passive and Active Voltage Stabilization." *Nucl. Inst. Meth. Phys. B* **463**, 348–56 (2020).
- [Wolf12] Wolf, R. N. et al. "Static-mirror ion capture and time focusing for electrostatic ion-beam traps and multi-reflection time-of-flight mass analyzers by use of an in-trap potential lift". *Int. J. Mass Spectrom.* **313**, 8–14 (2012).

- [Wolf13a] Wolf, R. N. et al. "Plumbing neutron stars to new depths with the binding energy of the exotic nuclide ^{82}Zn ". *Phys. Rev. Lett.* **110**, 041101 (2013).
- [Wolf13b] Wolf, R. N. et al. "ISOLTRAP's multi-reflection time-of-flight mass separator/spectrometer". *Int. J. Mass Spectrom.* **349-350**, 123-133 (2013).
- [Yord13] Yordanov, D. T. et al. "Spins, Electromagnetic Moments, and Isomers of $^{107-129}\text{Cd}$." *Phys. Rev. Lett.* **110**, 192501 (2013).

Acknowledgements

A dissertation in modern research is never the work of a single person. Special thanks hence go to the following, essential people in my life. Without you, this thesis would have never been so successful!

- First and foremost, I want to thank my *Doktorvater* Klaus for facilitating this thesis at one of the most prestigious physics institutes in the world. Not only did he manage to supervise me remotely, but he also gave me the chance to grow with augmented responsibilities and freedom at a faster pace compared to the average graduate student. Since our unique meeting on a plane, he became my mentor and close friend, and I am looking forward to our future collaboration.
- Second, I want to thank my faithful local colleagues, Maxime and Ivan, for a fabulous time at CERN, the fruitful discussions about God and the world, the courage for the successful horizontal alignment project, the amicable environment also outside working hours and the support during the writing phase of my thesis.
- Third, I want to thank the previous generation of postdocs at the ISOLTRAP experiment, Vladimir, Dinko, and Frank, for teaching me the operation and maintenance of an elaborate experiment with radioactive ions, and the ethics and mindset of an experimental physicist.
- Fourth, I want to thank Gerda for the supervision and support, Michael for the organization, and the German Federal Ministry of Education and Research for the sponsoring of my stay at CERN via the Wolfgang Gentner Ph.D. Scholarship.
- Fifth, I want to thank Volker and Feng for providing me with the optimal environment at LBNL Berkeley for writing a dissertation.
- Sixth, I want to thank my family and friends for providing me with their best support far away from home. In CERN's exclusive and isolated environment, one can quickly lose connection to reality. Hence, sound roots from home are vital for success at work. Special thanks go to my parents, Britta and Manfred, and my sister Toska for always supporting my decisions and education.
- Last but not least, I would like to thank my smart and beautiful, soon-to-be wife, Jamie, for all her support, time, and love. Managing a relationship across up to 9333 km and nine time zones for almost two years gave us the chance to grow as a couple and gave me the confidence that I want to spend my life with you! I am excited about our shared future with all it has to offer 🤴❤️👸